Modeling and Analysis of Extrusion-Spin Coating: An Efficient and Deterministic Photoresist Coating Method in Microlithography

by

Sangjun Han

Master of Science in Mechanical Engineering
Massachusetts Institute of Technology, 1997

Submitted to the Department of Mechanical Engineering
In partial fulfillment of the requirements for the degree of

Doctor of Philosophy in Mechanical Engineering

at the

MASSACHUSETTS INSTITUTE OF TECHNOLOGY

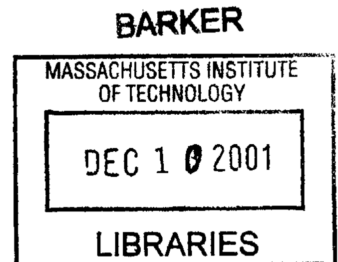
BARKER
MASSACHUSETTS INSTITUTE OF TECHNOLOGY
DEC 1 0 2001
LIBRARIES

February 2001

© Massachusetts Institute of Technology 2001. All rights reserved.

Author ....
Department of Mechanical Engineering
January 19, 2001

Certified by ....
Jung-Hoon Chun
Associate Professor of Mechanical Engineering
Thesis Supervisor

Certified by ....
Ain A. Sonin
Chairman, Departmental Committee on Graduate Students

Modeling and Analysis of Extrusion-Spin Coating: An Efficient and Deterministic Photoresist Coating Method in Microlithography

By

Sangjun Han

Submitted to the Department of Mechanical Engineering
on January 19, 2001, in partial fulfillment of the
requirements for the degree of
Doctor of Philosophy in Mechanical Engineering

Abstract

In the fabrication of microelectronic chips, microlithography is used to transfer a pattern of circuit geometry from mask to semiconductor wafer. An important step in this process is the deposition of a thin and uniform layer of photoresist (often called resist) on which the lithographic image is exposed. Typical photoresist layers are less than 1 μm thick with a variation of 5 Å for advanced chips. Spin coating is the prevalent coating method to produce the required thickness and uniformity, but it typically wastes over 90% of the photoresist applied. A more efficient method needs to be developed for two reasons. The first is that 80% of the photoresist is an environmentally hazardous solvent. The second is the cost increase of photoresist. As the target of semiconductor industry moves toward the fabrication of smaller devices with larger capacity, the trend in photoresist shifts from i-line to deep UV resists, which allow for narrower linewidths on a chip. The price of this new resist is four to ten times higher than that of i-line resists. Reducing photoresist waste is desirable for both environmental and economical reasons.

The current spin coating method has another problem in addition to low coating efficiency. Results from spin coating are unpredictable. The relationships between the inputs (process variables) and outputs (coating thickness and uniformity) can only be obtained by trial and error. Thus, a number of experiments have to be conducted to attain a certain coating thickness and uniformity. A more effective method would yield the predictable coating thicknesses and uniformities for given inputs. Both the cost and time required for process development can be reduced this way.

Extrusion-spin coating achieves high coating efficiency with predictable coating results. This new method uses an efficient extrusion coating technique to apply a thin film of resist to a wafer before spinning. This initial layer of photoresist eliminates the spreading phase, the most inefficient step of spin coating. The initial layer also provides the existing spin coating models with determined initial conditions and thereby renders its results predictable.

A prototype extrusion-spin coater has been designed and fabricated. Initial experiments have been conducted to determine, test and optimize process variables. One variable, the solvent concentration degree in the environment, is most critical. As the initial coating layer deposited by extrusion coating is only 20~40 μm, solvent contained in the photoresist evaporates rapidly at the absence of a solvent concentration in the environment.

Evaporation causes the viscosity of photoresist to be nonuniform over the wafer. The outcome of the spin coating process becomes less uniform.

Experimental results are compared with Emslie et al.'s predictive models of spin coating. A solvent concentration of 80% or higher in the environment was found to be necessary to attain a predictable coating thickness with 5 Å uniformity. With optimized process variables, mean coating thickness matches theoretical predictions with a variation of 0.01 μm. Defect-free coating results with coating efficiencies as high as 40% were achieved.

Thesis Supervisor: Jung-Hoon Chun

Title: Associate Professor of Mechanical Engineering

Acknowledgments

Five years that seemed everlasting have now become five seconds of memory. At this moment, nothing is left in my heart but gratitude for those who made the five seconds' memory worth each second.

My sincere and utmost gratitude goes to Prof. Chun who has been the most wonderful advisor in my life. He has taught me not only how to conduct scientific research but how to survive in the real world.

Thank you, Prof. Mikic and Prof. Boning for helping me throughout my research. Both of you have shown me the true qualities of MIT professors.

I also had a marvelous opportunity to work with people at SVG. Jae Park was fully responsible for my unforgettable memories at San Jose. Beverly Roberts helped me create comfortable environment to conduct successful experiments in every aspect. John Lewellen and Emir Gruer provided me with valuable advices whenever I needed them. Daniel Hanjojo was never hesitant to help me out with any mechanical problems. Dikran Babikian was there to support me fully when I faced any problems. Larry Oh always pulled me along to achieve my goals. Tom and Karen were always in the lab and helped my experiments. I, again, would like to show my sincere gratitude to all the people at SVG for their helps.

I would like to thank my new friends at California for their hospitality: Jung-Woo Lee and his wife, Hye-Jung, Joong-Soo Kim and his wife, Yoonjung, Jae-Joon Jang and his wife, Linda. Those are definitely unforgettable three months in my life.

I would like to thank my friends in the Heat Transfer Lab: Prof. Griffith, Marc, Matt, Jim, and Daxi.

I thank Lisa Falco for her humors and encouragements.

Thank you all my friends: Sokwoo Rhee, Andy Kim, Shinsuk Park, Seungkil Sohn, Chanil Chung, Jinpyung Chung, Sungjun Kim, Jaehyun Kim, Heungsoo Kim, Peter Park, Steve Rhee, Junbum Kim, Woosok Chang, Chunho Kang, Jinwoo Bae, Taesik Lee, and Yongsuk Kim.

I would like to thank Jin-Whan Ohr for his patience and trust.

Finally, I will just make this short. This thesis is for you all, Father, Mother and my lovely Sister.

Contents

1. Introduction **18**

1.1 Microlithography 18
1.2 Photoresist 20
1.2.1 Photoresist Material Properties 20
1.2.2 Photoresist Types 25
1.3 Coating Requirements 27
1.4 Mean Coating Thickness 27
1.5 Coating Uniformity 28
1.6 Defect Level 29
1.7 Coating Efficiency 30
1.8 Coating Time 31
1.9 A New Coating Technology 31
1.9.1 Potential Methods 32
1.9.2 Comparison of Potential Methods 35
1.10 Extrusion-Spin Coating 35
1.11 Photoresist Selection 37
1.12 Thesis Overview 37

2. Spin Coating: Application and Modeling **38**

2.1 Introduction 38
2.2 General Overview of Spin Coating 39
2.3 Spin Coating Characterized by Dispensing Method 40
2.4 Development of Dispense Stage for Extrusion-Spin Coating 41
2.5 Possible Defects from Spin Coating 42
2.6 Behavior of Fluid on a Rotating Disk 44
2.6.1 Fundamental Spin Coating Model 44
2.6.2 Photoresist Film Thinning with Evaporation 49
2.6.3 Analysis of Flow over a Spinning Disk 51

2.6.4 Laminar Regime ... 53
2.6.5 Transient Regime ... 55
2.6.6 Turbulent Regime ... 55
2.7 Requirements for Model Validity ... 55
2.8 Process Variables for Spin Coating ... 56
2.8.1 Spin Speed ... 56
2.8.2 Spin Coating Time ... 56
2.8.3 Relative Humidity ... 57
2.9 Summary ... 58

3. Extrusion-Slot Coating: A Method for Applying an Initial Coating Layer 59

3.1 Introduction ... 59
3.1.1 Description of Extrusion-Slot Coating ... 59
3.1.2 Classes of Extrusion Coating ... 61
3.2 Extrusion Head ... 62
3.3 Coating Fluid for Extrusion-Slot Coating ... 64
3.4 Modeling of Extrusion-Slot Coating ... 65
3.4.1 Analysis of Flow Extruded from Head ... 65
3.4.2 Process Variables of Extrusion-Slot Coating ... 66
3.5 Defects from Extrusion-Slot Coating ... 74
3.6 Theoretical Window of Coatability ... 77
3.7 Summary ... 79

4. Extrusion-Spin Coating 80

4.1 Description of Extrusion-Spin Coating ... 80
4.2 Establishment of Initial Coating Layer ... 81
4.3 Coating Pattern Requirements ... 84
4.3.1 Spiral Coating ... 84
4.3.2 Spiral Pattern Analysis ... 86
4.3.3 Center Modification ... 88

4.3.4 Spiral Coating Time 90
4.4 Neck-in of Extruded Flow 91
4.5 Maximum Gap Distance 95
4.6 Overlap Effect 97
4.7 Alignments 98
4.7.1 Z-Motion Alignment 99
4.7.2 Y-Motion Alignment 105
4.8 Modeling and Theoretical Analysis of Extrusion- Spin Coating 106
4.8.1 Flow over a Rotating Disk during Extrusion-Spin Coating 106
4.8.2 Evaporation of Solvent from a Spinning Disk 107
4.8.3 Physical Properties of PGMEA Solvent in Gas State 112
4.8.4 Effect of Spin Speed and Solvent Concentration on Flow above Rotating Disk 113
4.9 Summary 115

5. Experimental Apparatus of Extrusion-Spin Coater with Solvent-concentrated Environment System 117

5.1 Extrusion Head 120
5.2 Positioning System 122
5.3 Gap Measurement Sensor 124
5.4 Photoresist Dispensing System 125
5.4.1 First Generation Pump 125
5.4.2 Second Generation Pump 127
5.5 Spin Coater 129
5.6 Control System 129
5.7 Solvent Vaporizing Equipment 130
5.8 Solvent Concentration Measurement 131
5.9 Alignment and Calibration 132
5.10 Operation of Extrusion Coating Module 133
5.11 Operation of Spin Coating Module 135

6. Experimental Procedures, Results and Discussion **136**

6.1 Experimental Window of Coatability 136
6.2 Inspection of Coated Wafers 138
6.3 Experimental Procedure 138
6.4 Experimental Conditions 140
6.5 Initial Experimental Results 140
6.6 Initial Solvent-concentrated Environment 144
6.7 Extrusion-Spin Coating with Solvent-concentrated Environment 146
6.7.1 Solvent Concentration Measurements during Extrusion-Spin Coating Process 146
6.7.2 Unsteady Solvent-concentrated Environment 149
6.8 Initial Coating Layer Thickness 151
6.9 Experimental Observations 152
6.10 Prediction of Coating Uniformity 153
6.10.1 Mass Transfer Coefficient 154
6.10.2 Coating Uniformity Prediction Curve 156
6.11 Mean Coating Thickness 157
6.11.1 Coating Thickness Coefficient 160
6.12 Summary 163

7. Conclusions and Future Work **164**

7.1 Evaluation of Extrusion-Spin Coating Method 164
7.2 Evaluation of Process Variables 164
7.3 Solvent Consumption 166
7.4 Concluding Remarks 166
7.5 Future Work 167

Appendix A: Behavior of Resist Films with Evaporation **168**
Appendix B: Center Overlap **170**
Appendix C: Pump Stability **172**
Bibliography **173**

List of Figures

Figure 1-1 Microlithography.

Figure 1-2 Schematic of optical lithography techniques (a) proximity and (b) projection lithographic systems.

Figure 1-3 Historical improvement of coating efficiency.

Figure 1-4 Comparison of spin coating and extrusion-spin coating.

Figure 2-1 Spin coating process.

Figure 2-2 Different dispense methods for spin coating.

Figure 2-3 Particle-induced coating nonuniformity.

Figure 2-4 Striation of coated wafer.

Figure 2-5 A schematic diagram for film formation on a spinning disk.

Figure 2-6 Characteristic curves and surface contours for an arbitrary initial fluid distribution.

Figure 2-7 Schematic diagram of spin coating exhaust system.

Figure 2-8 Schematic diagram showing three flow regimes above spinning wafer.

Figure 2-9 Mass transfer coefficient, k, calculated in laminar regime.

Figure 3-1 Extrusion coating.

Figure 3-2 Comparison of curtain coating and extrusion-slot coating.

Figure 3-3 Extrusion-slot coating with bead vacuum.

Figure 3-4 Extrusion head (T-die).

Figure 3-5 Cross sectional view of modified extrusion head.

Figure 3-6 Cross section of the lips of an extrusion head.

Figure 3-7 Theoretical maximum coating speeds with various gap distances and flow rates.

Figure 3-8 Theoretical minimum coating thicknesses with various gap distances and coating speeds.

Figure 3-9 Various possible defects from extrusion-slot coating.

Figure 3-10 Theoretical window of coatability for i-line resist.

Figure 3-10 Theoretical window of coatability for deep UV resist.

Figure 4-1 Illustration of extrusion-slot coating on a rotating disk.
Figure 4-2 Initial coating thicknesses according to various total pump dispense volumes.
Figure 4-3 Coating efficiencies with various initial coating thicknesses.
Figure 4-4 Variations in final coating uniformities with variations of initial coating uniformities.
Figure 4-5 Spiral coating pattern formed on 200-mm wafer with extrusion head of 20 mm width.
Figure 4-6 Bead formation at the edge of the wafer.
Figure 4-7 Disk rotational speed during extrusion-slot coating.
Figure 4-8 Comparison of coating times for extrusion-slot coating.
Figure 4-9 Neck-in of extruded flow.
Figure 4-10 Experimental data of neck-ins for i-line resist.
Figure 4-11 Experimental data of neck-ins for deep UV resist.
Figure 4-12 Maximum coating gap distances in extrusion-slot coating.
Figure 4-13 Overlap of photoresist on a rotating wafer.
Figure 4-14 Cartesian coordinate on a rotating wafer.
Figure 4-15 Total misalignment of extrusion head and wafer.
Figure 4-16 Extrusion head and wafer alignment.
Figure 4-17 Extrusion head and wafer alignment with sensor.
Figure 4-18 Error in gap distance when spindle rod is misaligned.
Figure 4-19 Allowable range of angles ψ and ϕ for 40 μm gap distance.
Figure 4-20 Range of rotational speeds for the flow above the rotating wafer to remain in laminar regime.
Figure 4-21 Mass transfer rate of PGMEA solvent.
Figure 4-22 Evaporation on a rotating disk during extrusion-slot coating.
Figure 4-23 Molecular structure of PGMEA solvent.
Figure 4-24 Effect of solvent-concentrated environment on flow above the rotating disk.

Figure 5-1 Schematic diagram of extrusion-spin coater.
Figure 5-2 Top view of extrusion-spin coater.
Figure 5-3 Schematic diagram of extrusion head.
Figure 5-4 Pressure drop in extrusion head with various flow rates.
Figure 5-5 Required pressure drop to maintain a stable bead.
Figure 5-6 Picture of X-Z motion table.
Figure 5-7 Gap variation measurement.
Figure 5-8 First generation pump calibration.
Figure 5-9 Second generation pump calibration.
Figure 5-10 Schematic diagram of installed atomizer.
Figure 5-11 Atomizer calibration.
Figure 5-12 Extrusion coating operation

Figure 6-1 The window of coatability for extrusion-slot coating.
Figure 6-2 Uniformity data for an i-line resist.
Figure 6-3 Uniformity data for a deep UV resist.
Figure 6-4 Coating thickness profile from initial coating results.
Figure 6-5 Coating uniformity improvement with steady-state pump dispense.
Figure 6-6 Solvent concentration measurement at center of wafer.
Figure 6-7 Solvent concentration measurement at periphery of wafer.
Figure 6-8 Comparison of coating uniformities.
Figure 6-9 Coating thickness profile with spin coating speed of 2500 RPM in 100% solvent-concentrated environment.
Figure 6-10 Coating thickness profile with spin coating speed of 1500 RPM in 100% solvent-concentrated environment.
Figure 6-11 Calculated mass transfer coefficient k in various radial positions.
Figure 6-12 Coating uniformity results with different spin coating speeds.
Figure 6-13 Mean coating thickness results with 30 seconds of spin coating time and different high spin speeds.
Figure 6-14 Mean coating thickness results with 40 seconds of spin coating time and different high spin speeds.

Figure 6-15 Mean coating thickness results with 50 seconds of spin coating time and different high spin speeds.

Figure 6-16 Values of thickness coefficient *K* with different spin speeds and spin coating times.

Figure B-1 Center problem occurs when proper amount of suckback at the center is missing.

Figure B-2 Coating thickness profile with excessive dispense at center.

Figure C-1 Coating uniformity improvement with steady-state pump dispense.

List of Tables

Table 1.1 Typical photoresists and their properties.

Table 1.2 Various types of photoresist and their cost comparison.

Table 1.3 Photoresist applying techniques.

Table 3.1 Properties of experimental liquids used by Tallmadge et al.

Table 4.1 Comparison of density and viscosity of PGMEA solvent vapor with other gases.

Table 5.1 Specifications of Cybor pump.

Table 5.2 Measurement specifications of BMI sensor.

Nomenclature

B	Coating factor
B_s	Mass transfer driving force
c	Solid content percentage
C	Coefficient
C_s	Solvent concentration degree in environment
D	Diffusion coefficient
e	Solvent evaporation rate
G	Gap distance between extrusion head slot and substrate
h	Coating thickness
j	Diffusive mass flux
k	Mass transfer coefficient
K	Coating thickness prediction coefficient
L	Extrusion head lip width
M	Molecular weight
P	Pressure
q	Flow rate per unit length of circumference
Q	Photoresist flow rate
r	Radial distance from the center of a disk (wafer)
R	Wafer radius
s	Extrusion head slot width
t	Time

T	Temperature
V	Coating speed
w	Extrusion head slot width
w'	Necked-in flow width
Δw	Amount of overlap
w_s	Distance between extrusion head and gap measurement sensor

Greek

α	Misaligned angle: extrusion head lips not parallel to substrate
β	Dynamic contact angle between photoresist and moving substrate
ε	Coating efficiency
μ	Viscosity
ρ	Density
σ	Standard deviation, surface tension
ν	Kinematic viscosity
ϕ	Misaligned angle: between spinner axis and substrate axis
η	Non-dimensional viscosity
φ	Misaligned angle: extrusion head motion not perpendicular to spinner rotation
θ	Angle of wafer rotation
τ	Time constant
Ω	Rotating speed
∇	Volume

Superscripts and Subscripts

0	Initial
c	Critical
f	Final
l	Liquid
r	Radial direction
s	Solid
dry	Dry coating
max	Maximum
min	Minimum
$spiral$	Spiral coating
$solv$	Solvent
sub	Substrate
wet	Wet coating

Dimensionless Numbers

Ca	Capillary number
Ca^*	Critical Capillary number
DR	Drawdown ratio
Re	Reynolds number
Nu	Nusselt number
Pr	Prandtl number
Sc	Schimidt number
Sh	Sherwood number

Chapter 1

Introduction

Microelectronic devices have driven the rapid advancement of technology over the past few decades. The fabrication of smaller, faster, and cheaper microelectronic devices is the most important issue among device manufacturers. Fabrication consists of thousands of different, sequential processes. This thesis focuses on improving one of those processes, photoresist coating in microlithography.

1.1 Microlithography

Microlithography is a process used to construct three-dimensional microelectronic devices using a sequence of planar processes [Middleman and Hochberg, 1993]. Each planar process adds one layer of the microelectronic circuit geometry. Twenty or more layers complete one complex circuit geometry. Precisely controlled quantities of impurities are introduced into tiny regions of the silicon substrate of each layer. These regions are subsequently interconnected to create components and circuits. Lithographic processes create the patterns that define such regions. Figure 1-1 illustrates the basic steps of the microlithographic processes [Moreau, 1988]. The photoresist (also called resist) is applied as a thin film to the substrate (e.g., SiO_2) and then irradiated through a mask. The mask contains clear and opaque features that define the pattern to be created in the photoresist layer. The areas in the photoresist exposed to the light are made either soluble or insoluble in a specific solvent known as a developer. When the irradiated (exposed) regions are soluble, a positive image of the mask is produced in the resist. Such material is therefore termed a positive resist. If the nonirradiated regions are dissolved by the developer, a negative image results. Hence that resist is termed a negative resist. Following the

development process, etching removes the regions of silicon substrate no longer covered by resist, thereby replicating the mask pattern in that oxide layer [Wolf and Tauber, 1986]. The photoresist is then stripped from the substrate in preparation for the next layer.

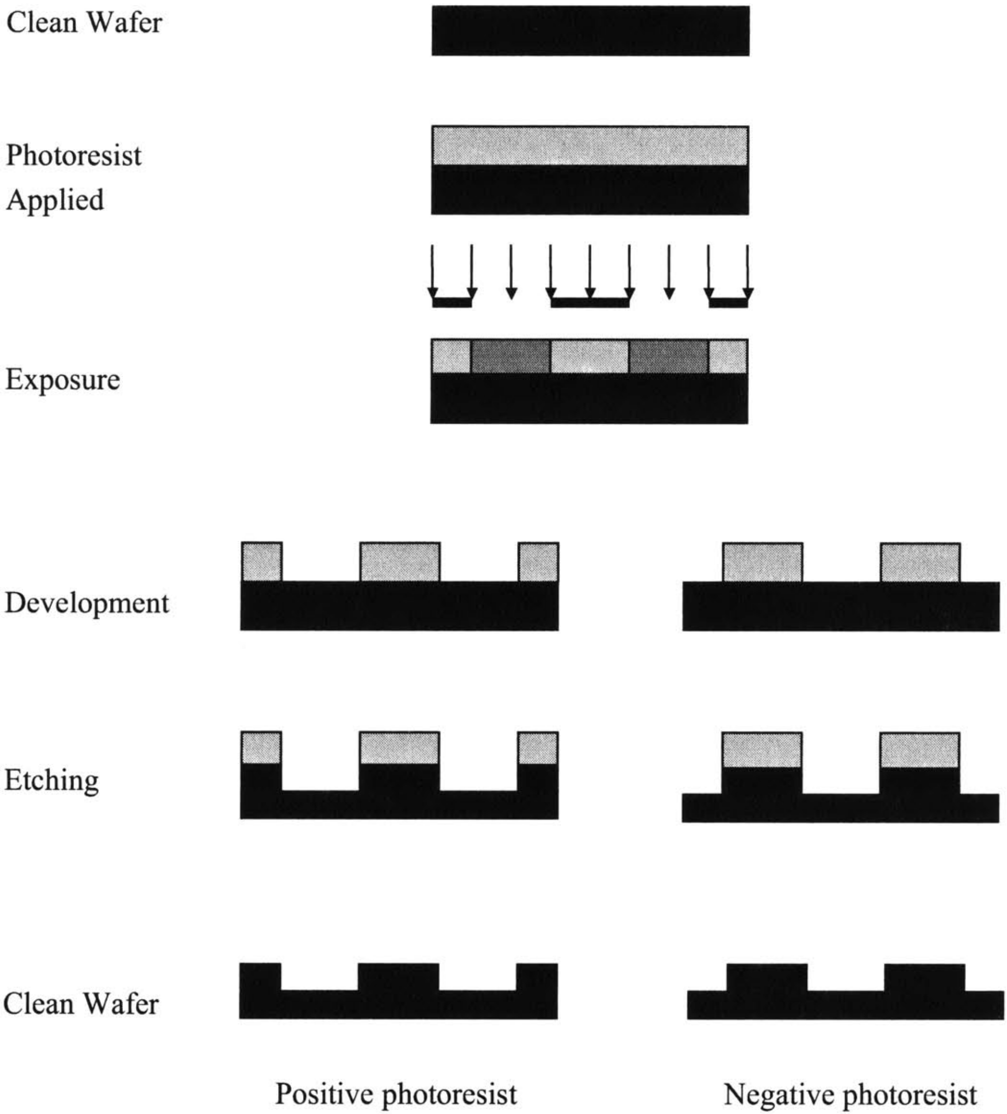

Figure 1-1: Microlithography.

1.2 Photoresist

Photoresist is used to coat silicon wafers due to its distinctive features. First, photoresist responds to exposing radiation in such a way that the mask image is replicated in the resist. Second, the remaining areas of resist protect the underlying substrate during the subsequent development process.

1.2.1 Photoresist Material Properties

The material properties of photoresist can be grouped into two categories:

- Mechanical/chemical properties, including density, viscosity, solid content, surface tension, etch resistance, thermal stability, and adhesion.
- Optical properties, including resolution and sensitivity.

Photoresist Composition

Conventional optical photoresist is composed of three types of materials:

- Polymer base (also called the resin) which establishes the mechanical properties of the coated film (adhesion and etch resistance).
- Photosensitizer (also called the inhibitor) which reacts to a particular wavelength, making the photoresist sensitive or resistant to a developer solution, depending on the resist used (positive or negative, respectively).
- Solvent which keeps the resist in a liquid state. The amount of solvent affects density, viscosity, and surface tension of the photoresist. It evaporates almost entirely after the coating process.

The proportion of the materials is approximately 15~30% polymer base, 1~5% photosensitizer, and 65~85% solvent [Photoresist, 1993]. Table 1.1 shows some typical photoresist properties.

Table 1.1: Typical photoresists and their properties

Photoresist Name	Density (kg/m^3)	Viscosity (mPa-sec)	Solid Contents	Surface Tension (N/km)
Shipley SPR2	1060	19 ~ 46	0.22 ~ 0.29	
Shipley SPR500-A	1050	0.53 ~ 5.1	0.16 ~ 0.32	
Shipley 510A	1060	26.5	0.23	22
AZ1512	1040	19	0.26	32
AZ1518	1060	36	0.30	32
AZ DX 1200P	1000	11	0.20	30
AZ 5602	1000	9.0	0.18	30
PGMEA Solvent	996	8.0	NA	40
Water	1000	1.0	NA	74

Density

The density of photoresist can be calculated from:

$$\rho = \rho_1(1-c) + \rho_s c \tag{1.1}$$

where ρ_1 is the solvent density, ρ_s is the polymer base density, and c is the solids content. Photoresist density is closely related to viscosity. The amount of solvent contained in the photoresist determines both properties. They easily change in the presence of evaporation.

Viscosity

The solids content and temperature determines the viscosity of a photoresist. Photoresist viscosity has been modeled in several different ways. Meyerhofer [1978] assumed the

photoresist to be a Newtonian fluid to model the viscosity as a function of concentration of the solid contents. Sukanek [1985] used a non-dimensional form to analyze the viscosity:

$$\eta = \frac{\nu}{\nu_0} = \frac{\nu_l}{\nu_0} + \left(1 - \frac{\nu_l}{\nu_0}\right)\left(\frac{c}{c_0}\right)^n \qquad (1.2)$$

where η is non-dimensional viscosity, ν is the viscosity of photoresist, ν_0 is the initial viscosity, ν_l is the solvent viscosity, c is the solids content, c_0 is the initial solids content, and n is a constant. Viscosities of non-Newtonian fluids have also been studied [Flack et al., 1984]. They are especially useful for explaining the behavior of flow on a rotating disk when the proportion of solvent in photoresist is smaller than 10%. However, today's photoresist contains more than 70% solvent. Jenekhe [1986] compared the theoretical prediction of coating thickness with experimental data, assuming Newtonian photoresist viscosity. He proved that the assumption of Newtonian photoresist viscosity is valid for spin coating. Lawrence [1988] asserted that the Non-Newtonian behavior of photoresist flow does not explain the actual behavior of spreading flow. This thesis assumes that the viscosity of photoresist is Newtonian.

Solids Content

Solids content, c, specifies the fraction of the resist that will remain as a solid after the complete evaporation of the solvent. Solids content is expressed as the fraction of the original liquid mass left behind as a dried mass. The typical solids content ranges from 0.15 to 0.35. ASTM Std. F66 84 [American Society, 1984] gives the procedure for measuring solids content. The solids content is important because it affects coating thickness and resist flow properties. Photoresists may experience a change in solids content over time. In positive resists, the sensitizer can decompose with time, causing formation of precipitates, which result in a net solids content change when filtered from the resist.

Solids content also changes by evaporation. In the typical resist coating process, the solvent contained in the resist continues to evaporate until a desired coating thickness is obtained. The amount of evaporation can either be calculated or obtained experimentally at

a specific time. The solids content can be calculated when the amount of evaporation is known. Consequently, density and viscosity at the moment can be obtained by using Equations 1.1 and 1.2.

Surface Tension

The surface tension of photoresist (σ) is very difficult to model during solvent evaporation. Photoresists consist mainly of solvent and thus have low surface tensions, as indicated in Table 1.1. Surface tension is an important variable in determining a stable coating flow and thickness during extrusion coating [Mues et al., 1989]. However, its effect on coating thickness and uniformity during spin coating is relatively small, as compared to other process variables such as density and viscosity of photoresist [Adamson, 1982; Wang and Yen, 1995].

Etch Resistance and Thermal Stability

Etch resistance specifies the ability of a resist to endure the etching procedure. Resist materials typically exhibit excellent resistance to wet etchants. Conventional positive resists of the novolac resin family possess a reasonable resistance to a variety of dry-etching conditions. Some dry-etch processes are conducted at higher temperatures than wet-etch processes. The resist in such applications must show thermal stability at process temperatures of 200°C or higher. Requests from industry have led to the development and commercial availability of products designed to be used at such elevated temperatures [Singer, 1985].

Adhesion

The resist must adhere to the substrate throughout the resist coating, development, and etch processes. Poor adhesion causes severe undercutting, loss of resolution, and possibly the complete pattern loss. Several techniques increase the adhesion between resist and substrate:

- Dehydration bakes prior to coating.
- Use of adhesion promoters such as hexamethyldisilazane (HMDS) and vapor priming systems.
- Elevated temperature post-bake cycles.

Resolution and Sensitivity

Resolution and sensitivity are the utilitarian metrics for resist performance. Resolution refers to the smallest feature that can be reproduced in a given resist. The term linewidth describes the resolution of the lithographic process. Linewidth is the horizontal distance between the resist material and air boundaries at a specified height above the resist-substrate interface in a given cross-section of the line.

The resolution of a lithographic process can be limited by many aspects of the process [Bargon, 1984; Bowden, 1984; Willson, 1983] including:

- Hardware (e.g. diffraction of light, lens aberrations, and mechanical stability of the system).
- Optical properties of the resist material.
- Process characteristics (e.g. softbake, develop, postbake, and etching steps).

If the resist volume increases during the development step (swelling) because the developer penetrates the resist material, it alters the feature size of the pattern created. Swelling is common in most negative resists. This produces a change in feature size that is unacceptably large for features smaller than 3 μm. Positive resists do not exhibit such swelling, due to a different dissolution mechanism during development.

Thinning the photoresist improves resolution. Conversely, because positive resist has higher contrast and exhibits negligible swelling as compared to negative resists, it can be used in thicker layers than negative resist and still provide equal resolution. If equal resolution can be obtained, a thicker resist is more advantageous because it provides better step coverage, more defect protection, and greater dry-etch resistance than a thinner resist.

Sensitivity refers to the amount of light energy necessary to create the chemical change of the photosensitizer. For photo-chemical reactions, the response is expressed quantitatively in terms of the photo-efficiency, or quantum yield, Φ, defined as the number of photo-induced events divided by the number of photons absorbed. A positive resist that operates by the photo-scission of sensitizer molecules must possess a high Φ to exhibit high sensitivity. The more sensitive a photoresist, the faster the process will be, because for a given exposure intensity, a shorter exposure time is required [Campbell, 1996].

1.2.2 Photoresist Types

Photoresist types are largely determined by two standards: resistivity to UV lights and sensitivity corresponding to the wavelength of UV lights.

Positive and Negative Resists

Positive resists are characterized by the photochemical transformation of the photosensitizer from a dissolution inhibitor to a dissolution enhancer when developer solution is applied. Negative resists react in exactly the opposite way.

Positive resists have higher resolution than negative resists. They are used in most applications in which the critical dimensions are less than about 3 μm [Willson, 1983]. Positive resists also exhibit improved etch resistance and better thermal stability than negative resists. However, negative resists cost less and have higher sensitivity, resulting in higher production rates than positive resists. Negative resists are still widely used for many lower resolution lithographic processes.

g-line, i-line, Mid-UV and Deep-UV Resists

Photoresist type is also defined by sensitivity to the various wavelength of UV light. Resolution can be increased significantly with a shorter and more energetic wavelength. This categorization is closely related to optics in microlithography. Techniques developed in the 1960s for the production of lithographic printing plates were utilized to make microcircuit patterns for semiconductor devices. These early techniques of contact or

proximity microlithography were refined to allow circuit resolution on the order of 3 to 5 μm. Problems encountered with proximity lithography, such as mask and wafer damage, alignment difficulty, and field size, limited its application for most photolithographic needs. The projection techniques of the mid-1970s minimized some of the problems with proximity lithography and led to the development of the current tools that allow resolution below 0.25 μm. Figure 1-2 diagrams proximity and projection techniques for microlithography. Figure 1-2(a) is a schematic of a proximity setup in which a mask is illuminated and held in close contact with a resist-coated substrate. The illumination source outputs radiation in the blue-ultraviolet portion of the electromagnetic spectrum. The mercury-rare gas discharge lamp produces radiation in the 350~450 nm range. The first wavelength used for positive resists was g-line (436 nm), which could produce a resolution of ~1 μm. The performance of the g-line stepper was improved to produce i-line (365 nm) lithography.

The ultraviolet regions from 300 to 350 nm and 150 to 300 nm are referred to as mid-UV and deep UV, respectively. A class of lasers well suited for microlithography is the excimer lasers. Excimer lasers using krypton fluoride (KrF) and argon fluoride (ArF) gas mixture produce radiations at 248 and 193 nm, respectively. The KrF excimer-based lithography system is the primary exposure tool for printing sub-0.2 μm features in IC manufacturing [Sturtevant et al., 1999; Vandenberghe et al., 1999]. The ArF excimer process is used for sub-0.15 μm features [Goethals et al., 1999; Okoroanyanwu et al., 2000]. Figure 1-2(b), a setup for a projection imaging system, shows details of these systems. Like a proximity system, a projection tool includes a source, a condenser lens, and a mask but utilizes an objective lens to project images toward a substrate. The condenser lens focuses an image of the source into the entrance pupil of the objective lens to provide maximum uniformity at the mask plane.

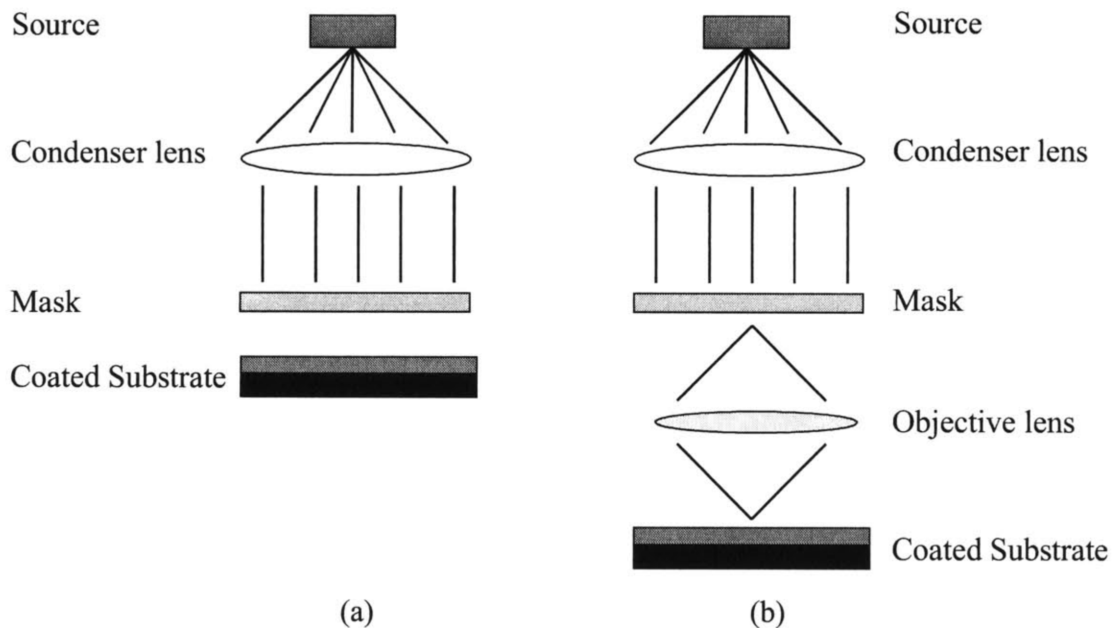

Figure 1-2: Schematic of optical lithography techniques (a) proximity and (b) projection lithographic systems.

1.3 Coating Requirements

A defect-free, uniform coating of photoresist film is critical to produce accurate and consistent circuit geometry. An adequate photoresist coating requires a consistent mean coating thickness, a thickness uniformity, and a low defect level. In addition, the coating process should also provide high efficiency and a short coating time. Sections 1.4 through 1.8 discuss coating requirements in detail.

1.4 Mean Coating Thickness

The mean coating thickness of an after-spin coating depends upon the spinning parameters. Film thickness can be measured in many ways. Contacting types of thickness measuring instruments are surface profilometers, capable of resolving 200 Å steps. Noncontact types

of thickness instruments use the optical techniques of ellipsometry or interferometry. Automatic interferometer-based instruments are widely used for resist thickness measurement. They are easy to use, accurate, and quick [Willson, 1983].

Required mean coating thickness is related to resolution. A thinner mean coating thickness can produce a higher resolution. Mean coating thickness must be consistent from wafer to wafer to produce consistent resolution. Although there is no specific relationship between mean coating thickness and resolution, the range of required mean coating thickness to produce certain resolution can be approximated. Coating thicknesses of 0.5 to 2 μm are used to obtain resolutions of 0.5 to 2.5 μm [Chen et al., 2000; Moreau, 1988].

1.5 Coating Uniformity

Coating uniformity across a wafer is defined as the standard deviation, σ, from the mean coating thickness. To obtain the standard deviation, certain locations are selected on a wafer and the coating thickness at each location is measured and collected. Typically 49 locations are selected for measurements. Increasing the number of measurement locations will yield more precise coating thickness and uniformity information. The mean coating thickness is obtained and the standard deviation calculated from the collected data. Typically, 1σ is represents the coating uniformity. When coating uniformity needs to be controlled tightly over the entire wafer, 3σ is used. Throughout this thesis, the term "coating uniformity" is understood as one standard deviation (1σ).

Producing a good coating uniformity is important in maintaining a constant exposure level across the surface of the wafer. Nonuniformities cause position overlay errors when optical steppers attempt to sense alignment marks beneath the photoresist film [Moreau, 1988]. As implanted patterns require increasingly more complex geometry in lithography, uniformity has to be improved correspondingly. In 1986, the required uniformity was 100 Å [Wolf, 1986]; today, it is 5 Å.

1.6 Defect Level

Defects in photoresist coating lead to failure of microelectronic devices. A number of factors can cause defects. Some steps to minimize defects in the microlithography process include the following [Elliott, 1986]:

- The resist film is sticky and easily entraps airborne particles until soft-baked. Spinning should be conducted in a Class-100 or better environment.
- The resist itself should be clean and free of all particles. Proper filtration is recommended.
- The resist solution should be free of all entrapped air. Air bubbles can cause defects in the resist image. Air and gases entrapped in resist should be dissolved prior to applications.
- Some wafers are inherently defective from the manufacturing process. Any coating of such wafers will have defects. All wafers must be inspected properly before use.
- Spun off resist can be re-deposited onto the wafer in droplet form by splashing back from the spin bowl. The spin bowl should be designed to prevent such splash back.
- The pump that controls the resist dispensing nozzle should provide a suckback after the resist volume is dispensed onto the wafer to prevent later dripping.
- Overly thin photoresist films may lead to high pinhole density and increased problems with small particles in photoresist. Proper ranges of coating thicknesses must be determined for the amount of photoresist used.

Defect level is closely connected to quality of the relevant manufacturing process. A typical chip in 1986 had an area of 0.25 cm^2 and a defect density of 5 defects/cm^2 per layer. These defects led to a yield of only 30% of good chips [Moreau, 1988]. There are no absolute standards for determining the acceptable/unacceptable defect level. However, various standards are set by different manufacturers to serve their particular quality levels.

1.7 Coating Efficiency

Photoresist coating efficiency, ε, is the percentage of photoresist remaining at the end of the coating process in comparison to the amount of photoresist applied:

$$\varepsilon = \frac{\nabla_{dry}}{\nabla_0 (c/100)} \tag{1.3}$$

where ∇_{dry} is the volume of dry photoresist remaining on the wafer at the end of spin coating, ∇_0 is the initial volume of photoresist applied, and c is the solids content percentage in photoresist.

The amount of photoresist required to achieve 100% coating efficiency is:

$$\nabla_{\varepsilon=100\%} = \frac{\nabla_{dry}}{(c/100)} = \frac{\pi R^2 h_{dry}}{(c/100)} \tag{1.4}$$

where R is the radius of the wafer and h_{dry} is the desired final coating thickness.

The corresponding wet coating thickness (before solvent has evaporated) is:

$$h_{wet_\varepsilon=100\%} = \frac{h_{dry}}{(c/100)} \tag{1.5}$$

For a typical photoresist with 25% solids content, 0.126 ml of photoresist will coat the entire wafer with 4 μm of wet coating, resulting in 1μm final dry coating thickness. Any excessive deposition of resist is waste.

Figure 1-3 illustrates the improvement in coating efficiency in the past [Photoresist, 1993; Moreau et al., 1995; Moreau, 1988]. For the estimations of coating efficiency, 25% solids content was assumed. Our experimental coater achieved an efficiency of 25% in 2000.

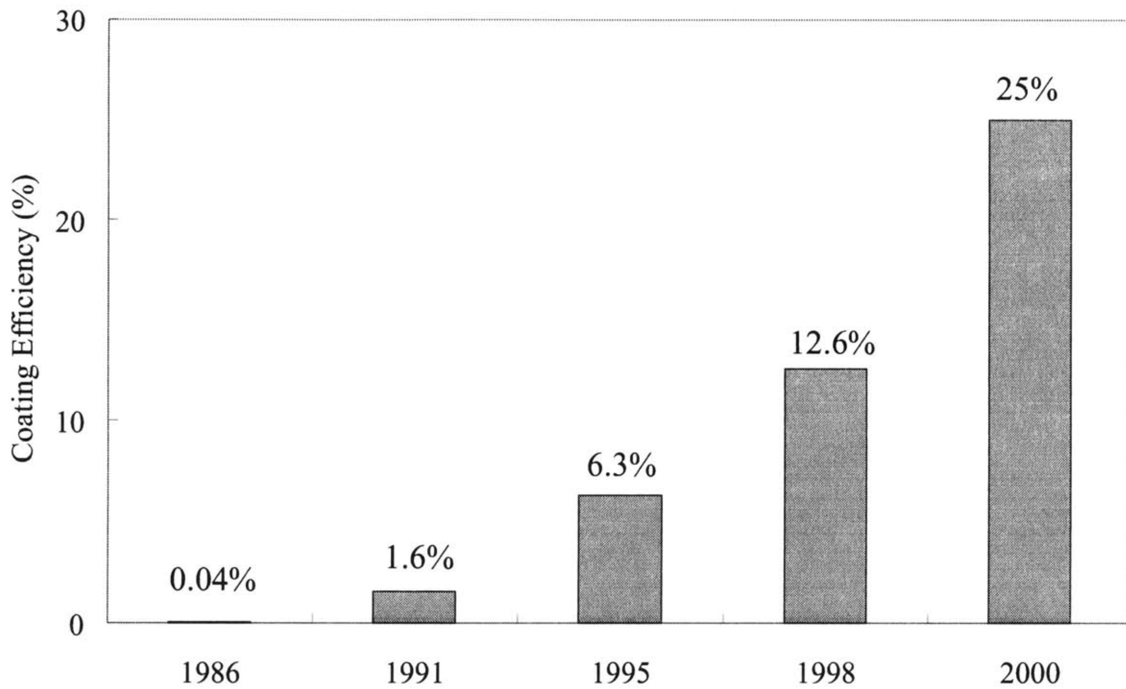

Figure 1-2: Historical improvement of coating efficiency.

1.8 Coating Time

Coating time is a very important parameter in the production rate. Typical coating time of the spin coating process includes aligning and loading of wafer to the coating position, dispense of photoresist, spin coating, and unloading of wafer. A conventional spin coating cycle takes 1~2 minutes.

1.9 A New Coating Technology

Spin coating is the method of coating semiconductor wafers with photoresist that meets today's required thickness and uniformity. Spin coating, however, typically wastes over 90% of the photoresist applied. About one million gallons of photoresist are consumed worldwide each year at a cost of $ 600 million. This represents 3% of the material costs of

the microlithography process [Moreau et al., 1995]. Industry needs a more efficient method for two reasons. The first is that 80% of the photoresist is composed of an environmentally hazardous material, the solvent. The other reason is the cost of photoresist. As the semiconductor industry continues to move toward smaller devices with larger capacity, the trend in photoresist is shifting from i-line resists to deep UV resists, which permit narrower linewidth on a chip. The price of this new resist is as much as 4 to 10 times greater than the previous generation resists, as shown in the first three columns of Table 1.2. Columns 4-6 indicate the approximate cost of annual photoresist consumption assuming 20 layers deposited on each wafer and 1,000 wafers produced per day. With the use of deep UV resists on 200 mm wafers, as much as ~$ 36 million per year can be saved if the amount of photoresist use can be reduced by one-fourth (from 4.0 cc/wafer to 1.0 cc/wafer). Thus, reducing the amount of photoresist waste is desirable for both environmental and economical reasons.

Table 1.2: Various types of photoresist and their cost comparison.

Material	Cost/ gallon	Cost/ cc	1.0 cc/ wafer 200 mm wafers	4.0 cc/ wafer 200 mm wafers	6.0 cc/ wafer 300 mm wafers
i-line	$ 550	$ 0.15	$ 1.35 M	$ 5.4 M	$ 81.0 M
Mid-UV	$ 1,500	$ 0.40	$ 3.6 M	$ 14.5 M	$ 21.7 M
DUV I	$ 2,000	$ 0.53	$ 4.8 M	$ 19.2 M	$ 28.9 M
DUV IV	$ 5,000	$ 1.32	$ 12.0 M	$ 48.1 M	$ 72.2 M

1.9.1 Potential Methods

Many methods could replace the current spin coating technology, including methods of deposit adopted from the paint industry [Patton, 1979]. A variety of solvent evaporative techniques can coat a target substrate with liquid resist. Table 1.3 lists the various coating methods and their useful range of thickness and uniformity [Moreau, 1988]. While all have the potential to reduce photoresist waste, they introduce other problems. The rest of

this section discusses those alternatives, as well as their advantages and disadvantages with respect to the current spin coating method.

Table 1.3: Photoresist application techniques.

Technique	Coating Thickness Range (microns)	Uniformity (%)
Spin Coating	0.1 ~ 10	± 1
Spray Coating	1 ~ 20	± 10
Roll Coating	1 ~ 20	± 5
Extrusion-Slot Coating	5 ~ 100	± 10
Chemical Vapor Deposition	0.01 ~ 2	± 5

Spray Coating

Spray coating deposits fine droplets onto a stationary wafer. It is potentially more efficient than spin coating except that the droplets have a great area of exposed surface area, which causes a high evaporation rate. The mechanisms to avoid such fast evaporation with droplets are complex [LaPorte, 1997]. The spraying nozzles must be designed to accommodate a fine, uniform spray. Droplet size ranges from 20 to 50 μm are produced to coat a target substrate [Doren et al., 1995; Wicks et al., 1994].

Because photoresist contains a polymer base, the resist solution tends to dry out. The nozzles easily clog if not controlled properly. Thus, failure to monitor all spraying nozzles frequently can lead to nonuniform and defective coatings.

Spray coating has attractive features such as fast application time, uniform coating thickness and the ability to apply uniform coatings to irregularly shaped objects. However, by itself, it is not adequate to produce a sub-1 μm coating thickness [Granger and Blunt, 1998].

Roll Coating

Roll coating is a method used in continuous manufacturing operations primarily for coating films. The general concept involves feeding the substrate between two rotating cylinders, while simultaneously metering the coating material into the nip between the cylinders. Coating liquid viscosity, web speed through the nip, metering rate, and distance between the rolls all contribute to coating thickness and uniformity [LaPorte, 1997]. Although roll coating is capable of producing uniform products while running at high speeds, the method cannot yield a sub-1 μm coating thickness [Choinski, 1991; Wicks et al., 1994].

Extrusion-Slot Coating

Extrusion-slot coating is very similar to roll coating except that the photoresist application method is more controlled and complex. An extrusion nozzle has the same width as the wafer diameter. The nozzle extrudes the photoresist while moving in one direction on the wafer. The method has the potential to meet uniformity and defects requirements. However, it cannot coat a round object. The extrusion head is typically unable to vary the slot width. When extrusion-slot coating is applied to a round silicon wafer, the resist deposited outside the edge of wafer can adhere to the backside of the wafer. This leaves a residue that leads to backside contamination problems. However, extrusion-slot coating is one of the most promising methods for replacing spin coating. Chapter 3 discusses in detail its advantages and disadvantages.

Chemical Vapor Deposition

Chemical vapor deposition (CVD) is widely used in the semiconductor industry when control of a precise growth of layers is required. The method has the advantage of precision in controlling coating thickness and uniformity. It is the only method besides spin coating that can produce a sub-1 μm coating thickness. However, its disadvantages are a long cycle time and the possible alteration of the inherent properties of the photoresist.

Growth rates of 0.05 to 0.3 μm/min are reported [Rees, 1996]. A nominal 1 μm coating thickness requires 3 to 20 minutes. Another drawback is that the polymer content in photoresist is not volatile and cannot be changed into a vapor form. Thus, conventional CVD is not applicable with the existing photoresist for the coating process.

1.9.2 Comparison of Potential Methods

Each potential method has its own advantages and disadvantages. However, in photoresist coating, three requirements must be considered:

- The new method should be able to produce a sub-1 μm coating thickness.
- Coating uniformity must be less than 5 Å.
- Cycle time should be less than one minute.

None of the potential methods were able to meet these requirements individually. Spin coating is the only method capable of meeting the above requirements. One major shortcoming of spin coating, however, is its excessive waste. If the conventional spin coating method can be modified to accommodate a more efficient use of photoresist, it will then satisfy the coating requirements and the need for a more efficient photoresist coating method.

1.10 Extrusion-Spin Coating

Section 1.9 describes the results of the search for a process to replace spin coating. Because none of the methods explored could meet all the requirements of the photoresist coating process, spin coating was examined to determine if modifications could improve its efficiency.

Figure 1-4(a) shows the typical process stages in spin coating. During the first stage, a small volume of photoresist is dispensed onto the wafer. In the second stage, the wafer is accelerated to create a centrifugal force which spreads the photoresist toward the edge of

the wafer. At the end of the second stage, a uniformly thick layer, referred to as the "initial coating layer" is achieved. When 4 ml of photoresist is dispensed onto the wafer, it takes 5~10 seconds from deposition to establishment of "initial coating layer." Approximately 85~90% of the total photoresist waste occurs during this transition. The efficiency of spin coating can be greatly improved by eliminating the waste of this point.

The extrusion-spin coating method eliminates the greatest material wastes of spin coating. This new method uses the efficient extrusion-slot coating technique to apply a thin film of fluid on a wafer before the spinning, thus eliminating the most inefficient phase of spin-coating, as shown in Figure 1-4(b).

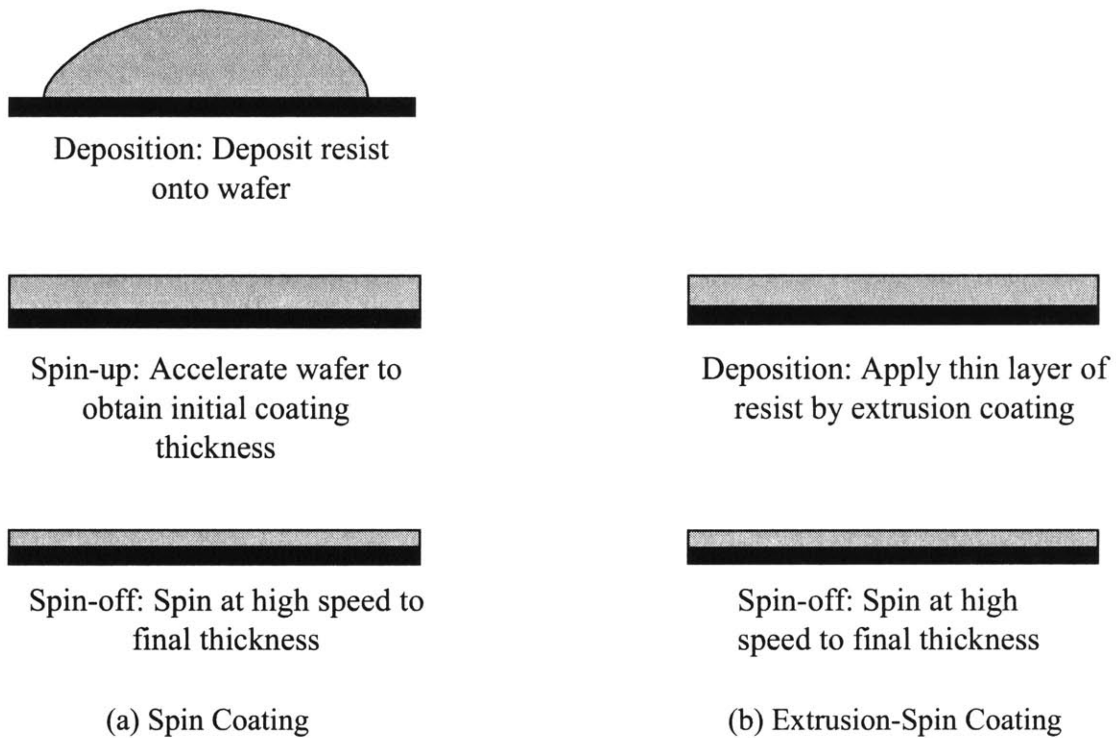

Figure 1-4: Comparison of spin coating and extrusion-spin coating.

1.11 Photoresist Selection

Among the various types of photoresists listed in Table 1.1, two particular resists were selected for experiments: i-line (AZ1512) and deep UV (AZ 1200P) resists. The theoretical analysis and experimental data of this thesis are obtained using these two resists. They were selected for the following reasons:

- Prior research indicates that among the physical properties of resists, viscosity is the most effective variable on both coating thickness and uniformity. The two resists have similar physical properties except for their viscosities. This makes the examination of the effect of viscosity on coating thickness and uniformity easy.
- The chemical composition of the two resists is identical except for the photosensitizer. This affects the outcome of the microlithography process, but does not affect the coating results in the spin coating stage. Thus, any defects in the coating are not caused by the chemical behavior of the resists. Only physical behavior needs to be studied.

1.12 Thesis Overview

The remainder of this thesis describes an extrusion-spin coating method. The newly developed process improves coating efficiency without compromising mean coating thickness or uniformity. Chapter 2 studies spin coating in detail and discusses modelings of spin coating and their limitations. Chapter 3 describes extrusion-slot coating, the process which, combined with spin coating, will produce an efficient photoresist coating. Chapter 4 describes extrusion-spin coating. Chapter 5 describes in detail the experimental apparatus for conducting extrusion-spin coating. Chapter 6 provides experimental results and their complete analysis. Finally, Chapter 7 evaluates the extrusion-spin coating method, draws conclusions, and discusses future works.

Chapter 2

Spin Coating: Application and Modeling

2.1 Introduction

Spin coating is the predominant method in the semiconductor industry of applying thin layers of photoresist to wafers. Spin coating is well adapted to the fabrication of integrated circuits, which need a uniform, adherent, and defect-free polymeric film of a desired thickness over an entire wafer. Although many factors contribute to the popularity of spin coating, consistency and simplicity are its major attractions. However, its unique way of dispensing photoresist has inherent problems. Photoresist is dispensed through a nozzle onto a wafer either in puddle form or in nonuniform streams. Such applications cause two problems. Over 90% of the photoresist applied is wasted at the end of the coating cycle. As photoresist is not recyclable, reducing the amount of photoresist is necessary for two reasons. First, photoresist contains an environmentally hazardous solvent. Second, the price of resist has increased dramatically. As the semiconductor industry develops smaller devices with larger capacities, the trend in photoresist is shifting from i-line resists to deep UV resists. The new resist costs as much as 4 to 10 times more than the older. The second problem with spin coating is that the method is non-deterministic. Coating thickness and uniformity are difficult to predict from process variables. Outputs are only obtained experimentally. As a result, experiments have to be repeated to predict thickness and uniformity. The following sections discuss the causes of these problems. Chapter 4 provides solutions.

2.2 General Overview of Spin Coating

Figure 2-1 shows a schematic diagram of a typical photoresist application. Spin coating uses centrifugal force to spread photoresist over the surface of a semiconductor wafer to produce a thin film. The process has three phases: photoresist is dispensed onto a wafer, photoresist is spread across the wafer, and the wafer is spun at a high angular speed to decrease the thickness of the photoresist to the final film thickness and uniformity. Sub-1 μm feature sizes require a mean coating thickness of less than 1 μm. Coating uniformity, which represents deviation from the mean coating thickness, should be 5 Å or better (smaller) to maintain a constant exposure level across the surface of the wafer to ensure a good transfer of the mask pattern to the coated photoresist.

During the first phase, a small volume of photoresist is dispensed onto the wafer surface. The amount of photoresist dispensed does not affect the final film thickness as long as it is sufficient [Daughton and Givens, 1982]. In practice, the minimum volume which results in consistent uniformity is used [Elliott, 1986]. In the second phase, the wafer is accelerated to create a centrifugal force which spreads the photoresist toward the edge of the wafer. During this spreading phase, the photoresist flow is unstable and nonlinear. The boundaries of the flow do not have consistent shapes. The flow rates in various directions are also unpredictable. There are no theoretical estimations or models to explain the behavior of fluid during this stage [Sukanek, 1985]. Daughton and Givens [1982] used high-speed photography to capture rotating "arms" of photoresist which flow quickly off the wafer when the wafer is accelerated rapidly. These arms of photoresist have narrow areas of uncoated wafer which are covered as the arms advance.

In the third phase, the wafer spins at the final high speed. The “initial coating layer” is established at the outset of the third phase. The photoresist film then thins to its final thickness by flowing outward off the wafer in concentric "waves" and by solvent evaporation due to the high convection over the wafer surface. As the solvent fraction in the photoresist decreases, the viscosity of the photoresist gradually increases, causing the outward flow of photoresist to almost completely stop. Subsequent thinning of the photoresist comes almost entirely from solvent evaporation [Bornside et al., 1989; Sukanek,

1985]. When the solvent is mostly evaporated (typically after 30 seconds), spinning stops and the wafer is soft baked at a high temperature to evaporate the remaining solvent.

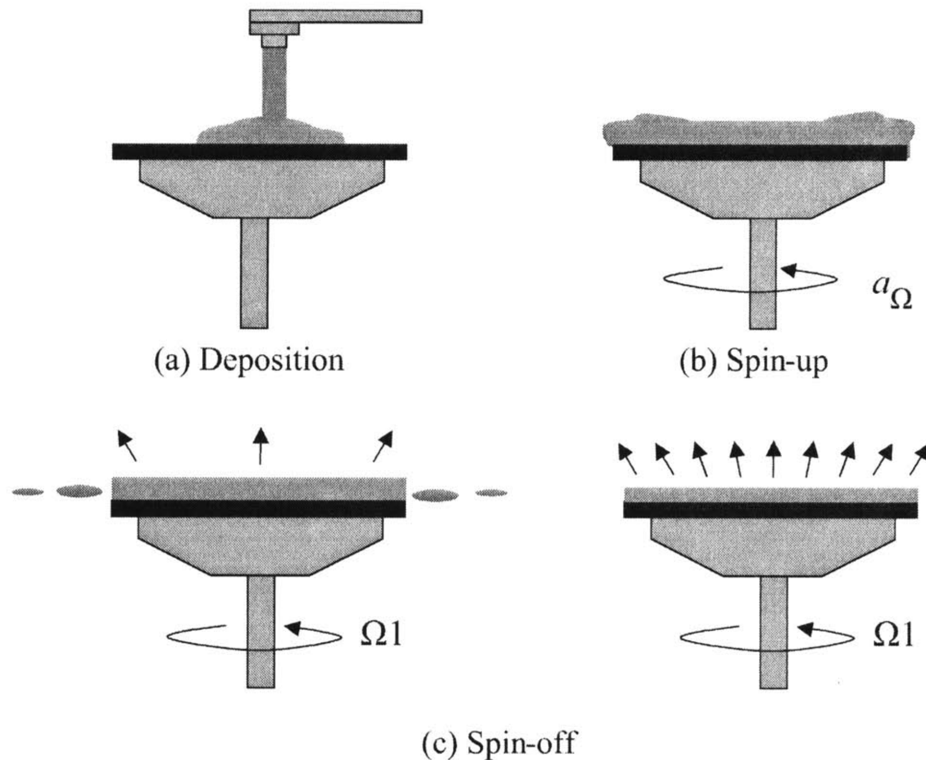

Figure 2-1: Spin coating process.

2.3 Spin Coating Characterized by Dispensing Method

Spin coating has successfully but wastefully achieved required coating thickness and uniformity. Many attempts have been made to minimize the amount of coating liquid waste by optimizing each stage. The investigation of various dispense methods was most promising because it is the easiest stage to modify. Figure 2-2 shows three different dispensing methods: center dispense; forward radial dispense; and reverse radial dispense. Of those, the reverse radial dispense method is accepted experimentally as the one providing the desired uniformity with the least amount of photoresist.

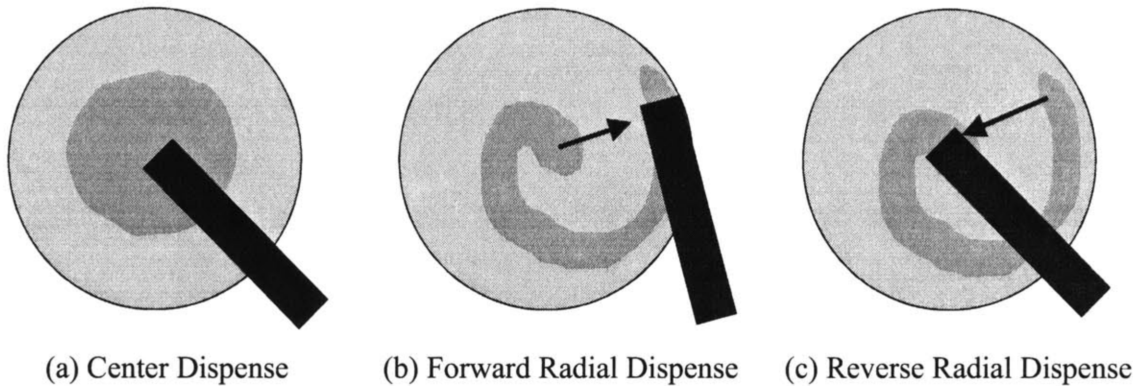

Figure 2-2: Different dispense methods for spin coating.

2.4 Development of Dispense Stage for Extrusion-Spin Coating

The purpose of testing dispense methods in spin coating is to optimize the deposited pattern of photoresist. Optimization in the deposition stage makes it easy to acquire a fully covered and uniform initial coating at the beginning of the spin-off stage. However, deposition has only been experimentally investigated because theoretical analysis of the behavior of such patterns as shown in Figure 2-2 (b) and (c) is nearly impossible.

The extrusion-slot coating method was chosen to establish a uniform initial coating layer before spinning. The new dispense method eliminates the nonlinear spreading behavior inherent in spin coating. It can minimize the waste while maintaining a uniform initial thickness. Chapter 3 discusses extrusion-slot coating. Chapter 4 describes and discusses in detail the combination of extrusion-slot coating with the spin coating method.

2.5 Possible Defects from Spin Coating

Section 1.6 discusses the general defects produced during resist coating. The discussion included the quality of coating environment, resist, wafers, and design and requirements of the experimental apparatus such as spin bowl and pump system. Then, assuming that all the conditions to eliminate general defects are met, those coating defects solely caused by the spin coating process can be addressed.

Although using a minimum amount of photoresist is desirable with respect to efficiency, three factors must be considered when determining the lower limit of photoresist coating: complete coverage, uniformity, and defect levels. Complete coverage is paramount. Uniformity and defect levels are closely interrelated. Once uniformity over the whole wafer is obtained, defects cannot be detected in the coated layer. However, various kinds of defects begin to occur with an insufficient resist volume. Correspondingly, the required coating uniformity is not attained. The most common defects in spin coating are voids, comets, and striations. Voids are spots left uncoated. The presence of voids demonstrates that the amount of applied photoresist was insufficient. Adding more resist is the only solution to the problem [Daughton and Givens, 1982]. Submicron particles encapsulated by a thicker resist layer can cause coating nonuniformities in a layer 4000 to 5000 Å thick. Figure 2-3 shows these streaks with a particle nucleus, called "comets." The region of comets is characterized by a thinner layer of coating. To eliminate comets, particles must not be allowed into the coating at any cost [Elliott, 1971].

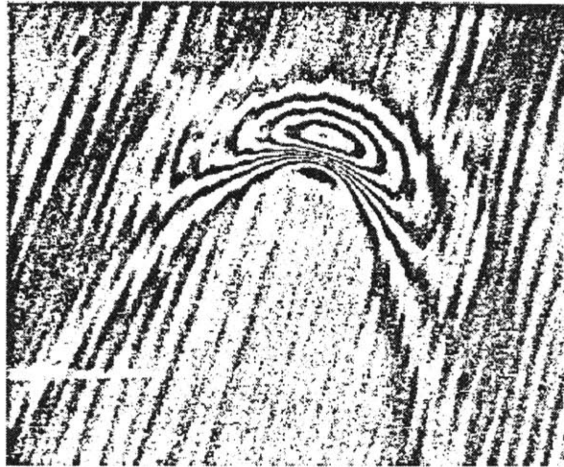

Figure 2-3: Comets, particle-induced coating nonuniformity.

Striations are strips that form toward the edge of a wafer due to the molecular interactive attraction between photoresist particles. Figure 2-4(a) shows that when the wafer is spun at high speed, some streams of photoresist attract others, which causes the photoresist to spread unevenly [Fraysse and Homsy, 1994]. By the time the initial coating layer is established, most of the wafer is covered with a uniform film. Some areas, however, have either a thinner or no initial coating layer due to unstably spreading rivulets. As a consequence, the areas with striation are more thinly coated. The triangular shape illustrated in Figure 2-4(b) represents the striations. While striations are only small undulations in the resist film, they are large enough to cause variations in line geometries after developing or etching. Increasing the amount of photoresist to cover the entire wafer can eliminate striations. Formulating a resist system with a special solvent system that prevents drying in the spin environment will also remove striations. Another chemical approach is to put a wetting agent or surfactant additive in the resist that keeps the resist film uniform [Elliott, 1986].

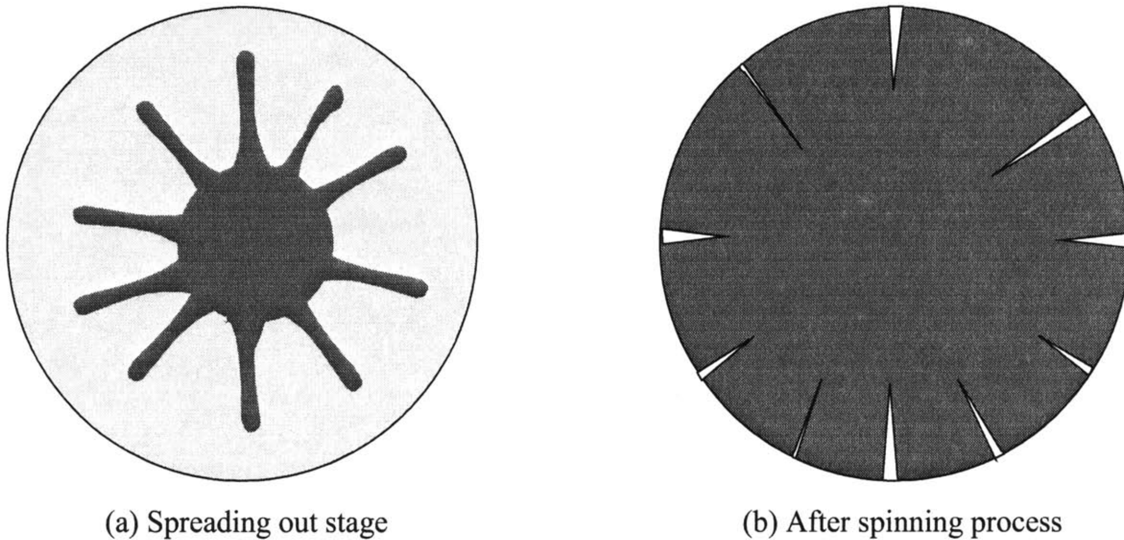

(a) Spreading out stage (b) After spinning process

Figure 2-4: Striation of coated wafer.

2.6 Behavior of Fluid on a Rotating Disk

2.6.1 Fundamental Spin Coating Model

Emslie et al. [1958] developed a model of liquid spreading over a spinning disk. The following assumptions were made for simplicity:

- The rotating disk is infinite in extent.
- The plane is horizontal so that there is no radial component of gravitation.
- The liquid is not viscoelastic, i.e., the liquid is Newtonian.
- The liquid layer is radially symmetric.
- The liquid layer is so thin that differences in gravitational potential normal to the surface of the disk are negligible in comparison to the effect of centrifugal forces in distributing the liquid.
- The liquid layer is so thin that shear resistance is appreciable only in horizontal planes.
- The viscosity and density of liquid are maintained constant.

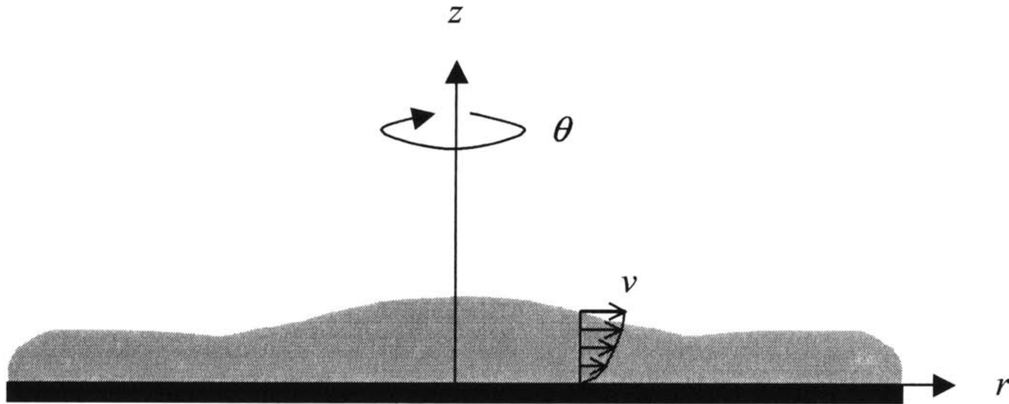

Figure 2-5: A schematic diagram for film formation on a spinning disk.

In cylindrical coordinates (Figure 2-5), the force balance between the viscous drag and centrifugal forces per unit volume will give:

$$-\mu\frac{\partial^2 v}{\partial z^2} = \rho\Omega^2 r \tag{2.1}$$

where μ is the fluid viscosity, ρ is the fluid density, Ω is the rotational speed of the wafer, and v is the linear velocity of the fluid toward the edge of the wafer.

Equation 2.1 can be integrated employing two boundary conditions: $v = 0$ @ $z = 0$ and $\partial v/\partial z = 0$ @ $z = h$, resulting in:

$$v = \frac{1}{\mu}\left(-\frac{1}{2}\rho\Omega^2 r z^2 + \rho\Omega^2 r h z\right) \tag{2.2}$$

From Equation 2.2, the flow rate per unit length of circumference, q, can be obtained:

$$q = \int_0^h v\,dz = \frac{\rho\Omega^2 r h^3}{3\mu} \tag{2.3}$$

From mass conservation, the differential equation for h is obtained:

$$r\frac{\partial h}{\partial t} = -\frac{\partial (rq)}{\partial r} \tag{2.4}$$

The behavior of the film thickness is of prime interest. Substituting the values of h from Equation 2.3 to Equation 2.4 results in:

$$\frac{\partial h}{\partial t} = -C\frac{1}{r}\frac{\partial}{\partial r}\left(r^2 h^3\right) \tag{2.5}$$

where $C = \rho\Omega^2/3\mu$.

General Solution

The general solution can be obtained by considering an equivalent set of two simultaneous first order ordinary differential equations. Equation 2.5 can be written as:

$$-2Ch^3 = \frac{\partial h}{\partial t} + 3Crh^2\frac{\partial h}{\partial r} \tag{2.6}$$

Assume that the successive surface contours defined by Equation 2.6 are given by the instantaneous positions of a set of points, which move along a family of characteristic curves. The height, h, of any one of these moving points varies according to the total derivative expression:

$$\frac{dh}{dt} = \frac{\partial h}{\partial t} + \frac{\partial h}{\partial r}\frac{dr}{dt} \tag{2.7}$$

The differential equations for the characteristic curves can now be obtained from the conditions for mutual consistency of Equations 2.6 and 2.7:

$$\frac{dh}{dt} = -2Ch^3 \tag{2.8}$$

and:

$$\frac{dr}{dt} = 3Crh^2 \tag{2.9}$$

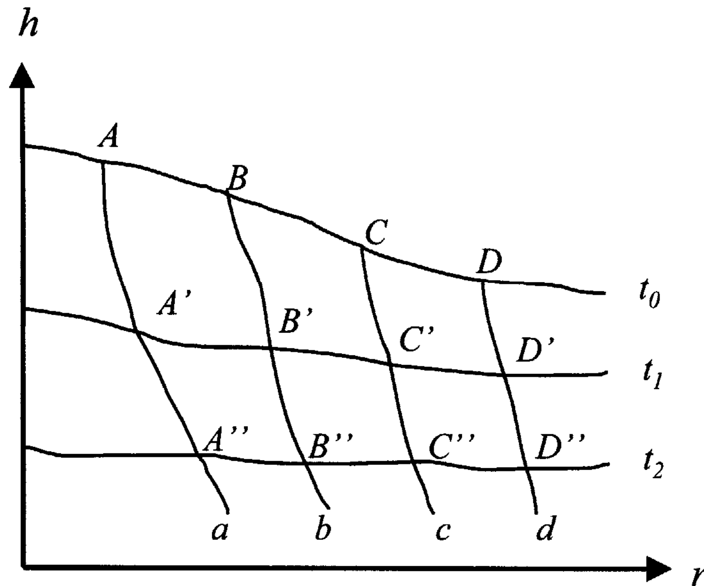

Figure 2-6: Characteristic curves and surface contours for an arbitrary initial fluid distribution.

Figure 2-6 illustrates the solution of the simultaneous Equations 2.8 and 2.9. This figure schematically represents the fate of an arbitrary initial distribution at time $t = t_0$. The set of points *A, B, C, D* travel along characteristic curves *a, b, c, d*, and are found at positions *A', B', C', D'* at time $t = t_1$, *A'', B'', C'', D''* at time $t = t_2$. The loci of points of *A', B', C', D'*, and *A'', B'', C'', D''* represent the new surface contours at times t_1 and t_2. Note that the characteristic curves *a, b, c, d* are not the flow lines of particles on the surface of the liquid, but rather a mathematical artifice for calculating the positions of successive surface contours.

Equation 2.8 integrates immediately to give:

$$h = \frac{h_0}{\left(1 + 4Ch_0^2 t\right)^{\frac{1}{2}}} \tag{2.10}$$

Substituting this expression for h into Equation 2.9 gives:

$$\frac{dr}{dt} = \frac{3Ch_0^2 r}{1 + 4Ch_0^2 t} \tag{2.11}$$

which has the integral:

$$r = r_0 \left(1 + 4Ch_0^2 t\right)^{\frac{3}{4}} \tag{2.12}$$

Equations 2.10 and 2.12 give the coordinates (r, h) after time t of a point on the surface in terms of its original coordinates (r_0, h_0). Thus, it is possible to construct the new contour after any given time of centrifugation from any initial surface contour.

Initially Uniform Distribution

Because extrusion coating deposits an initially uniform layer of photoresist, h is independent of the radial distance from the center r and dependent only upon time t. In such a case, Equation 2.5 can be simplified as Equation 2.8. Thus, Equation 2.10 represents the final coating thickness.

Equation 2.10 implies that if the initial distribution of the film is uniform everywhere, it will remain uniform throughout the whole spinning process. Equation 2.10 can be rewritten by introducing the time constant, τ:

$$h = \frac{h_0}{\left(1 + t/\tau\right)^{1/2}} \tag{2.13}$$

where $\tau = 1/4Ch_0^2$. Equation 2.13 shows that the thickness of the fluid layer decreases by a factor of $1/\sqrt{2}$ in a time τ. Thus, a thicker coating tends to thin out at a faster rate than a thinner coating.

Other investigators used the Emslie et al.'s model as the basis for improved spin coating models. Acrivos et al. [1960] investigated non-Newtonian fluids. Their model assumed that shear resistance is appreciable in the horizontal planes and. They showed that with non-Newtonian fluid viscosity, a fluid film thins more rapidly near the periphery of the disk than at the center. However, they were unable to explain the practical success of the spin coating process because in spin coating, fluids usually exhibit nearly Newtonian properties [Lawrence 1988]. Meyerhofer [1978] investigated the effects of solvent evaporation on coating thickness. Many other models improve on early developments by modeling other phenomena such as fluid and gas-phase resistance to solvent diffusion [Bornside et al., 1993], the effects of topography [Stillwagon and Larson, 1990], and the effects of relative humidity in the air flowing over the wafer [Bokelberg and Venet, 1995; Chen, 1983]. Among those models, those of developed by Meyerhofer [1978] and Bornside et al. [1987, 1989, 1993] provide good approximations for estimating the effect of evaporation and the flow over a rotating disk. The following sections discuss them in detail.

2.6.2 Photoresist Film Thinning with Evaporation

Meyerhofer extended Emslie et al.'s model by incorporating evaporation. The spin-off and evaporation stages are sequential and uncoupled in Meyerhofer's model. The concentration of the solute is uniform over the entire wafer at the start of spinning. The solvent evaporates uniformly over the entire surface area, causing the solids concentration in photoresist to increase. As h is independent of r as shown in Equation 2.9, the solids concentration is also independent of the radial position. When convective outflow ceases and the film thins solely by evaporation, the right-hand term in Equation 2.8 can be assumed to be equal with evaporation rate, e (Appendix A):

$$(1-c_0)\frac{2\rho\Omega^2}{3\mu}h_{wet}{}^3 = e \tag{2.14}$$

where h_{wet} is the wet thickness.

The expression of wet film thickness at that instant can be obtained as:

$$h_{wet} = \left[\left(\frac{3\mu}{2(1-c_0)\rho\Omega^2}\right)e\right]^{1/3} \tag{2.15}$$

At the end of the evaporation stage, the dry film thickness is obtained as:

$$h_{dry} = c_0\left[\left(\frac{3\mu}{2(1-c_0)\rho\Omega^2}\right)e\right]^{1/3} \tag{2.16}$$

where h_{dry} is the dry film thickness and c_0 is the initial concentration of solid in photoresist. The evaporation rate, e, is found using the principle of continuity of mass flux at the free surface:

$$\rho e = k\rho^s \tag{2.17}$$

where ρ is the density of the solvent, k is the mass transfer coefficient for transport from the surface of the wafer and ρ^s is the density of solvent in the air at the surface of the wafer. Equation 2.16 can be rearranged by using Raoult's law [Denbigh, 1981]:

$$e = k\frac{p^* x_0 M}{\rho RT} \tag{2.18}$$

where p^* is the vapor pressure of the pure solvent, M is the molecular weight of the solvent, R is the ideal gas constant, and T is the temperature. Substituting Equation 2.18 into Equation 2.16 gives:

$$h_{dry} = c_0 \left[\left(\frac{3\mu}{2(1-c_0)\rho^2\Omega^2} \right) \frac{p^* M}{RT} k x_0 \right]^{1/3} \tag{2.19}$$

Equation 2.19 is a steady state equation predicting that the dry thickness of the photoresist film scales with the cubic root of the mass transfer coefficient k. For example, when the mass transfer coefficient varies by 0.3% from the center of the wafer to its periphery, the dry film thickness correspondingly varies by 0.1%.

2.6.3 Analysis of Flow over a Spinning Disk

The uniformity of the photoresist coating thickness on a silicon wafer critically influences microlithographic resolution. The coating thickness depends mostly on evaporation of the solvent during the spin-off stage. The amount of evaporation determines the photoresist viscosity. The viscosity variation changes the viscous drag term defined in Equation 2.1 and thus affects the final coating thickness. Bornside and Brown [1993] modeled the effect of gas phase convection on mass transfer during the spin coating stage. They calculated the mass transfer coefficient on a rotating disk at a spin speed of 2000 RPM with the exhaust flow rate of 100 *l*/min. The model assumed a compressible, laminar, steady-state, and axisymmetric air flow in a spin coating apparatus for 6 inch diameter wafers. Flow fields were computed by a finite-element-Newton method to evaluate the radial profile of the mass transfer coefficient at the surface of the rotating wafer. The results predicted that the mass transfer coefficient is independent of the radius. Meyerhofer showed that, if solvent evaporates from the free surface of a uniformly thick film of photoresist thinning by convective outflow at a rate independent of the radial position, the coating thickness of the dry photoresist film will also be independent of the radial position. Kreith [1959] and Sparrow [1960] proposed an ideal situation for producing a uniform film by assuming an infinite spinning disk and a semi-infinite gas. The rate of mass transfer is independent of the radial position, provided that the flow of the gas induced by the rotating disk remains laminar and steady.

In reality, spin coating does not satisfy these conditions. The wafer has a finite size. It is usually located within a catch cup that constrains the gas flow as illustrated in Figure 2-7. The airflow within the catch cup is complicated due to the interactions between the flow fields induced by the spinning disk and the exhaust suction. Experiments have shown that there are three different regimes above the spinning wafer [Clarkson et al., 1980; Kobayashi et al., 1980; Kohama, 1984; Smith, 1947; Wilkinson and Malik, 1985]. These regimes are illustrated in Figure 2-8. These states are strongly related to the radial position on the wafer for a fixed rotational speed and fixed viscosity and density of the gas. The first transition occurs at $Re = 1 \times 10^5$. The second transition occurs at $Re = 3 \times 10^5$.

Different flow regimes over a rotating disk provide different diffusion rates of the solvent in interaction with its environment. Therefore, these regimes must be studied carefully to understand the behavior of solvent evaporation.

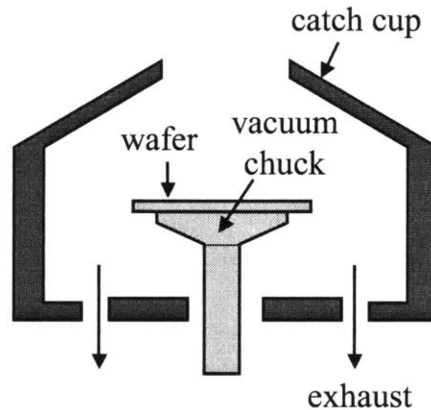

Figure 2-7: Schematic diagram of spin coating exhaust system.

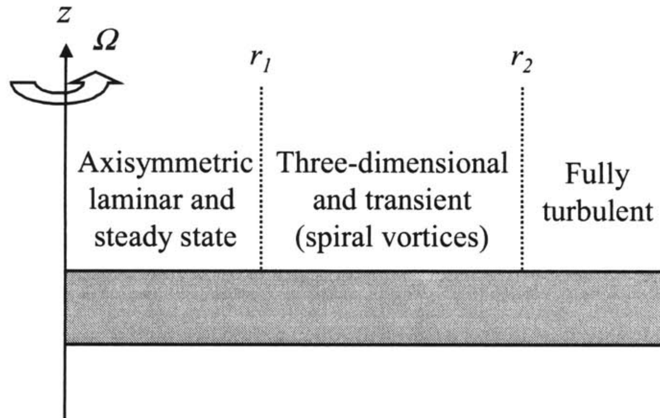

Figure 2-8: Schematic diagram showing three flow regimes above spinning wafer.

2.6.4 Laminar Regime

In the first regime ($r < r_1$), the flow is laminar, axisymmetric, and steady. The mass transfer coefficient is independent of radial position. The critical radius is found as:

$$r_1 = \sqrt{\frac{1\times10^5 \nu}{\Omega}} \tag{2.20}$$

The mass transfer coefficient in this regime is independent of radius. Von Karman [1921] predicted that the flow induced by an infinite spinning disk was responsive to a similarity solution if the flow is incompressible, laminar, axisymmetric, and in a steady state. Kreith et al. [1959] and Sparrow et al. [1960] extended Von Karman's work to compute the mass transfer coefficient in the laminar regime:

$$k = \kappa D(\Omega/\nu)^{1/2} \tag{2.21}$$

where κ is the constant that depends on the Schmidt number ($Sc = \nu/D$) and D is the binary diffusivity of the solvent in air, Ω is the rotational speed of the rotating disk, and ν is the kinematic viscosity of the surrounding gas, respectively. Kreith et al. experimentally

determined that for a Schmidt number smaller than 10, κ is given by $0.386(Sc)^{0.462}$. Equation 2.20 shows that the mass transfer coefficient does not depend on the radial position on the surface of the wafer. Combining Equation 2.21 with 2.19 shows that the dry photoresist thickness will be independent of radial position in the laminar regime, provided that the binary diffusivity remains constant in the same regime. Figure 2-9 shows the values of the mass transfer coefficient, k, varying with rotational speed Ω in the laminar flow regime. The analysis uses PGMEA solvent as an evaporating solvent and air as a surrounding gas. The kinematic viscosity of air is 1.51×10^{-5} m^2/sec and PGMEA solvent diffusivity in air is 2×10^{-5} m^2/sec [Reid et al., 1987]. In reality, this value is lower because the concentration of the solvent in the surrounding atmosphere increases as evaporation of the solvent takes place. However, this analysis is useful to estimate the order of magnitude for the mass transfer coefficient. Chapter 6 presents the actual mass transfer coefficients obtained through the experiments.

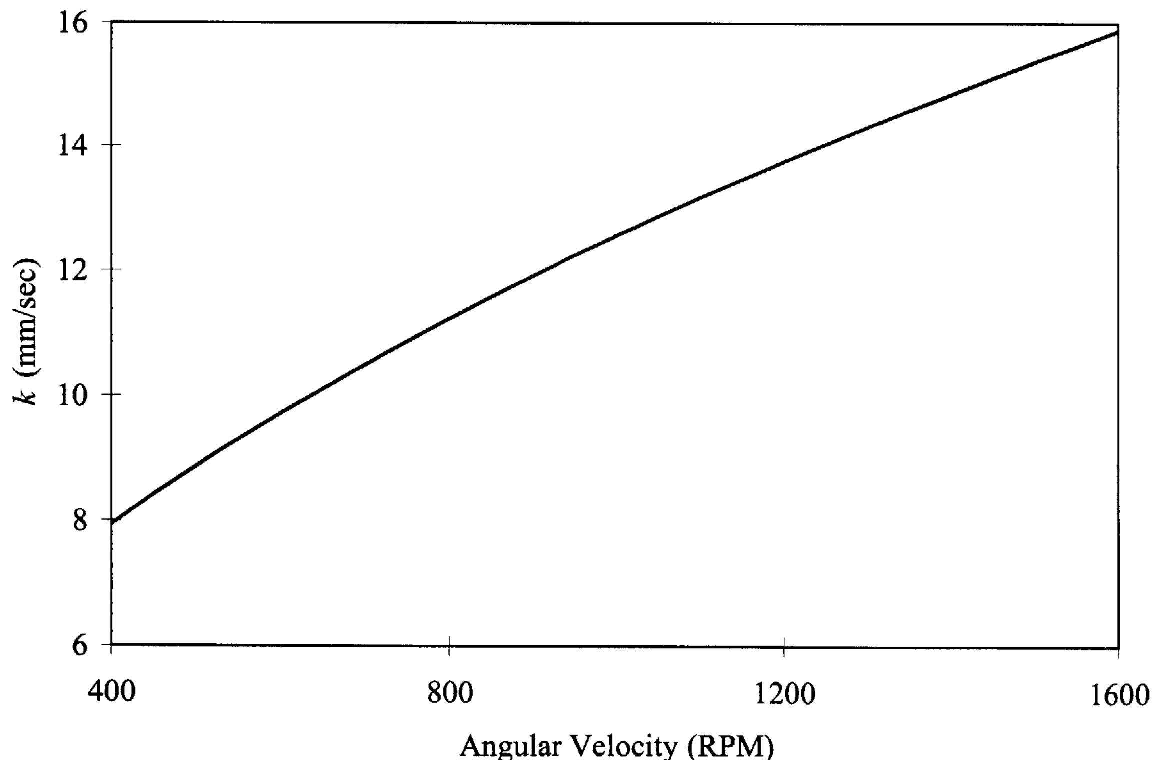

Figure 2-9: Mass transfer coefficient, k, calculated in a laminar regime.

2.6.5 Transient Regime

A transient regime exists between r_1 and r_2, where r_2 is found as:

$$r_2 = \sqrt{\frac{3\times10^5 \nu}{\Omega}} \quad (2.22)$$

The flow is three-dimensional and transient [Ellison and Cornet, 1971]. The mass transfer coefficient is undetermined and can only be experimentally deduced. It is probable that it will have an intermediate value between the mass transfer coefficients in laminar and turbulent regions [Bornside and Brown, 1993].

2.6.6 Turbulent Regime

Flow is turbulent in the third regime ($r > r_2$). The mass transfer coefficient is a nearly linear function of the radius and is greater than in the laminar regime [Ellison and Cornet, 1971]. The mass transfer coefficient increases as $r^{0.9}$. The dependence of the mass transfer coefficient on the radius and Equation 2.23 implies that dry film thickness at the periphery of the wafer will increase with the radius.

2.7 Requirements for Model Validity

All spin coating models have limitations when applied to real spin coating. All models assume that the wafer is initially entirely covered with photoresist. This assumption is not true with current dispensing methods, as shown in Figure 2-2. An initial coating layer is achieved during the spin-up stage (Figure 2-1). It is difficult to estimate actual initial conditions (initial coating thickness and uniformity). It is also difficult to predict the outcomes (final coating thickness and uniformity) without experiments when initial conditions are not known. To use spin coating models properly, providing an initial layer

of photoresist with known initial thickness is critical. The viscosity and density of the initial layer also must be maintained constant for the existing models to be valid.

2.8 Process Variables for Spin Coating

2.8.1 Spin Speed

Spin speed is the rotational speed at which a wafer is spun for a specific time. Spin speed mainly contributes to obtaining a certain film thickness. Spin speeds between 3000 and 5000 RPM produce 1 μm thickness with typical i-line resists. With deep UV resists, spin speeds between 1500 and 3000 RPM produce a sub-1 μm coating thickness. Daughton and Givens [1982] experimented to show that the thickness of photoresist is approximately proportional to $\Omega^{-1/2}$ when solvent evaporated during the coating process.

Levinson [1993] conducted a set of experiments to investigate the effect of spin speed on coating results. He used N-Methylpyrrolidone solvent, which is fairly non-volatile. Thus the coating results should be similar to the case where solvent does not evaporate. The coating thickness was proportional to Ω^{-1}, which agrees with the prediction of the model of Emslie et al. (Equation 2.10).

2.8.2 Spin Coating Time

Spin coating time affects the final coating thickness. Typically, 20 to 40 seconds of spin coating time attains a desired coating thickness. Additional time does not result in a thinner coating. The coated layer is no longer a liquid and ceases to spread once most of the solvent evaporates.

Meyerhofer's model [1978] estimates typical spin coating times. His model provides the required time for the spin-off stage. He assumed that there is no evaporation during the spin-off stage and that there is an imaginary stage at which all evaporation takes

place, called the "evaporation stage." Times for the spin-off and evaporation stages are represented in Equations 2.24 and 2.25 respectively:

$$t_{spin\ off} = \frac{3\mu_0}{4\rho\Omega^2}\left(\frac{1}{h_{spin\ off}^2} - \frac{1}{h_0^2}\right) \tag{2.24}$$

$$t_{evaporation} = \frac{V_{solvent}}{e} = h_{spin\ off}\frac{\rho_{solv}^0}{\rho e} \tag{2.25}$$

Total time, excluding the short deposition and spin-up stages, to reach the final thickness would simply be:

$$t = t_{spin\ off} + t_{evaporation} \tag{2.26}$$

Levinson [1993] investigated the effect of spin coating time on coating results. He used three different coating times (30, 60, and 90 seconds) at different spin speeds (800 ~ 3000 RPM). When spin speed and other process variables are constant, the coating thickness varies proportional to $t^{-1/2}$, which corresponds with Emslie et al.'s model.

2.8.3 Relative Humidity

Bokelberg and Venet [1995] investigated the effects of relative-humidity variation on photoresist thickness after spin coating. Relative humidity was varied from 30 to 60%. Their results indicate a strong linear correlation between relative humidity and coating thickness. As the relative humidity increased, the coating thickness decreased. The increased humidity acted as a solvent-concentrated environment to decrease the evaporation rate of solvent. The viscosity of photoresist correspondingly decreased to yield a thinner coating. Although the relationship between relative humidity and coating uniformity was not as evident as the case of relative humidity and coating thickness, coating uniformity also improved as relative humidity increased.

2.9 Summary

This chapter presented theoretical predictions and experiments done by others to explain the behavior of flow on a rotating disk. Emslie et al.'s and Bornside et al.'s equations allow the prediction of the coating thickness in the absence and presence of solvent evaporation, respectively. However, current dispense methods do not provide known initial conditions, making prediction of final coating thickness and uniformity difficult. If the initial coating layer can be established with known conditions, Bornside et al.'s model would be effective in predicting coating thickness. If the initial coating layer exists and solvent evaporation during spin coating can be eliminated, coating thickness will be predictable and controllable according to Emslie et al.'s model.

The following chapter explains extrusion-slot coating, the method selected for establishing an initial coating layer before spin coating.

Chapter 3

Extrusion-Slot Coating: A Method for Applying an Initial Coating Layer

3.1 Introduction

Extrusion-slot coating is one surface coating method widely used to produce a continuous and uniform film on a substrate. All the fluid fed to the extrusion head is used for coating, consequently the coating efficiency is near 100%. Extrusion-slot coating is an excellent candidate for providing an initial coating layer for spin coating because it can produce a continuous and uniform coating layer with high efficiency.

This chapter describes extrusion-slot coating in general terms. Its process variables will be defined and their effects on coating thickness and uniformity will be studied. In addition, a window of coatability will be established using theoretical analysis to estimate the proper range of process variables for extrusion-slot coating.

3.1.1 Description of Extrusion-Slot Coating

Extrusion-slot coating is a premetered coating system. All the material metered to the coating die coats the substrate as shown in Figure 3-1. Once the coating speed, coating width, and flow rate are known, the coating thickness can be calculated as:

$$h_{wet} = \frac{Q}{V_{sub} w} \tag{3.1}$$

where h_{wet} is the coating thickness before evaporation occurs, Q is the coating fluid flow rate, V_{sub} is the coating speed, and w is the width of the slot in the extrusion head, respectively. At the end of a complete coating cycle, all solvent in the coating liquid

evaporates to leave only the solid content. The final dry coating thickness, h_{dry}, is expressed in terms of solids content and wet coating thickness:

$$h_{dry} = ch_{wet} \tag{3.2}$$

where c is the solids content as defined in Section 1.2.1.

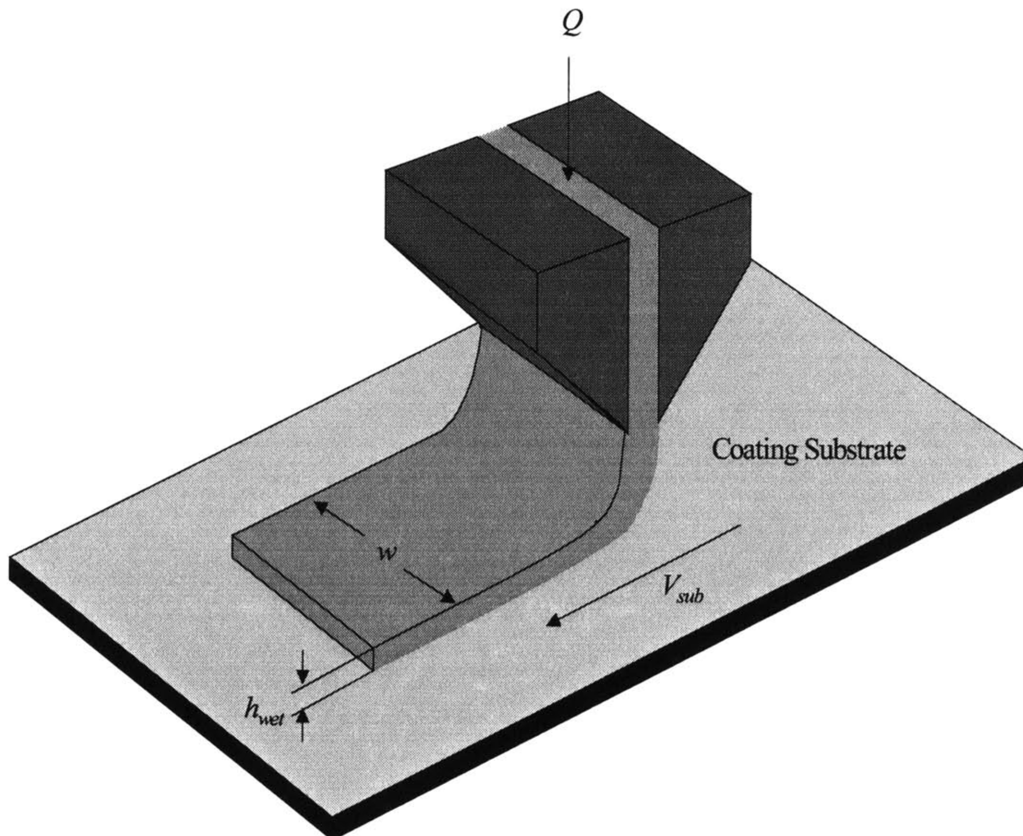

Figure 3-1: Extrusion coating.

3.1.2 Classes of Extrusion Coating

Extrusion coating comprises two major classes: curtain coating and extrusion-slot coating. The two are distinguished by gap distance between the extrusion head and coating substrate. In curtain coating, the gap distance is wide enough to allow a flow to be squeezed from an extrusion head to lie upon a substrate, as illustrated in Figure 3-2(a). The name curtain coating comes from the way the extruded flow draws down like a curtain. Extrusion-slot coating is sometimes called bead coating after its major characteristics of a bead formed on the fore coating lip, as illustrated in Figure 3-2(b). The gap distance between the extrusion die and substrate has to be small enough for this bead to be formed.

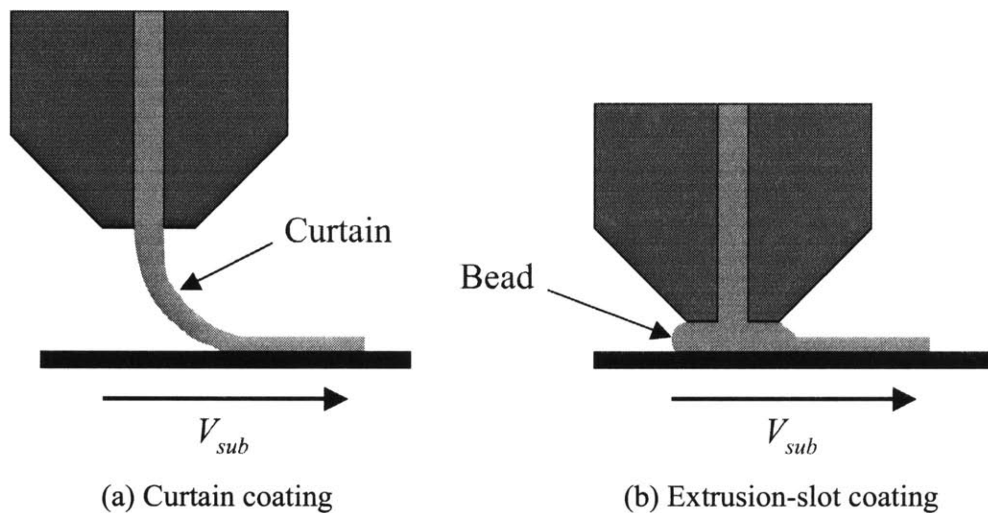

(a) Curtain coating (b) Extrusion-slot coating

Figure 3-2: Comparison of curtain coating and extrusion-slot coating.

Extrusion-slot coating is appropriate when good coating uniformity and low level of defects are required [Gutoff, 1992]. Many theoretical analyses and experiments demonstrate that to create such defect-free, smooth coatings, a well-shaped bead must be formed and maintained on the fore lip and throughout the coating process [Choinski, 1991; Mues et al., 1989; Sartor, 1990]. A vacuum can create an adequate pressure difference across the bead to maintain a well-shaped bead [Sartor, 1990]. Figure 3-3 shows the

extrusion-slot coating with a vacuum introduced at the fore coating lip. The vacuum is useful when a thinner film coating or higher coating speed is required [Beguin, 1954].

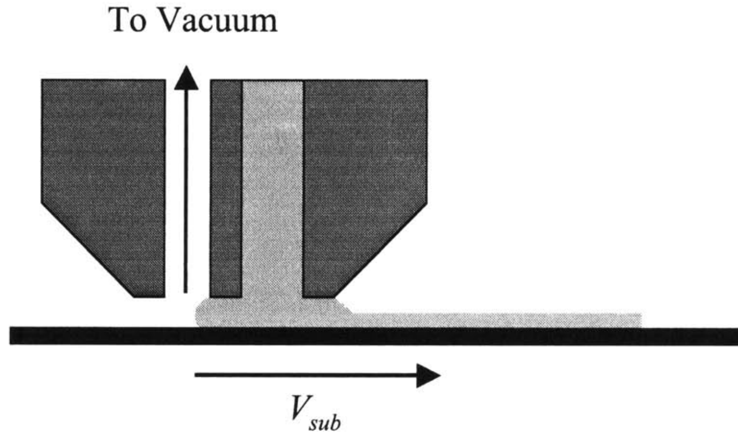

Figure 3-3: Extrusion-slot coating with bead vacuum.

3.2 Extrusion Head

Figure 3-4 illustrates a design of a typical extrusion head (also known as a T-die). Coating fluid from the reservoir enters the extrusion head through an inlet path. This path directs the coating fluid to the flow channel, which is created by a shim inserted between two flat plates. The gap of the flow channel is equal to the size of the inserted shim, *s*. The coating fluid exits the extrusion head through the gap to be deposited onto the target substrate. If the length of the gap from the channel to the slot exit is constant, the only way a uniform flow can occur across the width of the coating head is for the pressure to be constant throughout the length of the channel. However, a pressure drop is created when photoresist flows in the channel. The pressure in the channel is highest where the resist enters the channel, at the center. Because the pressure is highest there, the flow rate through the slot will be greater at the center than at each edge. This creates a nonuniform coating profile that is higher in the center and lower at the edges. Figure 3-5 illustrates one of the head designs to convert such a nonuniform profile to a uniform one. The length of the flow path along the flat, from the channel to the exit, decreases at the edges (l_{edge}) relative to the center (l_{center}), so that the pressure drop per unit length along the width of the flat is constant,

and thus the flow rate is constant. With exact correction, the pressure above the flat at any distance from the front edge will not vary across the width, so that the flow rate across the width is constant [Sartor, 1990].

The internal geometry of the extrusion head affects the pressure drop created across the internal die. Equation 3.3 indicates that for a laminar steady viscous flow, when the path is rectangular, the pressure drop variation is proportional to the flow rate, Q, the viscosity of the coating fluid, μ, and the path length, l. It is inversely proportional to the cube of the slot thickness, s [Gutoff, 1993]:

$$\Delta P = \frac{12\mu l Q}{s^3} \tag{3.3}$$

The pressure drop should remain within a reasonable range to maintain a stable flow rate for coating fluid. Chapter 5 discusses the design of the actual extrusion head for the experiments.

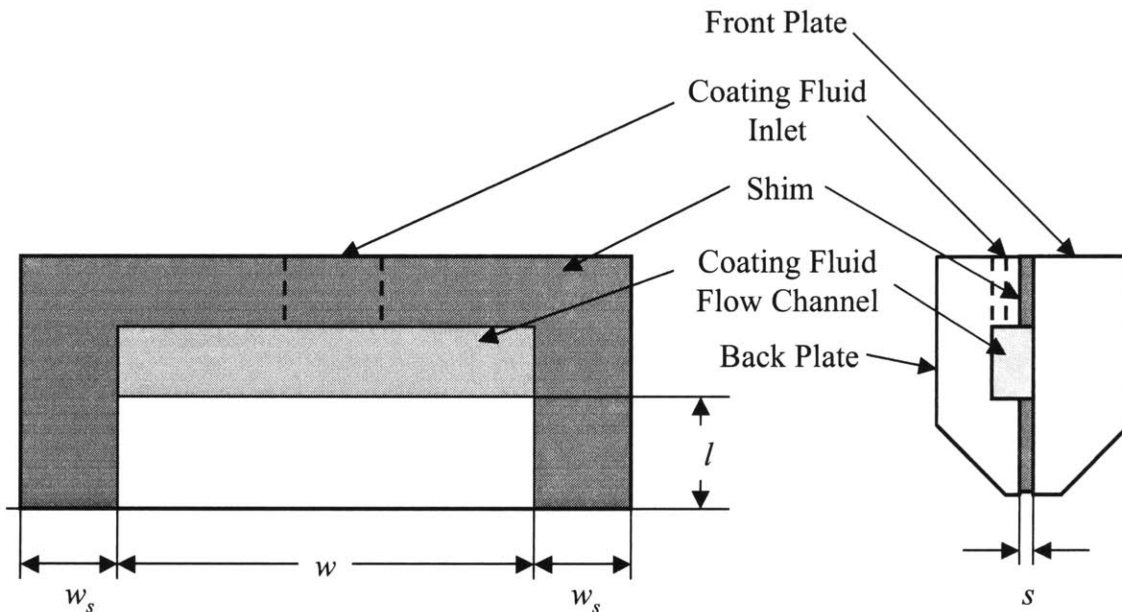

3-4: Extrusion head (T-die).

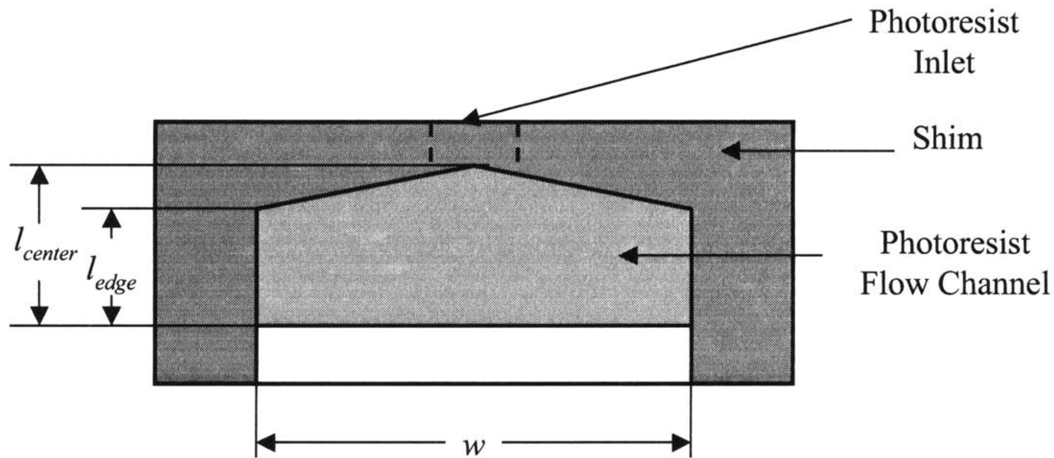

3-5: Cross sectional view of modified extrusion head.

3.3 Coating Fluid for Extrusion-Slot Coating

Extrusion-slot coating works with a variety of coating fluids and substrates. A common application of extrusion-slot coating is the coating of flat panel displays. An extrusion head that has the same slot width as the display applies thin films to the display substrate [Bagen and Newquist, 1996].

Coating liquids with wide ranges of viscosities use extrusion-slot coating: from as low as 10 mPa-sec [Lee et al., 1992] and as high as 1,000 mPa-sec [Mues et al., 1988; Lee et al., 1992]. A typical photoresist has a viscosity of 10 ~ 46 mPa-sec. Extrusion-slot coating is well suited for the photoresist application, yielding a coating uniformity of less than 2% [Bagen and Newquist, 1996].

3.4 Modeling of Extrusion-Slot Coating

3.4.1 Analysis of Flow Extruded from Head

Figure 3-6 shows how the gap between the lips and the substrate is filled with a bead of coating fluid in extrusion-slot coating. The menisci at the leading and trailing edges of the coating bead are pinned to the corners of the extrusion head lips. According to Fahrni and Zimmerman [1978], these corners must have a radius of curvature less than approximately 50 μm to maintain the pinned menisci.

Choinski [1991] analyzed the relationships between bead coatability and coating parameters. He asserted that in extrusion-slot coating, bead formation dynamics are the key to producing a defect-free and uniform coating. He enumerated factors that are closely related to the dynamics. Equation 3.4 shows the relationship of bead coatability and those parameters:

$$Bead\ Coatability \propto Bh_{wet} / \mu V_{sub} G \tag{3.4}$$

where B is the coating factor, h_{wet} is the wet thickness, μ is the fluid viscosity, V_{sub} is the coating speed, and G is the gap distance between the extrusion head and substrate, respectively. Bead coatability represents how uniform the coated area is. Higher bead coatability means more uniform coating. The relationship reveals much useful information. The coating factor, B, depends on many factors including extrusion head design and alignments between extrusion head and substrate. It is a coefficient typically obtained through experimentation. The thicker wet coatings provide a better bead coatability because more resist has been applied [Doren, Freitag, and Stoye, 1995]. Liquids with lower viscosities tend to spread out more smoothly and thus result in better coating uniformity [LaPorte, 1997]. Unpredictable fluid dynamics occur at high coating speeds, worsening bead coatability. The same applies at large gap distances. A large gap distance usually causes neck-ins of extruded flow which, again, lead to unstable fluid dynamics and bad bead coatability. However, relationships do not indicate the quantitative effect of each

variable. For example, doubling the wet thickness and coating velocity does not necessarily guarantee the same bead coatability.

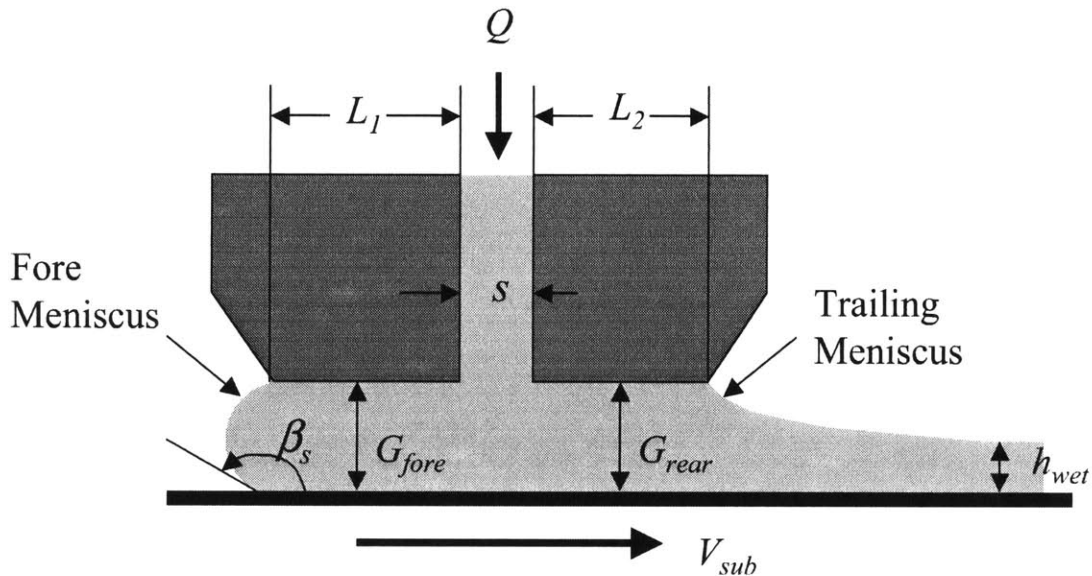

3-6: Cross-section of the lips of an extrusion head.

3.4.2 Process Variables of Extrusion-Slot Coating

Extrusion-slot coating involves several process variables. Some of them are coupled and cannot be decoupled. A strong theoretical basis and experimental results are necessary to understand their interrelations.

Capillary number

Lee et al. [1992] experimented to determine the minimum wet thickness achievable by extrusion-slot coating. There is a critical Capillary number ($Ca^* = \mu V_{sub} / \sigma$) for Newtonian fluids; below Ca^*, the minimum wet thickness is independent of the Capillary number. It is a function of the coating gap only. As $Ca > Ca^*$, the minimum wet thickness will become constant as the coating speed increases. The critical Capillary number can be determined experimentally for a specific coating liquid.

Coating Speed

Coating speed is a process variable directly related to production rate. A high coating speed increases the production rate but can cause instabilities in the coating. The range of coating speeds which permits defect-free coating must be determined for each type of resist used.

Faust [1975] conducted an experimental study of bead coating stability limits. The study determined speed limits for several Newtonian liquids with different viscosities, over a range of volume flow rates and gap sizes. Ruschak [1976] derived a predictive model for estimating a range of coating speed in a pre-metered coating device. His model agreed well with Faust's experimental data. According to his theoretical analysis, the maximum coating speed, V_{max}, is:

$$V_{max} = \left(\frac{Q(1+\cos\beta_s)}{1.338wG} \right)^{\frac{3}{5}} \left(\frac{\sigma}{v} \right)^{\frac{2}{5}} \tag{3.5}$$

where all the parameters are defined in Figures 3-1 and 3-6.

Figure 3-7 shows theoretical maximum coating speeds by Ruschak with various gap distances and flow rates. Coating gaps of 40, 60, 80, and 100 μm are used for each resist because those are the gap distances that will be used in experiments in this thesis.

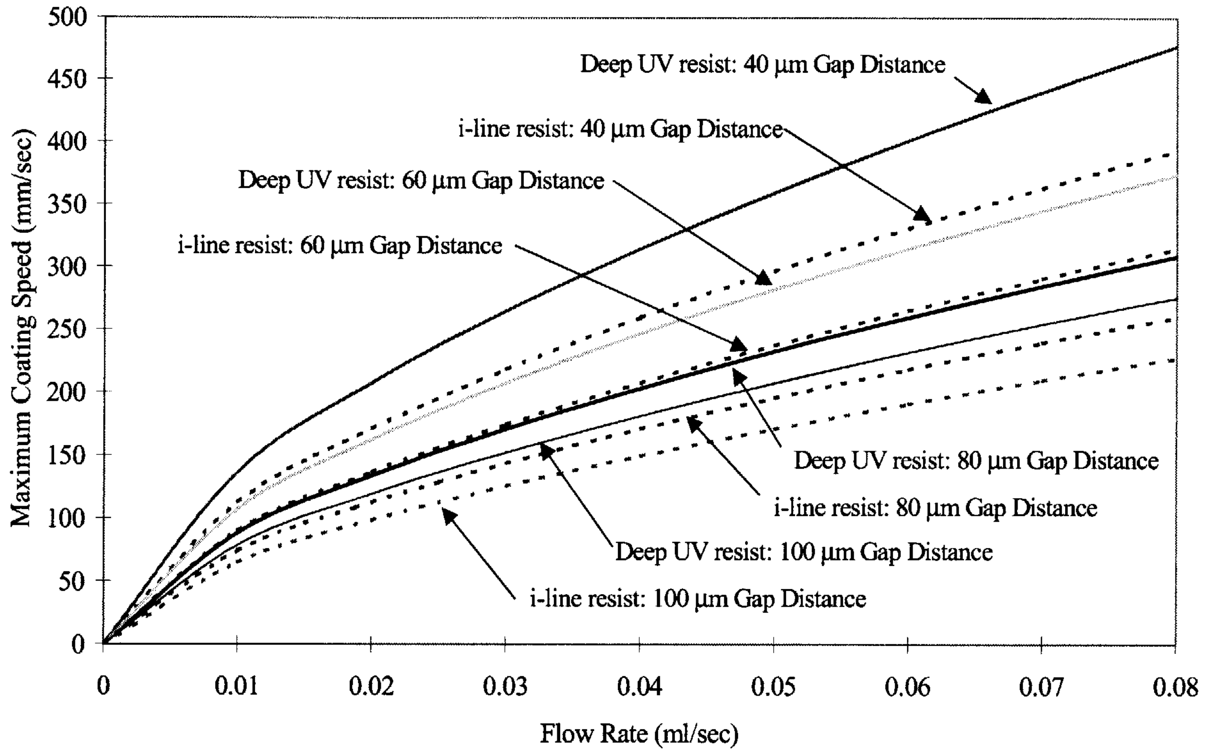

Figure 3-7: Theoretical maximum coating speeds with various gap distances and flow rates.

Tallmadge et al. [1979] compared experimental results with Ruschak's theoretical model. They acquired the operable range of the coating speed using three different liquids shown in Table 3.1. Those properties are also compared with typical properties of i-line and deep UV resists. The results with glycerin are useful because its physical properties are similar to typical photoresists. The lower limit of the coating speed is known as the "drip point" at which the bead becomes too large to be maintained between the extrusion head and the substrate and thus results in coating instability. The upper limit is known as the "split point" at which the amount of the fluid bridging the extrusion die and the substrate becomes insufficient to maintain the bead and coating uniformity.

Table 3.1: Properties of experimental liquids used by Tallmadge et al.

Coating Fluid	Density (kg/m^3)	Viscosity (mPA-sec)	Surface Tension (N/km)
Glycerin	1180	22	39.4
Paraffin Oil	865	68	34.1
Oil Mixture	902	281	33.6
i-line Resists	1040 ~ 1060	19 ~ 46	22 ~ 32
DUV Resists	998 ~ 1000	8 ~ 12	30

Their experimental data show that except for one process variable, Ruschak's theoretical analysis is a good approximation method of upper coating speed limit. The gap distance does not affect the result as predicted by the theoretical model. All the maximum coating speed data were smaller than the predicted data. The upper speed limit is found to vary with + 0.1 power of the gap size instead of Ruschak's predictive model that varies with – 0.6 power. Tallmadge et al. suggest that the effect of gap distance on the maximum coating speed should be investigated experimentally, for it can vary according to the physical properties of the coating liquid.

Another constraint for the maximum coating speed limit is air entrainment. Deryagin and Levi [1964] were the first to note that the dynamic contact angle, β_s, increases proportionally to the coating velocity. When the dynamic contact angle reaches 180°, the air film carried along by the moving substrate causes incomplete wetting, resulting in air entrainment. Joos et al. [1990] and Mues et al. [1989] predicted that air entrainment begins when the contact angle reaches 180°. Mues et al. explained that the contact angle, β_s, increases with the Capillary number. Air entrainment begins when the Capillary number reaches the value of 0.25. Thus the coating speed at which air entrainment begins can be derived as:

$$V_{air\ entrainment} = \frac{\sigma}{4\mu} \tag{3.6}$$

The maximum coating speed should not exceed $V_{air\ entrainment}$ to avoid unstable coating. For deep UV resist, the estimated air entrainment speed is 375 mm/sec.

The maximum coating speeds obtained by Ruschak (Equation 3.5) and Mues et al. (Equation 3.6) do not necessarily agree. Ruschak's model provides a maximum coating speed that does not create the defects described in Section 3.5. On the other hand, Mues et al.'s model only predicts the speed that creates air entrainment. Ruschak's model typically provides a better prediction of the maximum coating speed when the coating fluid has a low viscosity. Mues et al.'s model provides a better prediction when the coating fluid has a high viscosity. With i-line resist, the maximum coating speeds predicted by Ruschak and Mues et al.'s models are 396 and 375 mm/sec, respectively. With deep UV resist, they are 480 and 750 mm/sec, respectively. They are both useful to estimate the order of magnitude for the maximum coating speeds. However, the actual maximum speeds must be obtained experimentally.

Coating Thickness

Higgins and Scriven [1980] developed a model for extrusion-slot coating. They identified two primary flows within the coating bead. The motion of the substrate relative to the extrusion head creates a Couette flow. The pressure drop between the slot in the extrusion head and the edges of the coating bead creates a Poiseuille flow. Both flows must exactly cancel out at the leading edge of the coating bead to maintain a stable bead. The difference between the Couette and Poiseuille flows causes the outflow in the trailing edge.

The minimum coating thickness predicted by Higgins and Scriven is:

$$h_{min} = h_0\left(1+\frac{6Ca}{1+\cos\beta_s}\left(\frac{L_1}{G_{fore}}\right)\left(\frac{G_{rear}}{G_{fore}}\right)\left[1+\left(\frac{L_2}{L_1}\right)\left(\frac{G_{fore}}{G_{rear}}\right)^2-\frac{2h_0}{G_{fore}}\right]\right) \tag{3.7}$$

where:

$$h_0 = 1.34Ca^{2/3}\frac{G_{fore}}{(1+\cos\beta_s)} \tag{3.8}$$

All other parameters are defined in Figure 3-6.

Lee et al. [1992] verified the model experimentally. The Capillary number was smaller than the critical Capillary number: the gap was 0.2 mm and dynamic contact angle was near 45°.

Figure 3-8 shows Equation 3.7 for different gap distances and coating speeds. Coating gaps of 40, 60, 80, and 100 μm are used for each resist because those are the gap distances that will be used later. Chapter 6 compares theoretical minimum coating thicknesses with experimental data.

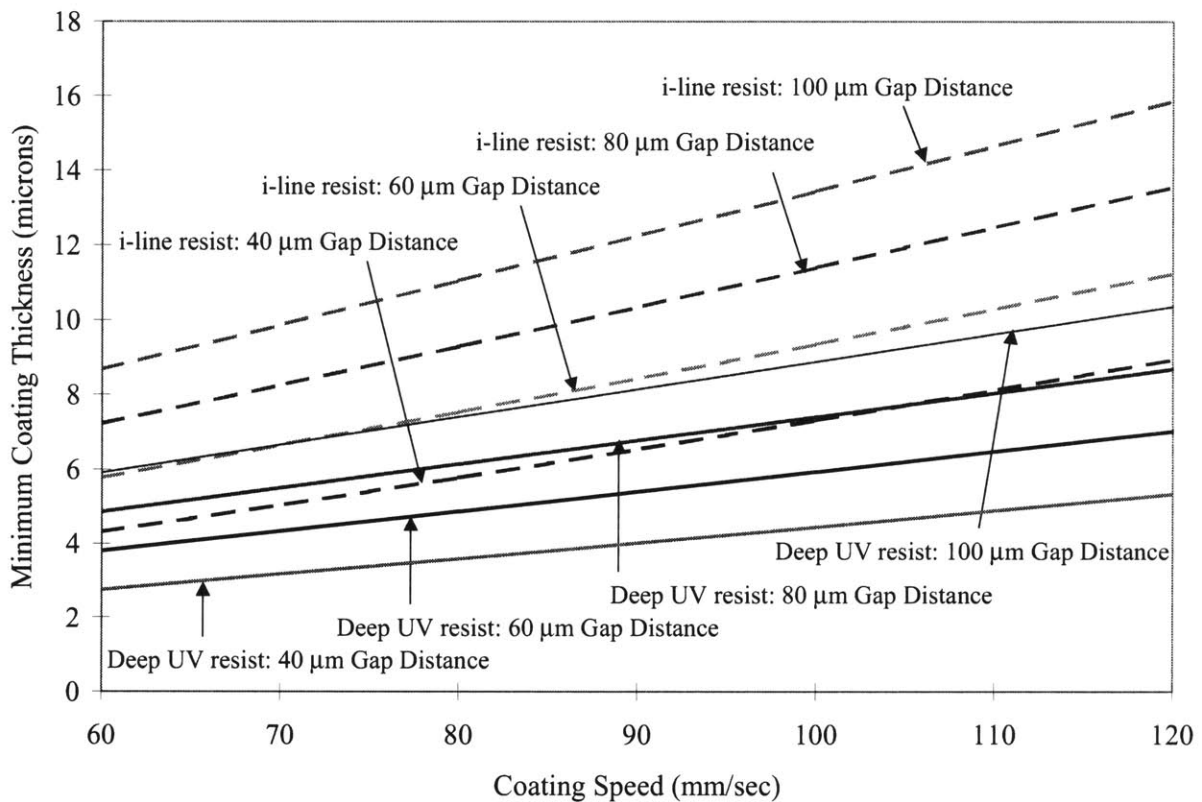

Figure 3-8: Theoretical minimum coating thicknesses with various gap distances and coating speeds.

Viscosity of Coating Fluids

Lee et al. [1992] experimented to determine the effect of the coating fluid's viscosity on both coating speed and minimum wet thickness. The minimum wet thickness can be reduced if the fluid viscosity is lower, especially for a larger coating gap. The maximum coating speed for the low viscosity coating solution is much higher than for the high-viscosity coating solutions.

Gap Distance

Gap distance is the distance between the extrusion head and substrate. It is one of the main parameters that distinguish the curtain coating process from the extrusion-slot coating process.

Choinski [1991] emphasizes the importance of the drawdown ratio, *DR*, in extrusion-slot coating. It indicates the ratio of gap distance, *G*, to wet coating thickness, h_{wet}:

$$DR = \frac{G}{h_{wet}} = \frac{GwV_{sub}}{Q} \tag{3.9}$$

Once a stable coating is reached, the coating fluid is drawn down uniformly along the slot at the bottom of the extrusion head. When the drawdown ratio is small, the bead remains stable and the coating thickness, h_{wet}, is unchanged. Even if the extrusion head is skewed, the coating thickness remains constant along the length of the extrusion head.

The range of the drawdown ratio for stable coating is different for various types of coating liquids. In conducting an extrusion-slot coating, the range of drawdown ratios for a specific coating liquid must be determined experimentally to obtain stable coating.

Bead Vacuum

Bead vacuum is necessary to maintain a stable bead with large gaps and high coating. The vacuum creates a pressure drop across the coating bead to balance the viscous forces and surface tensions. Higgins and Scriven [1980] predicted the minimum and maximum pressure drop across the bead as:

$$\Delta p_{\min} = 1.34 Ca^{2/3} \frac{\sigma}{h_{wet}} - \frac{\sigma(1+\cos\beta_s)}{G_{rear}} + \frac{6\mu v L_2}{G_{fore}^2}\left[1 + \left(\frac{L_1}{L_2}\right)\left(\frac{G_{rear}}{G_{fore}}\right)^2 - \frac{2h_{wet}}{G_{rear}}\right] \qquad (3.10)$$

$$\Delta p_{\max} = 1.34 Ca^{2/3} \frac{\sigma}{h_{wet}} + \frac{\sigma(1-\cos\beta_s)}{G_{rear}} + \frac{6\mu v L_2}{G_{fore}^2}\left[1 + \left(\frac{L_1}{L_2}\right)\left(\frac{G_{rear}}{G_{fore}}\right)^2 - \frac{2h_{wet}}{G_{rear}}\right] \qquad (3.11)$$

where all parameters are defined in Figure 3-6. Sartor [1990] later validated the model experimentally, showing the "window of coatability" that defines the pressure limits for establishing stable coating beads. If the upper vacuum limit is exceeded, fluid is sucked from the bead (swelling and weeping at the fore meniscus). When the bead vacuum is below the lower limit, ribbings and rivulets occur.

Viscous forces cause most of the pressure drop across the bead. The allowable range of pressure drop is very small with a small gap and a high coating speed. The allowable pressure drop is 26.2 ~ 29.1 kPa for a 14 mPa-sec fluid coated to 10 μm at 500 mm/sec [Sartor, 1990].

Lee et al. [1992] investigated the effect of bead vacuum. They found that increasing bead vacuum can effectively reduce the minimum wet thickness, particularly if the fluid viscosity is low and the coating gap narrow.

3.5 Defects from Extrusion-Slot Coating

Extrusion-spin coating is a sequential combination of extrusion-slot and spin coating. The purpose of applying extrusion-slot coating is to provide spin coating with a uniform initial layer that results in a uniform and final coating layer without any defects. One essential condition for an initial layer to be uniform is that it must be free of any defects. Defects from extrusion-slot coating and solutions to eliminate them must be studied.

Figure 3-9 shows the most common defects caused be extrusion-slot coating. They are mainly caused by coating speed problems. The upper speed limit is the speed below which uniform coating is made with no defects. Defects caused by excessive coating speed are air entrainment, ribbings, and rivulets. When the coating speed exceeds the upper limit, the coating liquid extruded from the fore lip becomes unstable and allows air to be entrained in the bead, as illustrated in Figure 3-9(a). This unstable phenomenon also occurs in the rear lip, causing ribbings, as in Figure 3-9(c). If the coating speed surpasses the limit even further, rivulets are formed, as in Figure 3-9(d), leaving part of the substrate uncoated. Figure 3-9(e) shows chatter, which is the fluctuating phenomenon of coating liquid. Chatter, ribbing, and rivulets are also related to the surface tension of the coating liquid. Swelling and weeping at the fore meniscus, as in Figure 3-9(b), appear when the vacuum rate is too high.

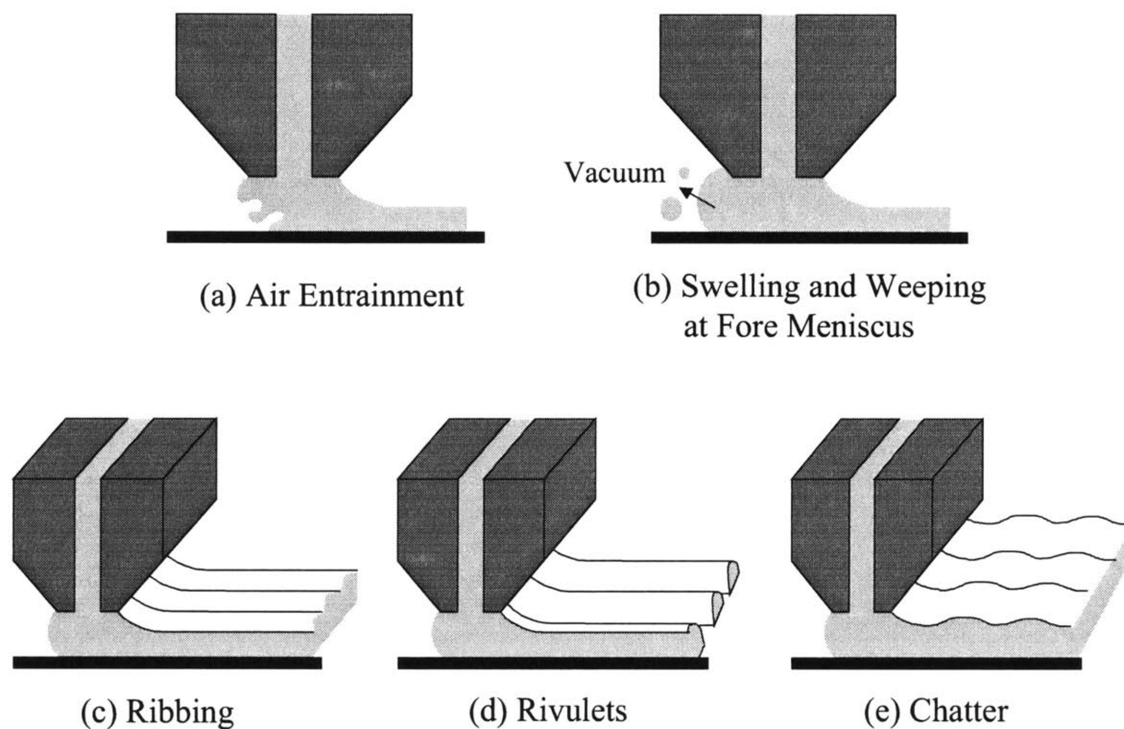

Figure 3-9: Various possible defects from extrusion-slot coating

Because defects are mainly caused by excessive coating speed, an upper speed limit must be known. Some defects have been studied carefully. Solutions to eliminate them are proposed.

Air Entrainment

Air entrainment in a coating bead causes bubbles to be entrapped in the coating layer [Sartor, 1990]. Air bubbles can cause defects in the resist image, as discussed in Section 1.6. When air bubbles are detected in the initial coating layer, decreasing the coating speed and increasing the vacuum can solve the problem.

Ribbing

Bixler [1982] described the ribbing in extrusion-slot coating using a finite element analysis technique. He reported that the following factors induce ribbing: high capillary number $Ca = \frac{\mu V_{sub}}{\sigma}$, low drawdown ratio, $DR = \frac{G}{h_{wet}}$ and low Reynolds number, $\mathrm{Re} = \frac{V_{sub} G}{\nu}$. Therefore, to decrease the risk of ribbing:

- Lower the viscosity of coating fluid.
- Decrease coating speed.
- Increase surface tension.
- Increase wet thickness.
- Decrease the gap distance between head and substrate.

Ribbing is not a particular problem by itself, but it can develop into rivulets, which will leave void areas on coated areas. Voids in the initial coating layer can lead to uneven coating thicknesses.

Chatter

Chatter is sometimes called barring because it appears as crossweb bars of fairly uniform width and period. When chatter occurs severely it can cause a discontinuity of coating flow in the direction perpendicular to the moving direction of extrusion head. In almost all cases, it is caused by mechanical vibration. The system must isolate the coating subsystem from any sort of vibrations to eliminate chatter [Cohen and Gutoff, 1995]. Chatter can also occur near the limits of coatability. In such cases, slowing down the coating speed, decreasing the gap distance, or increasing the vacuum can help resolve the instability.

Fat Edges

Fat edges are sometimes called "picture frames." Because the coating edges are thinner than the rest, with approximately the same evaporation rate, the concentration will increase faster at the edges. As a consequence, the edge surface tension will be higher than the middle, causing a flow toward the edges, creating fat edges. Fat edges can lead to a nonuniform initial layer. Increasing the coating speed or using a solvent-concentrated environment can reduce the total evaporation amount and prevent the forming of fat edges.

3.6 Theoretical Window of Coatability

Many factors influence the lower and upper coating speed limits in extrusion-slot coating, as discussed in Section 3.4.2. A low coating speed adversely affects productivity while a high coating speed causes incomplete coverage, nonuniformity, and defects. Within the parameters of coating speed, film thickness, and other process variables, there is a region within which the coated film is free of unacceptable defects: the "window of coatability."

Theoretical windows of coatability can be estimated with the analysis in Section 3.4.2. Figure 3-10 and 3-11 show the theoretical windows of coatability for i-line resist and deep UV resist, respectively. For both resists, a 40 μm coating gap is used. The width of the extrusion head slot is 20 mm. A flow rate of 0.01 ml/sec or higher is used. Ruschak's analysis (Equation 3.5) estimates the maximum coating speed. Constraints on the cycle time determine the lower bound for coating speed. With a coating speed of 60 mm/sec or lower, the extrusion coating cycle time exceeds 40 seconds for a 200 mm wafer, which is the maximum coating time allowable to meet overall cycle time. Higgin's analysis (Equation 3.7) gives the minimum coating thickness. However, these theoretical values cannot be achieved within the window of coatability due to the minimum flow rate of the actual resist dispensing pumps. The pumps used have a minimum flow rate of 0.01 ml/sec. Therefore, the minimum coating thickness is determined by the relationship between the coating speed, the wet coating thickness and the pump flow rate given in Equation 3.1.

Coating efficiency constrains the maximum wet coating thickness. When a 40 μm or thicker initial coating is applied, the coating efficiency is below 12.5%. Because the target of the new coating method is to achieve a coating efficiency higher than 12.5%, any thickness over 40 μm is undesirable.

The theoretical window of coatability helps to estimate the range of process variables before experimentation. However, the experimental window of coatability may be different from the theoretical one, as discussed in Section 3.4.2.

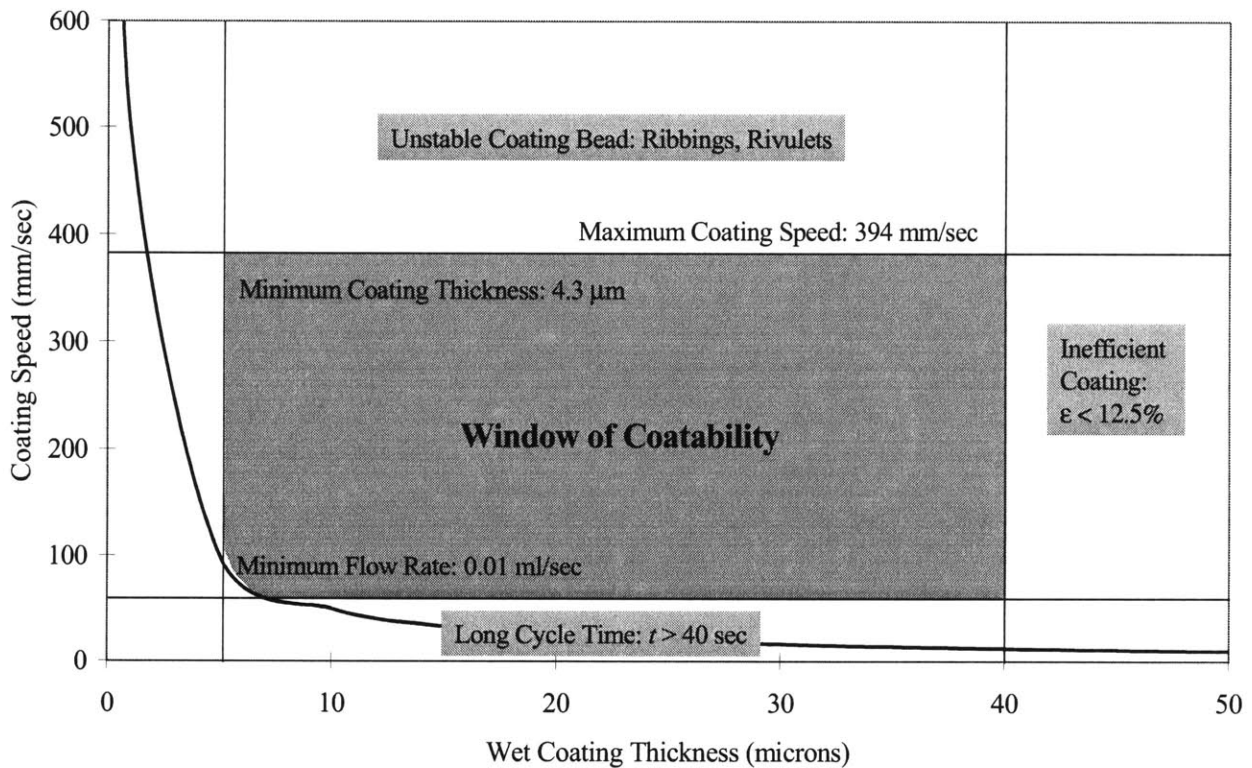

Figure 3-10: Theoretical window of coatability for i-line resist.

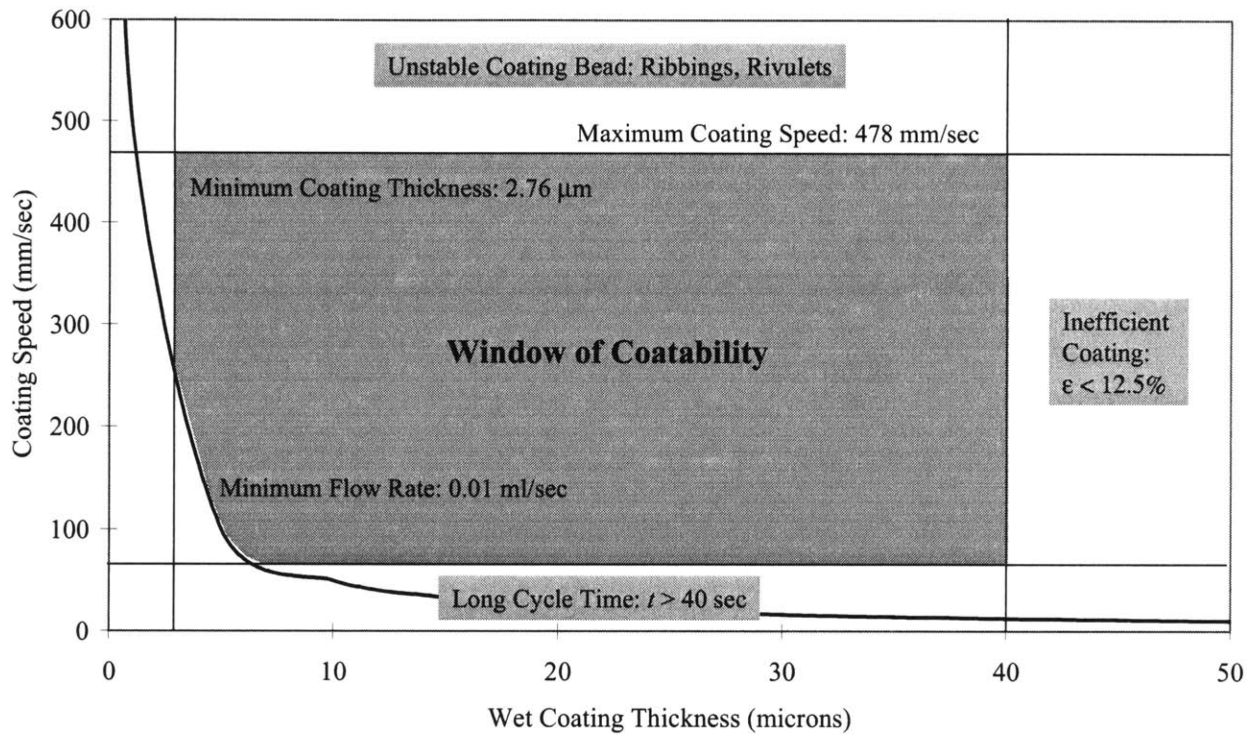

Figure 3-11: Theoretical window of coatability for deep UV resist.

3.7 Summary

A study of extrusion-slot coating revealed that the method can produce uniform, thin coatings with high efficiency. Such advantages make extrusion-slot coating an appropriate choice for providing an initial coating layer for spin coating. Proper design of the extrusion head for even distribution of photoresist was suggested. The approximate ranges of initial coating thicknesses and coating speeds were obtained. Minimum initial coating thickness is desirable for maximum coating efficiency. Maximum coating speed is desirable for minimum coating time. Using this information, extrusion-slot coating can now be applied to a rotating disk.

Chapter 4

Extrusion-Spin Coating

4.1 Description of Extrusion-Spin Coating

The extrusion-spin coating method replaces the dispense stage of conventional spin coating with an extrusion-slot coating method. Chapter 2 identifies the spin-off stage as the most inefficient stage in spin coating. Approximately 85~90% of the total resist applied is wasted during this stage. Extrusion-spin coating eliminates this stage by replacing the conventional dispense stage with extrusion-slot coating, as shown in Figure 1-4. Coating efficiency correspondingly improves because unnecessary waste is minimized. Figure 4-1 diagrams the extrusion-slot coating process applied to a rotating disk.

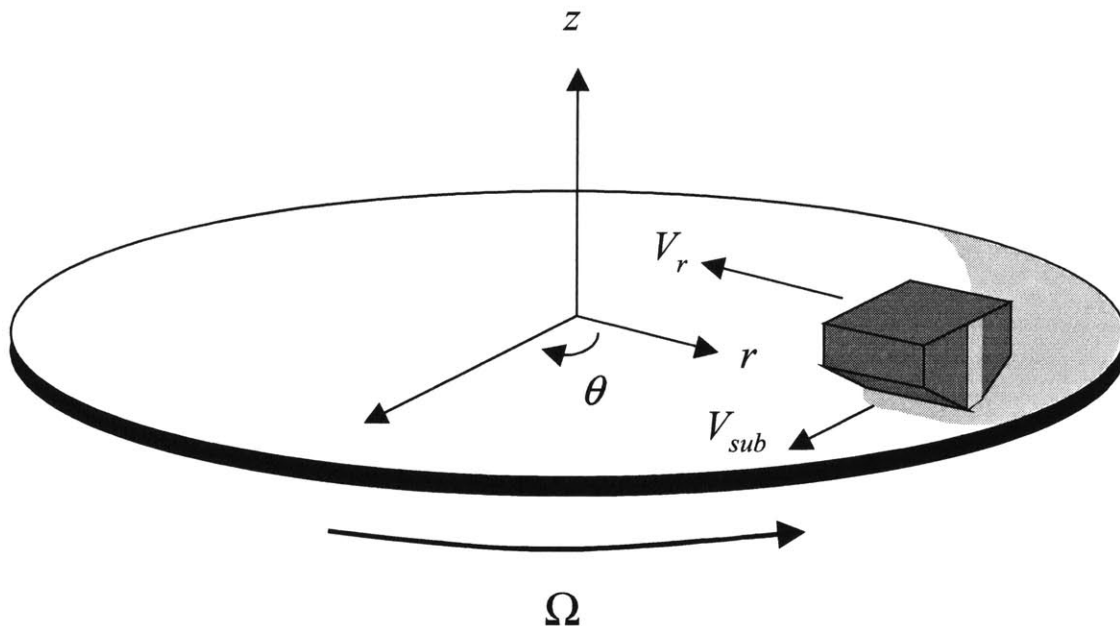

Figure 4-1: Illustration of extrusion-slot coating on a rotating disk.

Extrusion-spin coating not only improves coating efficiency, but also enables accurate predictions of coating thickness and uniformity. Chapter 2 notes that none of the existing spin coating models can determine initial conditions due to the dispense methods. Because the initial coating layer is applied by premetered extrusion-slot coating in extrusion-spin coating, initial thickness and uniformity can be controlled. When evaporation of the solvent occurs, Bornside et al.'s model can predict coating thicknesses at various locations on the wafer. Coating uniformity can be also predicted from this. When evaporation of the solvent is inhibited, Emslie et al.'s model can predict the coating thickness. Both models require establishment of a uniform initial coating layer.

4.2 Establishment of Initial Coating Layer

The most important aspect of extrusion-spin coating is establishing the initial coating layer. Coating thickness can be controlled by varying the flow rates and the extrusion head slot width with extrusion-slot coating. Coating uniformity, however, is unknown and must be measured experimentally.

Assuming that all dispensed photoresist is deposited on the wafer, the initial coating thickness, h_0, varies with the total volume of photoresist dispensed:

$$h_0 = \frac{\nabla_{total}}{\pi R^2} \tag{4.1}$$

where ∇_{total} is the total volume of photoresist dispensed and R is the wafer radius. Figure 4-2 shows the initial coating thickness according to various total pump dispense volumes for a 200 mm wafer. Figure 4-3 shows the coating efficiency (Equation 1.3) for various initial coating thicknesses. Initial coating thickness should not exceed 40 μm to obtain a coating efficiency of 12.5% or higher for deep UV resist. Thus, the total volume of dispense should be less than 1.25 ml to meet the coating efficiency requirement.

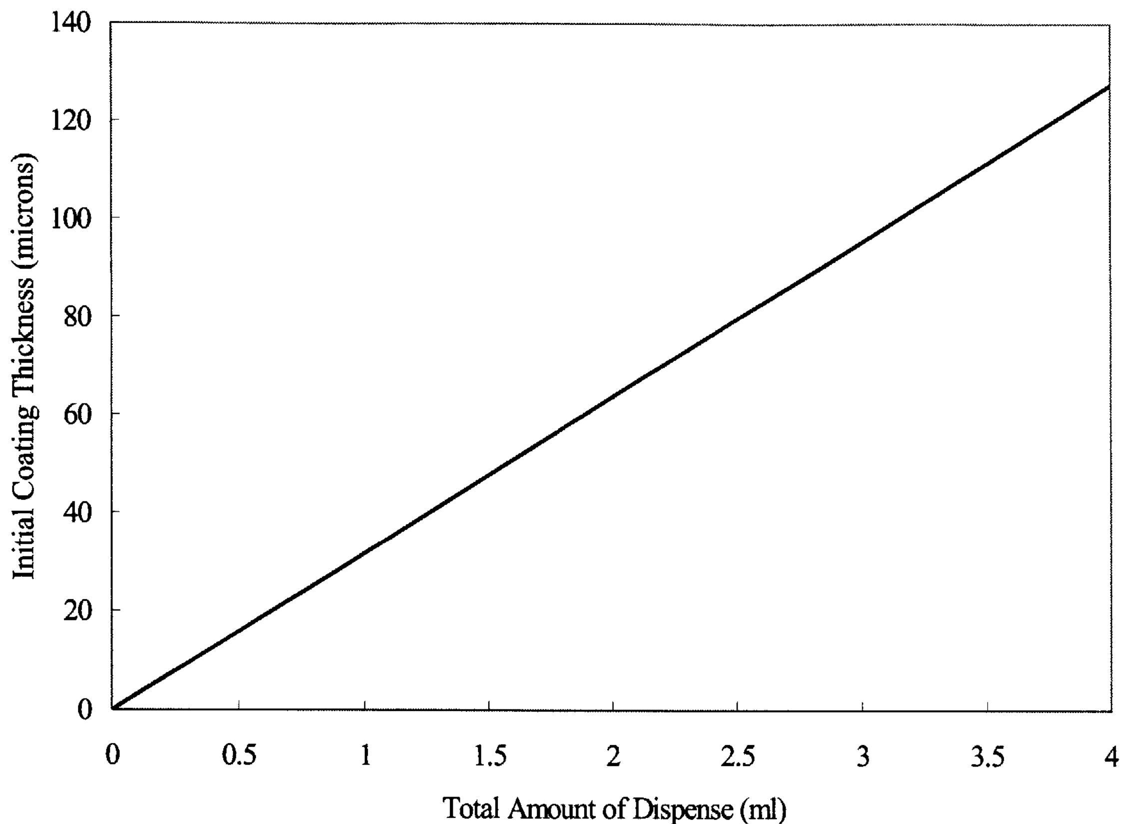

Figure 4-2: Initial coating thicknesses according to various total pump dispense volumes.

The initial coating layer must retain a certain uniformity level to meet the final coating uniformity requirement. The required initial coating layer uniformity is calculated to obtain the final coating uniformity of less than 5 Å based on Emslie et al.'s model (Equation 2.10). Figure 4-3 shows the allowable variation in initial coating thickness that will produce the final coating uniformity of 5 Å or better. The typical initial coating thickness and high spin speed used in experiments are 20~30 μm and 1500~2500 RPM, respectively. Therefore, this analysis is useful to estimate the coating uniformity level during an extrusion-slot coating on a rotating wafer. Figure 4-4 shows that the final coating uniformity of 5 Å can be met when a 20 μm initial coating layer is applied with a high spin speed of 1000 RPM and an initial coating layer uniformity of 35 Å. An initial coating uniformity of 900 Å is required to obtain same final coating uniformity when a 30 μm of

initial coating layer is applied with a high spin speed of 2000 RPM. This analysis, however, does not include the effects of evaporation. Coating uniformities are difficult to predict with evaporation unless the mass transfer coefficient, k, (Equation 2.18) is known at every location of the wafer.

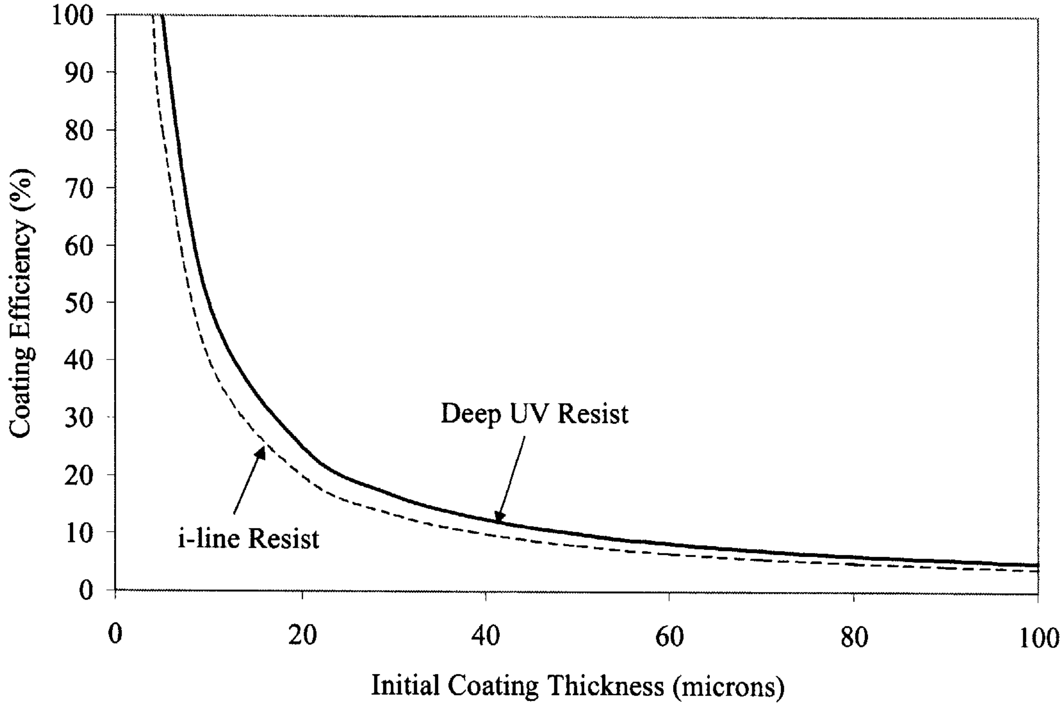

Figure 4-3: Coating efficiency with various initial coating thicknesses.

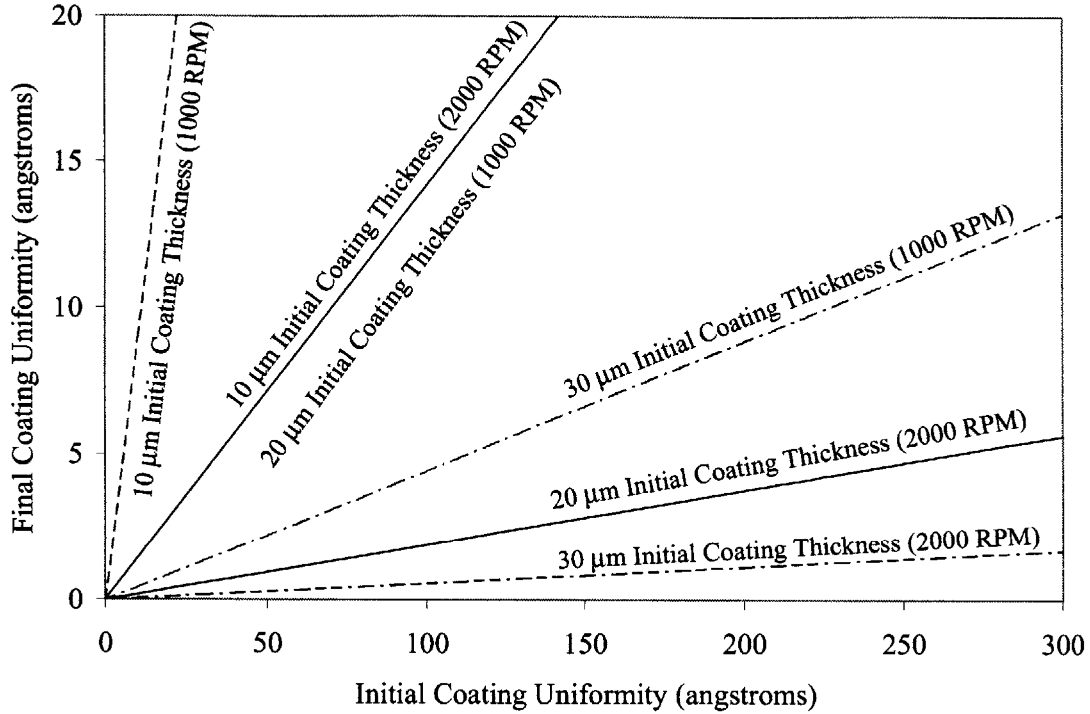

Figure 4-4: Variations of final coating uniformity with variations of initial coating uniformity.

4.3 Coating Pattern Requirements

Two principal goals must be satisfied in choosing a coating pattern: high efficiency and uniform coating. High efficiency can be obtained by minimizing the resist waste. Uniform coating can be obtained by maintaining a well-shaped bead in extrusion-slot coating. Many factors contribute to maintaining a well-shaped bead as discussed in Section 3.4. Most of all, continuous coating flow is essential.

4.3.1 Spiral Coating

The spiral coating pattern delivers continuous extrusion-slot coating with high coating efficiency. Figure 4-4 shows the spiral pattern formed on a rotating wafer whose diameter is 200 mm. The extrusion head has a 20 mm wide slot on its bottom. The extrusion head

moves toward the center, while the wafer rotates at a changing rotational speed due to the movement of the extrusion head in the radial direction.

The spiral coating pattern can provide a continuous stream of extruded flow on a spinning disk. Because maintaining a continuous stream is critical to a well-formed bead, it is the most important factor to extrusion-slot coating.

The outer shaded region in Figure 4-5 shows the initial dispense. An initial dispense is essential for two reasons. Photoresist at the tip of an extrusion head usually dries out between two consecutive coating processes. Dry photoresist must not be dispensed onto the wafer, for it could cause defects. The second reason is that extrusion-spin coating needs a stable coating bead to produce a uniform coating flow. The coating bead is formed within the first rotation of the wafer.

The shaded region at the center of the wafer denotes the overlapped region. The overlap at the center is inevitable because an infinite rotational speed at $r = 0$ is physically impossible. The amount of photoresist flow must be optimized to minimize the overlap at the center to avoid nonuniformities.

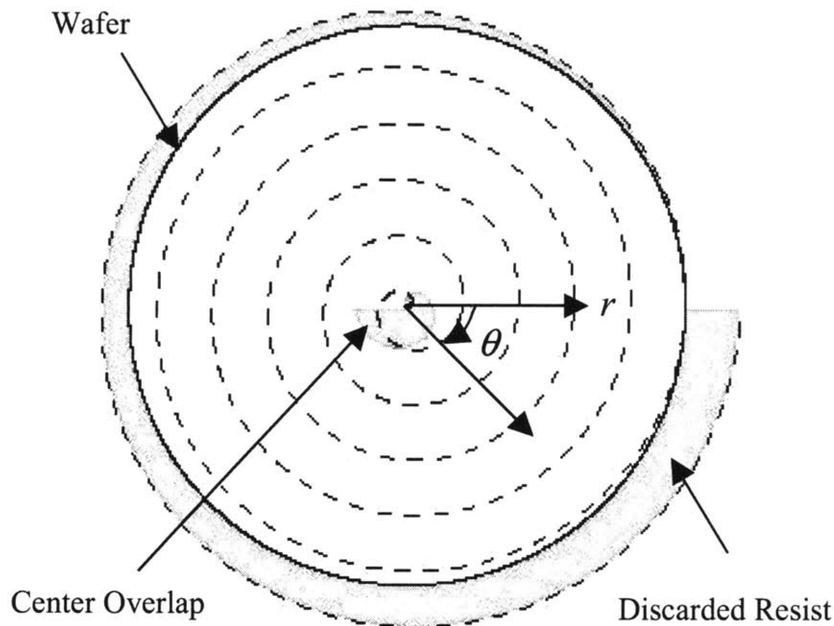

Figure 4-5: Spiral coating pattern formed on 200-mm wafer with extrusion head of 20 mm width.

It is also important to prevent contamination in applying extrusion coating on a rotating wafer. The extrusion head starts dispensing resist and then moves onto the wafer. If surface tension of the resist is almost negligible, the resist extruded from the extrusion head falls down vertically. In such cases, the part of the extrusion head slot that stays outside the wafer dispenses the resist outside the wafer, as shown in Figure 4-5. However, the surface tension of resist is not small enough to be negligible. At a certain point, capillary force exceeds gravitational force. All extruded resist then piles on the edge of the wafer, as illustrated in Figure 4-6. Experiments indicate that this starts to happen when the wafer rotates by one-quarter the rotation. Too much resist on the edge can slop over to contaminate the backside of the wafer. The amount of photoresist applied at the edge of wafer must be carefully determined to avoid this backside contamination problem.

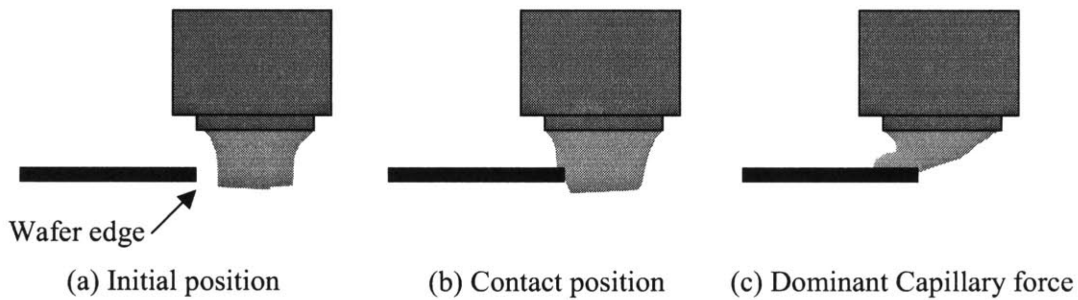

Figure 4-6: Bead formation at the edge of the wafer.

4.3.2 Spiral Pattern Analysis

The coating speed, V_{sub}, is a function of the radial position, r, and the rotational speed, Ω:

$$V_{sub} = r\Omega \tag{4.2}$$

The velocity in the radial direction, V_r, is a function of the extrusion head slot width, w, and the rotational speed, Ω. The radial velocity is expressed as:

$$V_r = \frac{w\Omega}{2\pi} = -\frac{dr}{dt} \tag{4.3}$$

With the initial condition $r = r_0$ @ $t = 0$, where r_0 is the initial start position equal the wafer diameter, R, plus the slot width in extrusion head, w. Integrating Equation 4.3 for the radial position, r, gives:

$$r = \sqrt{r_0^2 - \frac{wV_{sub}}{\pi} t} \tag{4.4}$$

By substituting r in Equation 4.2 by r in Equation 4.4, the rotational speed of the rotating disk can be obtained:

$$\Omega = \frac{V_{sub}}{\sqrt{r_0^2 - \frac{wV_{sub}}{\pi} t}} \tag{4.5}$$

Substituting Ω in Equation 4.3 with Ω in Equation 4.5 gives the radial velocity of the extrusion head:

$$V_r = \frac{wV_{sub}}{2\pi\sqrt{r_0^2 - \frac{wV_{sub}}{\pi} t}} \tag{4.6}$$

Because the rotational speed $\Omega = d\theta / dt$, the angle of the wafer, θ, can be determined by integrating Equation 4.5 using the initial condition of $\theta = 0$ @ $t = 0$:

$$\theta = \frac{2\pi r_0}{w}\left(1 - \sqrt{1 - \frac{wV_{sub}}{\pi r_0^2} t}\right) \tag{4.7}$$

4.3.3 Center Modification

The rotational speed in spiral pattern equations has a singularity at the center of the disk. As the extrusion head approaches the center of the wafer, the rotational speed increases toward infinity to maintain the constant tangential coating velocity. This is physically impossible. Thus, the spiral motion must be modified to stay within a reasonable rotational speed. One method of solving the center singularity problem is to maintain a constant rotational speed when the extrusion head reaches a critical radius. The radial velocity of the extrusion head and the rotational speed of wafer when that critical radius is reached are:

$$(V_r)_c = \frac{wV_{sub}}{2\pi r_c} \tag{4.8}$$

and:

$$\Omega_c = \frac{V_{sub}}{r_c} \tag{4.9}$$

The optimum critical radius is the point which guarantees the minimum overlap of photoresist at the center of the wafer and the maximum area of a uniformly deposited layer. This point is when the inner edge of the extrusion head reaches the center of the disk. At this position, the outer edge of the extrusion head is at a radius equal to its width, w. The corresponding extrusion head speed and rotational speed are respectively:

$$V_r = \frac{V_{sub}}{2\pi} \tag{4.10}$$

and:

$$\Omega = \frac{V_{sub}}{w} \tag{4.11}$$

Figure 4-7 shows the difference in the disk rotational speed between the original spiral shape and the modified spiral shape for a 200 mm wafer with a 20 mm wide extrusion head slot. The extrusion head follows the spiral path until it reaches the 5th revolution of the wafer, the position at which the outer edge of the head reaches the critical radius. The dotted lines indicate the original disk rotational speed without modification. The horizontal lines after the 5th revolution represent the modified disk rotational speed for the two different coating speeds. The 6th and last revolution has a constant rotational speed.

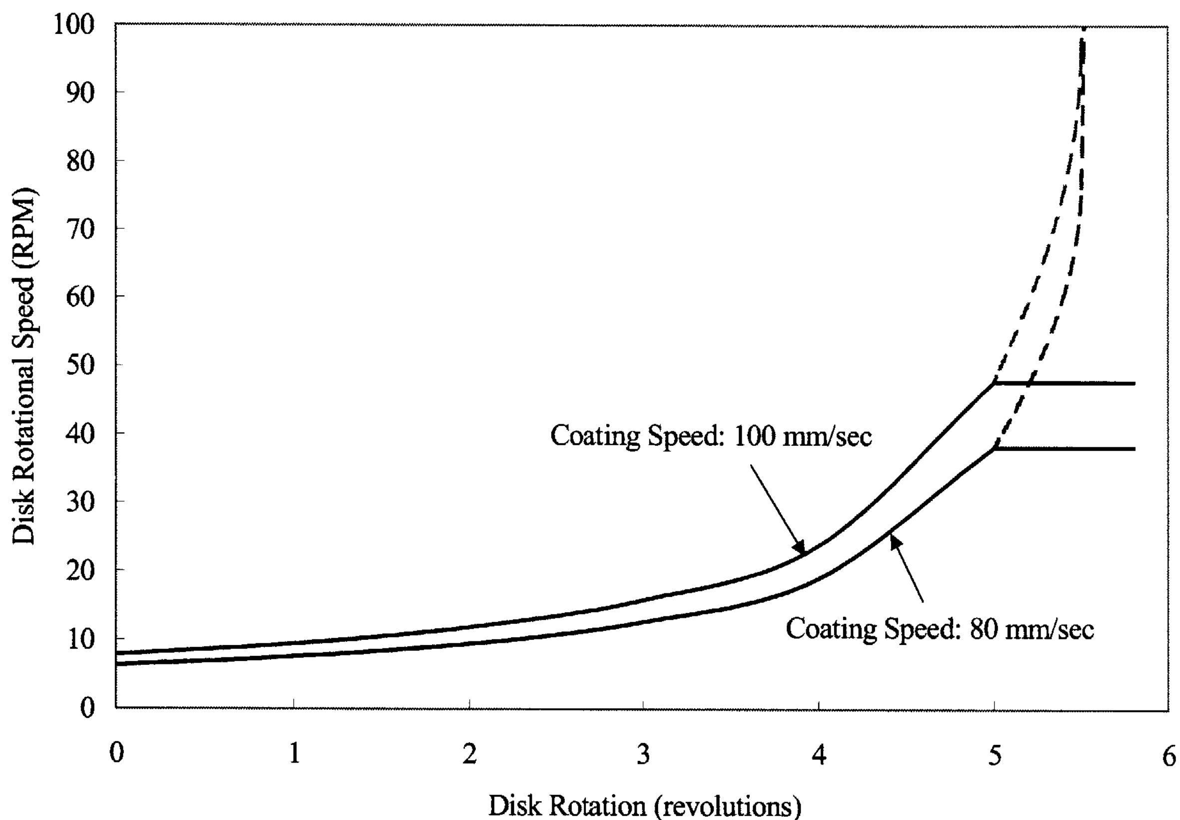

Figure 4-7: Disk rotational speed during extrusion-slot coating.

4.3.4 Spiral Coating Time

Solving Equation 4.4 for t yields the total time for the spiral coating:

$$t_{spiral} = \frac{\pi\left(r_0^2 - r_f^2\right)}{wV_{sub}} \tag{4.12}$$

where r_f is equal to the slot width in the extrusion head. However, the coating time increases when the spiral pattern is modified, as discussed in Section 4.3.3. The modified coating time is divided into two sections: the times required to coat the regions inside and outside the critical radius. The time required to coat the region inside is:

$$t_{<r_c} = \frac{2\pi r_c^2}{wV_{sub}} \tag{4.13}$$

The time required to coat from the outer edge to the critical radial position (outside the critical radius) is:

$$t_{>r_c} = \frac{\pi r_0^2}{wV_{sub}} - \frac{\pi r_c^2}{wV_{sub}} \tag{4.14}$$

Adding Equations 4.13 and 4.14 yields the total coating time for the modified spiral pattern:

$$t_{total} = \frac{\pi r_0^2}{wV_{sub}} + \frac{\pi r_c^2}{wV_{sub}} \tag{4.15}$$

Figure 4-8 compares the original spiral coating time (continuous line) and the modified spiral coating time (dotted line). The experimental coating speeds will be equal to or higher than 80 mm/sec because the extrusion coating time should not exceed 30 seconds to meet the coating time requirement. In this range, the modified spiral pattern adds one

second or less to the total coating time. Therefore, the modified spiral pattern can eliminate the singularity problem at the center while satisfying the coating time requirement.

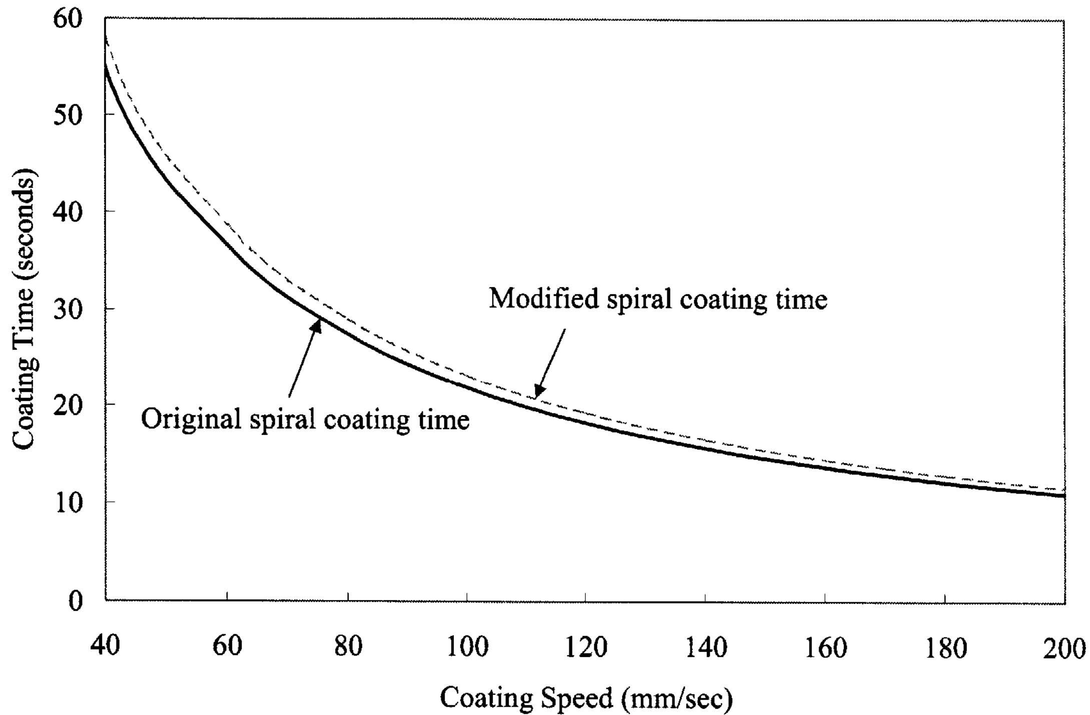

Figure 4-8: Comparison of coating times for extrusion-slot coating.

4.4 Neck-in of Extruded Flow

Neck-in is one of the important behaviors of the extruded flow. Figure 4-8 illustrates the neck-in of an extruded flow. Neck-in is the behavior of a fluid caused by its surface tension. When a flow is extruded from a narrow slot, it is so thin that viscous force becomes negligible. Surface tension is the dominant force in determining its behavior.

The behavior of neck-in is very important in extrusion-spin coating. An initial coating thickness depends on the amount of neck-in. Neck-in causes an extruded flow with an original width of w, to shrink to a new width w', as shown in Figure 4-9. A contracted

width causes a thicker coating layer. Thus, when the amount of neck-in, defined as $w - w'$, is not known, the thickness of coating layer cannot be determined.

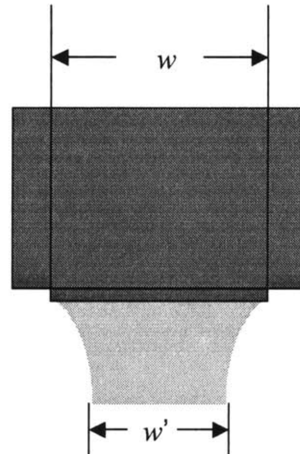

Figure 4-9: Neck-in of extruded flow.

Experiments estimated the amount of neck-in. Three parameters tracked the effect of neck-ins. The gap distance, flow rate, and viscosity of the photoresist influence neck-in [Burley and Kennedy, 1978]. Figures 4-10 and 4-11 demonstrate the neck-in as a function of gap distance for i-line and deep UV resists, respectively. Both figures indicate coating speeds, flow rates and maximum drawdown ratios. Coating speeds of 80 and 100 mm/sec were used for i-line resist. Flow rates varied from 0.04 to 0.06 ml/sec. The maximum drawdown ratios for i-line resist varied from 5.69 to 7.05. Deep UV resist used different flow rates (0.013, 0.016, and 0.024 ml/sec) with the same coating speed (80 mm/sec). 80 mm/sec will be used in later experiments.

These two plots clearly indicate that the amount of neck-in increases more rapidly as gap distance widens. In addition, the less viscous flow (deep UV) tends to neck-in more rapidly. This is because as flow is extruded away from the slot, the effect of surface tension increases while that of viscous force decreases. Maximum drawdown ratios of a specific resist stay within a close range, as shown in Figures 4-10 and 4-11. The drawdown ratio for each experiment must not exceed these values for a successful coating. As long as

the drawdown ratio remains below the maximum values, coating results are not significantly affected [Choinski, 1991].

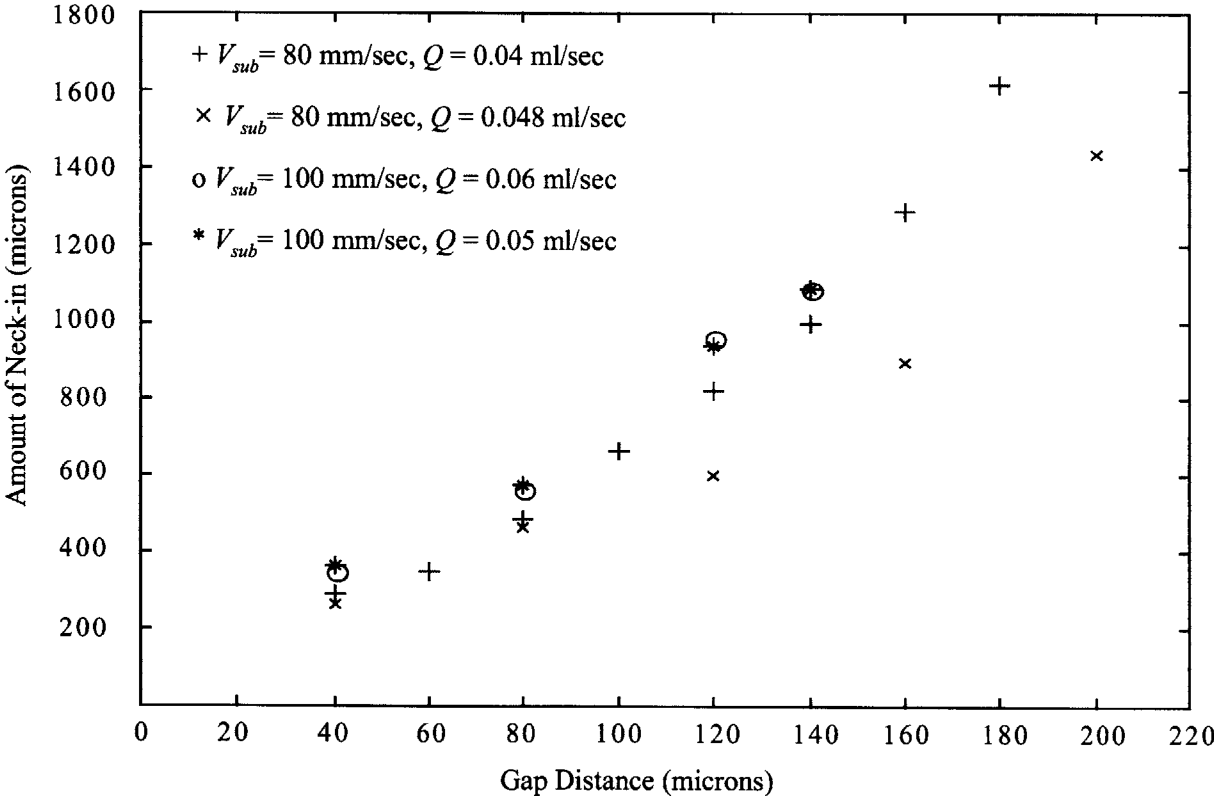

Figure 4-10: Experimental data of neck-ins for i-line resist.

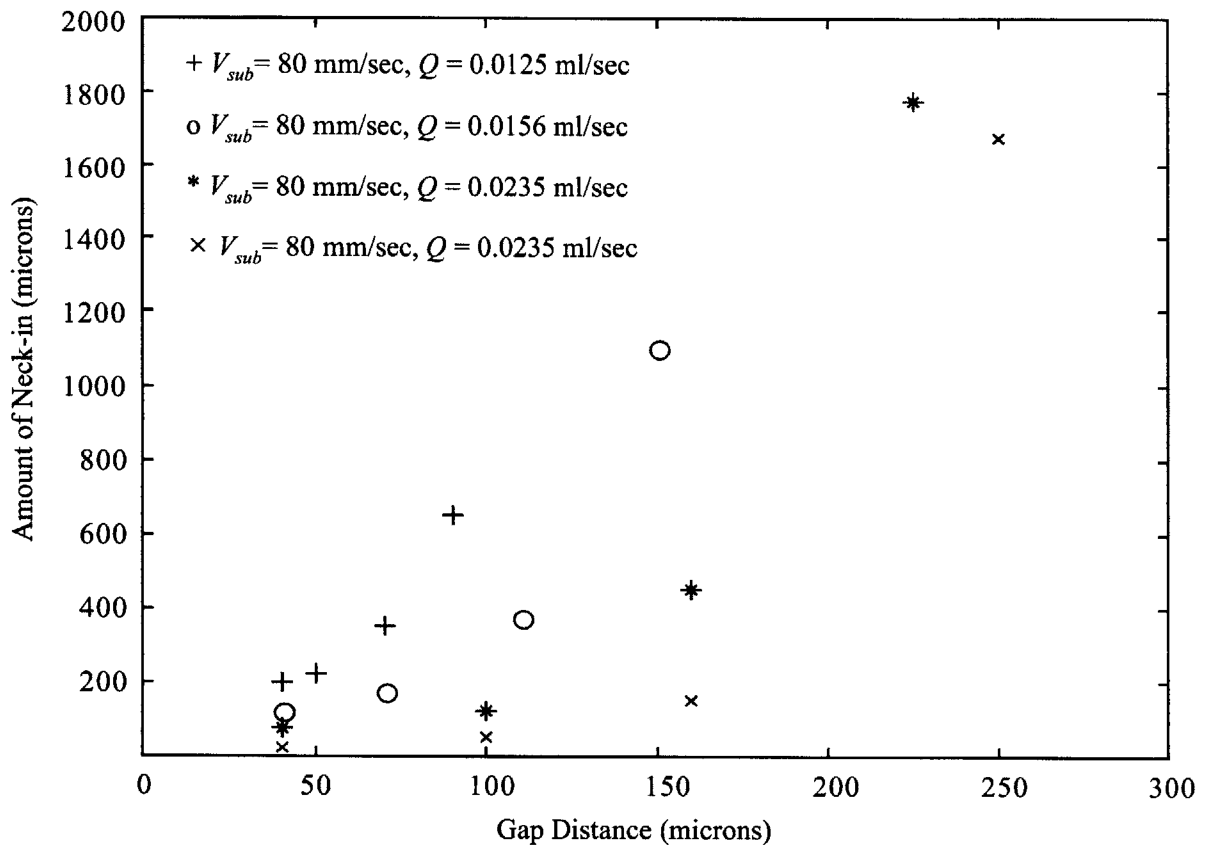

Figure 4-11: Experimental data of neck-ins for deep UV resist.

4.5 Maximum Gap Distance

Maximum gap distance is the maximum distance allowable between the extrusion head and the wafer that will yield a stable coating without any of the defects listed in Section 3.5. Extrusion-slot coating no longer provides a stable coating flow once the maximum gap distance is exceeded. It can cause defects such as rivulets and air entrainment.

Maximum gap distance between the extrusion head and wafer is constrained by photoresist viscosity, flow rate, and neck-ins. Figure 4-12 shows the maximum gap distances allowable with various flow rates. Two photoresists were used to obtain the maximum coating gap: i-line and deep UV. Maximum gap distance increased as pump flow rate increased. This result corresponds with the results in Figures 4-9 and 4-10. The amount of neck-in decreases as flow rate increases and therefore a wider gap distance is allowed. The plot also indicates that the amount of neck-in increases more rapidly as gap distance widens. In addition, deep UV resist, which has a lower viscosity, was observed to neck-in more rapidly than the more viscous resist (i-line).

Estimation of the maximum coating gap is important because when the extrusion head is too close to the rotating disk, the tip of the head can accidentally touch the surface of the wafer during the rotation, which can scratch the surface of the wafer. Therefore the gap distance must be wide enough to avoid contact between the extrusion head and wafer, but not wide enough to cause defects in the coating.

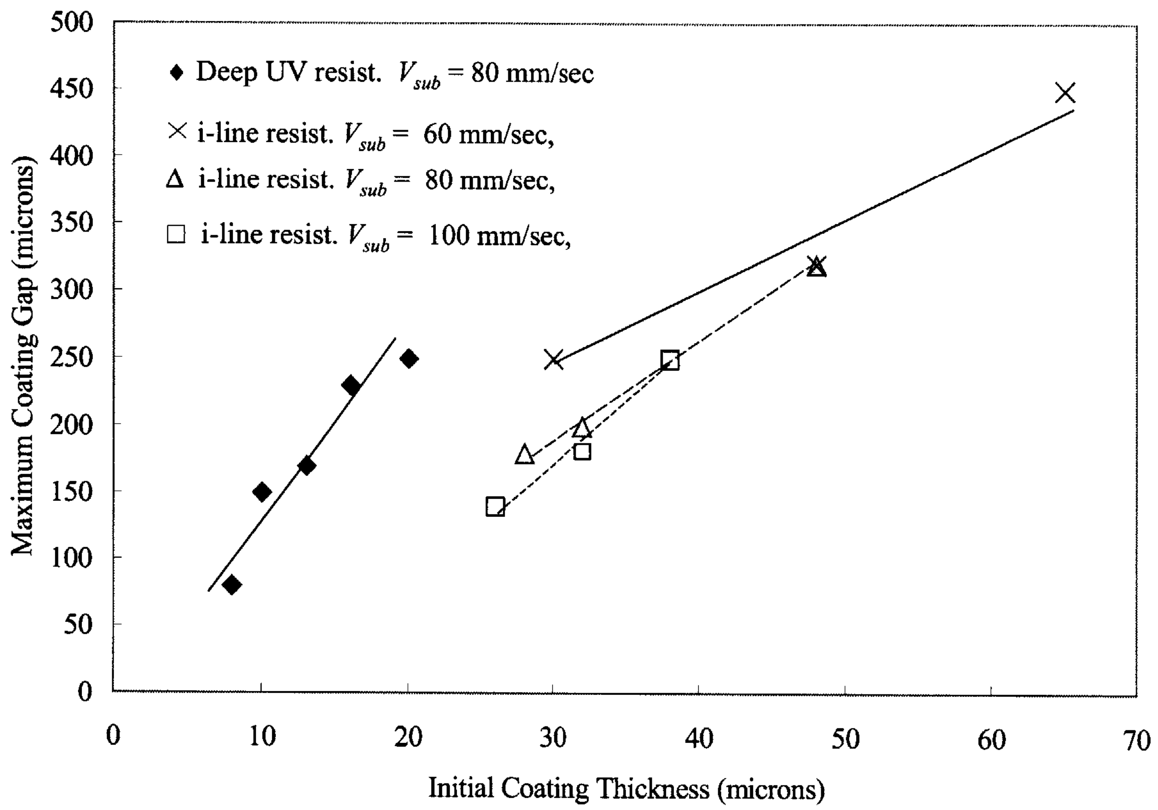

Figure 4-12: Maximum coating gap distances in extrusion-slot coating.

4.6 Overlap Effect

The photoresist overlap is set to avoid void spots on a rotating wafer. To create overlaps, the slot width of extrusion head, w, in Equations 4.3 ~ 4.15 is replaced with the new slot width, $w' = w - \Delta w$, where Δw is the desired amount of overlap. This yields the total coating time.

$$t_{total} = \frac{\pi r_0^2}{(w - \Delta w) V_{sub}} + \frac{\pi r_c^2}{(w - \Delta w) V_{sub}} \tag{4.15}$$

The original coating time was increased by $w/(w - \Delta w)$. The overlap was observed when the extrusion head meets the previously dispensed line of photoresist. Figure 4-13 shows the overlapped region caused by extrusion-slot coating. The overlap, A, is created in the previous rotation. The new overlap, B, is created when the extrusion head completes a rotation to meet with the previously dispensed coating layer between A and B. Derksen [1997] investigated overlap spreading. He found that these overlaps have little if any effect on final coating uniformity, provided other process variables are maintained constant. However, when the extrusion coating speed is fixed, increasing the overlap amount also increases the coating time, as shown in Equation 4.15. The photoresist overlap itself does not affect the final coating uniformity as long as the overlap is small compared to the extruded width. However, creating overlaps increases extrusion-slot coating time and cause an associated increase in evaporation amount and thus, affects the coating uniformity.

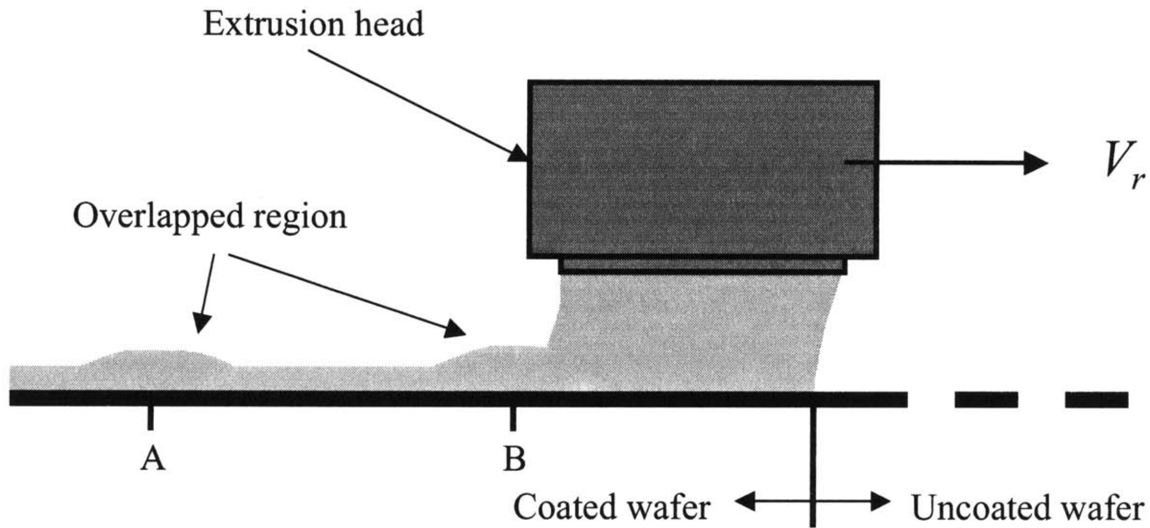

Figure 4-13: Overlap of photoresist on a rotating wafer.

4.7 Alignments

The gap distance between the extrusion head and wafer does not remain constant in practice. The prototype extrusion-spin coater was built with the platform of an existing spin coater designed for high rotational speeds (typically over 1000 RPM). When this spin coater is used to conduct extrusion-slot coating, the rotational speeds range from 0 to less than 60 RPM (Figure 4-6). At such low rotational speeds, the rotating wafer displayed wobbling. Due to this wobbling, the gap distance between extrusion head and wafer varies during rotations.

Extrusion-spin coating involves two major alignment issues. A Cartesian coordinate is used for the discussion of the alignments. Figure 4-14 shows the coordinates on a wafer. The X-axis is identical to the *r*-axis as defined in Figure 4-1. The Y-axis is the axis perpendicular to the X-axis in clockwise direction. The first issue of the alignments is the gap distance variations, addressed as the Z-motion alignment. This is a common problem encountered with the extrusion-slot coating method. The second issue arises from the unique spiral coating shape of the extrusion-slot coating applied to a spinning wafer. It

involves an appropriate deposition at the center of the wafer and is addressed as the Y-motion alignment.

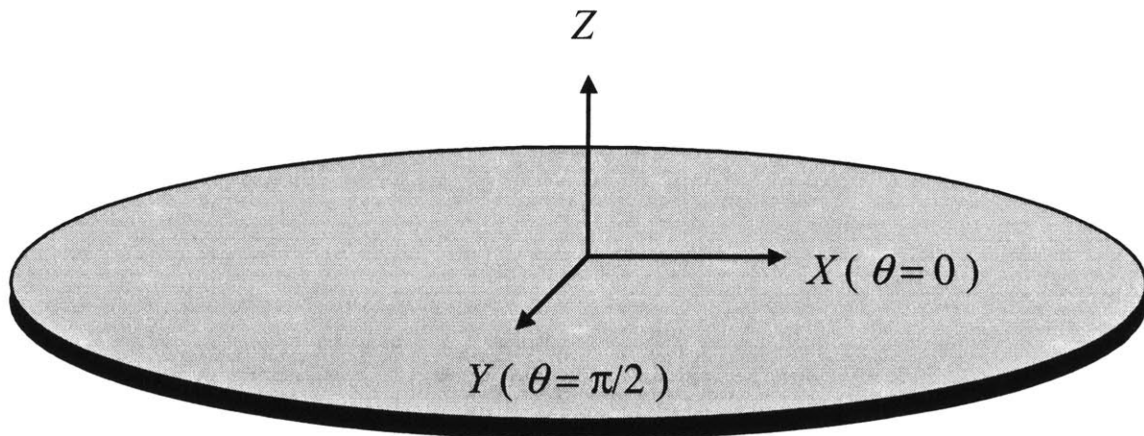

Figure 4-14: Cartesian coordinate on a rotating wafer.

4.7.1 Z-Motion Alignment

Two alignments have to be considered with Z-motion: the extrusion head alignment and the spindle chuck runout. Figure 4-15 illustrates the total misalignment error caused by both the extrusion head and the spindle chuck runout. The following sections will examine each alignment issue.

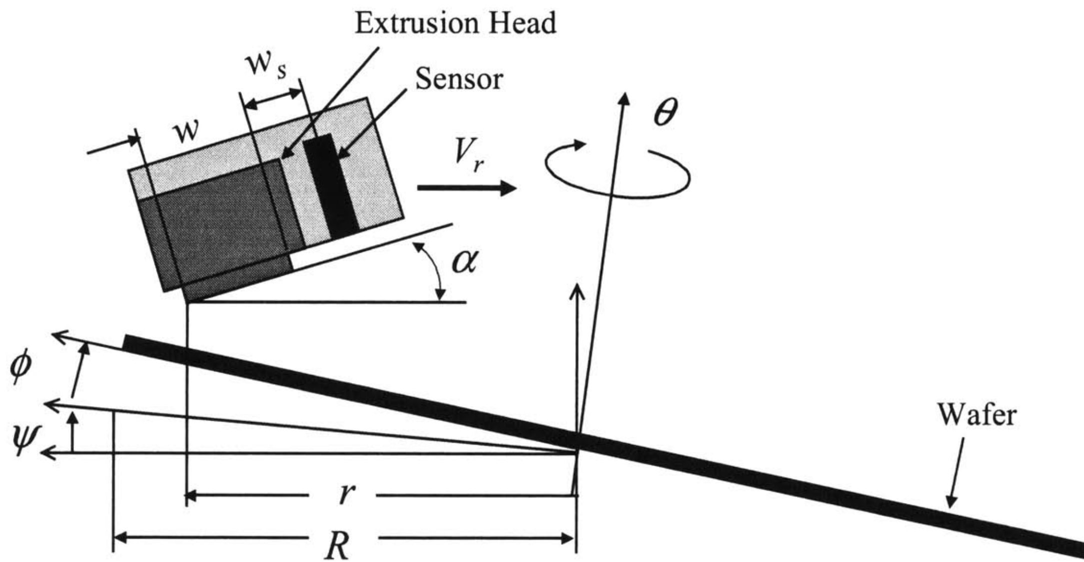

Figure 4-15: Total misalignment of extrusion head and wafer.

Extrusion Head Alignment

When the extrusion head is not aligned parallel to the axis of its motion, the gap distance between the extrusion head and the wafer does not remain constant. Figure 4-16 shows that the difference in gap distance from one end of the extrusion head to the other will be:

$$\begin{aligned} \Delta G &= \Delta G_{\alpha} \\ &= w \sin \alpha \end{aligned} \tag{4.16}$$

where α is the misalignment angle between the extrusion head and the substrate when the substrate is parallel to the horizontal axis.

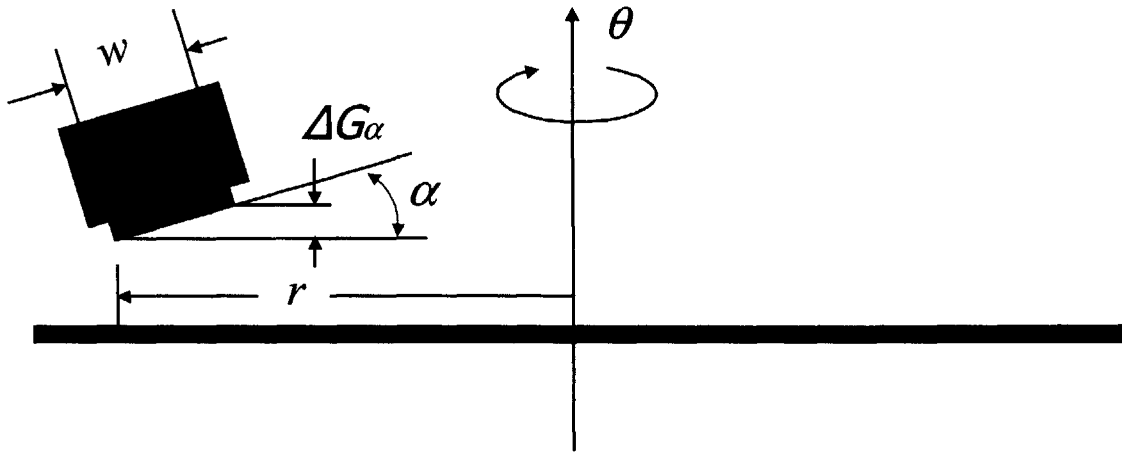

Figure 4-6: Extrusion head and wafer alignment.

Spindle Chuck Runout

When the axis of rotation of the disk is not perpendicular to the extrusion head, the gap between the extrusion head and the wafer varies periodically with the gap variation of ΔG_ϕ, expressed as:

$$\Delta G_\phi = -r \tan\phi \cos\theta \tag{4.17}$$

This misalignment also causes a gap distance variation within an extrusion head. Between the wafer and the extrusion head, the gap distance between one end and the other end of the extrusion head is different by an amount:

$$\Delta G_w = w \tan\phi \cos\theta \tag{4.18}$$

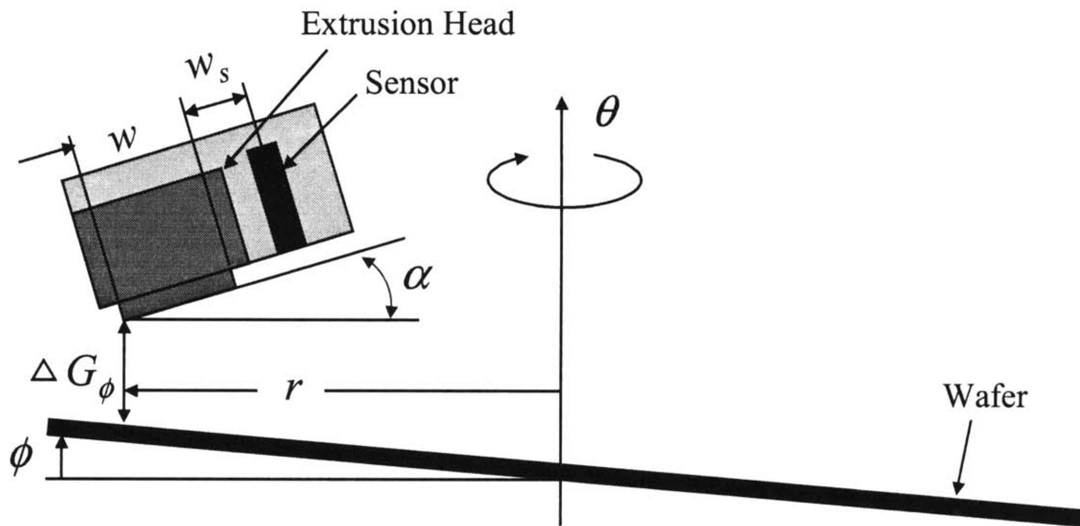

Figure 4-17: Extrusion head and wafer alignment with the sensor.

A feedback sensor is necessary because maintaining a constant gap distance is critical in extrusion-slot coating. Figure 4-17 shows the sensor installed next to the extrusion head. The sensor controls the gap distance actively through a closed loop control. Although it cannot control angular misalignment, the absolute gap distance error can be minimized. The remaining gap distance error, $\Delta G(\theta)$, is:

$$\Delta G(\theta) = -(w + w_s)\tan\phi\cos\theta \qquad (4.19)$$

where w_s is the distance between the inner edge of the extrusion head and the sensor measuring point.

Spindle Rod Misalignment

When the spindle rod is misaligned by ΔG_ψ to the perpendicular to the motion of extrusion head in r direction, as shown in Figure 4-18, the gap error due to the spindle rod misalignment is:

$$\Delta G_\psi = (R - r)\tan\psi \qquad (4.20)$$

where R is the r-direction projection of the radius of the wafer.

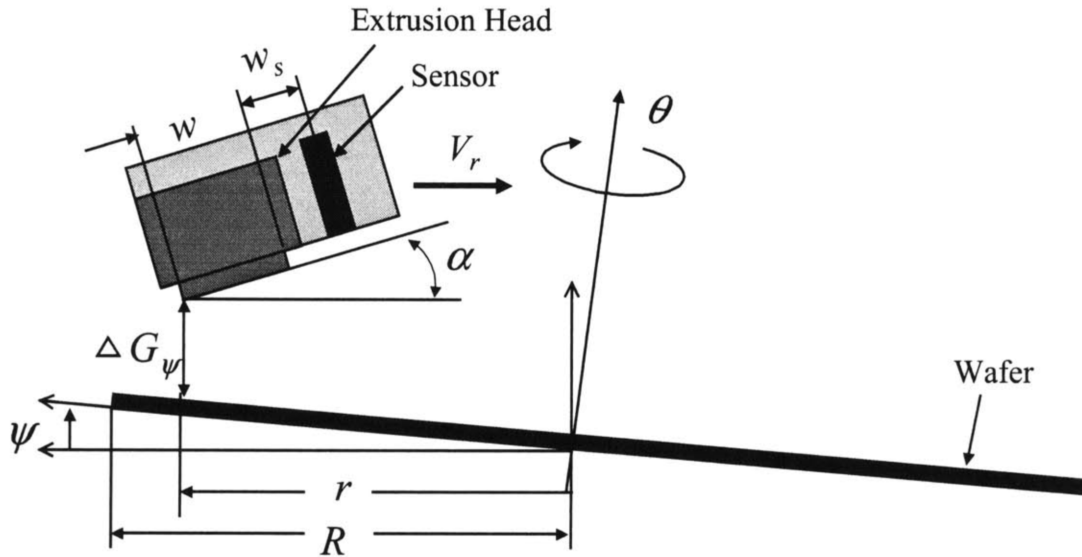

Figure 4-18: Error in gap distance with misaligned spindle rod.

Total Gap Distance Error due to Misalignment

The total gap distance error at a given location r is originally:

$$\Delta G_{original} = -r\tan\phi\cos\theta + (R - r)\tan\psi \tag{4.21}$$

However, with a sensor, the gap distance error is:

$$\Delta G_{sensor} = -(w + w_s)\tan\phi\cos\theta \tag{4.22}$$

Due to the angle of the wafer with respect to the horizontal axis, there is a gap variation:

$$\Delta G_w(\theta) = w\tan\alpha + w\tan\phi\cos\theta + \tan\psi \tag{4.23}$$

With Equation 4.23, the gap distance error at the inner (or leading) edge of an extrusion head is:

$$\begin{aligned} \Delta G_{r-w} &= \Delta G_w + \Delta G_{sensor} \\ &= w \tan\alpha + w \tan\phi \cos\theta + w \tan\psi - (w + w_s) \tan\phi \cos\theta \end{aligned} \quad (4.24)$$

For small angles ($\alpha, \phi, \psi << 1$), Equation 4.24 becomes:

$$\Delta G_{r-w} = w(\alpha + \psi) - w_s \phi \cos\theta \quad (4.25)$$

Minimizing the gap distance error is important in extrusion-slot coating,. If the gap distance cannot be precisely controlled, the amount of error needs to be determined. Equation 4.25 shows that gap distance error involves three angles α, ϕ, and ψ. Aligning the head and wafer in experiments can eliminate the misaligned angle, α, which is caused by the extrusion head and the wafer. However, the other misaligned angles, ϕ and ψ, are caused by the inherent dynamics of the spindle motor and cannot be controlled. Therefore, their values can only be measured by experimentation.

Most of the experiments in this thesis are conducted with a 40 μm gap distance. An estimation of the allowable range of misaligned angles to maintain that gap distance is useful. The maximum gap distance error must first be obtained to estimate the allowable range. The maximum gap distance error should be no bigger than the gap distance If it is bigger, the extrusion head will contact the wafer. An extrusion head fabricated of material harder than silicon wafer can scratch or even break the wafer.

Figure 4-19 indicates the range of allowable misaligned angles, ϕ and ψ, when the extrusion head misaligned angle, α, is eliminated. A gap distance of 40 μm and the same allowable gap distance error are used for analysis. Chapter 5 presents a method of controlling the Z-motion alignment as well as the actual data.

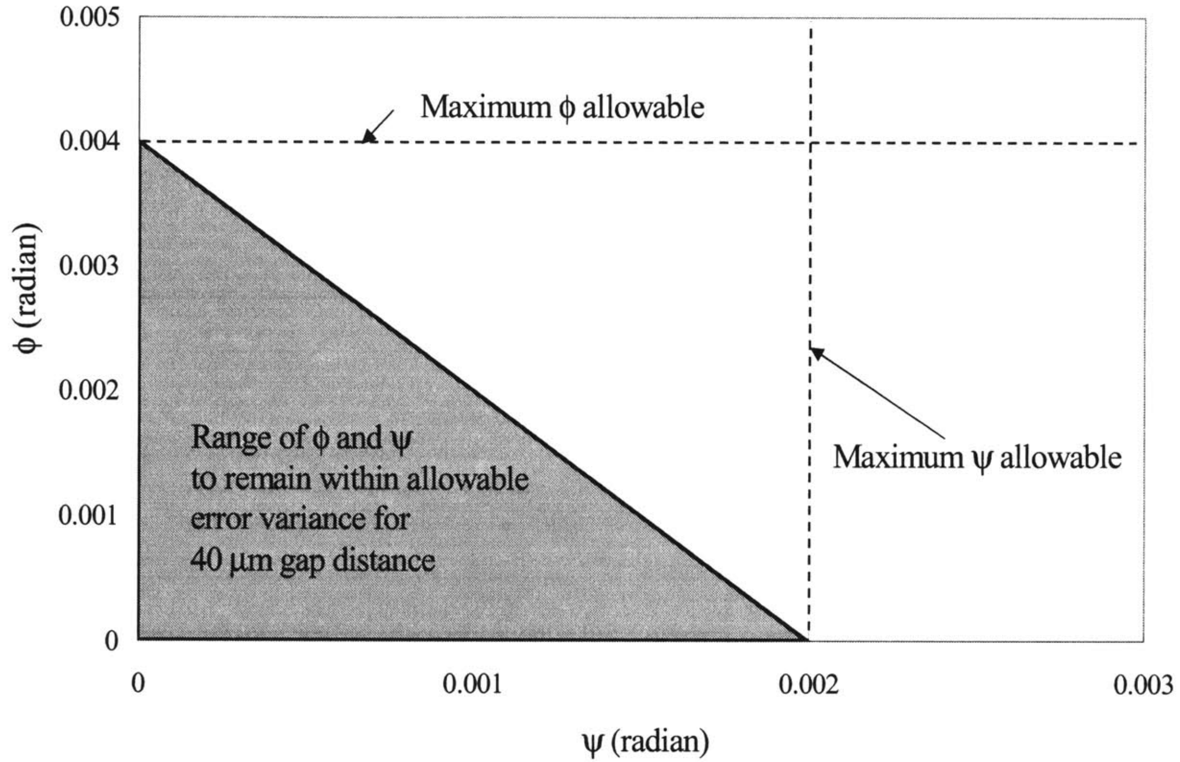

Figure 4-19: Allowable range of angles ψ and ϕ for 40 μm gap distance.

4.7.2 Y-Motion Alignment

The slot on the extrusion head must cross the exact axis of rotation on the wafer to obtain a complete coating. If not, the center of the wafer is not properly coated. It can either stay uncoated or entrap bubbles, either of which leads to a coating defect at the center. Chapter 5 presents a method of controlling Y-motion alignment in an experimental system.

4.8 Modeling and Theoretical Analysis of Extrusion-Spin Coating

Chapters 2 and 3 respectively presented modelings and theoretical analysis of spin and extrusion-slot coating. The two should not be considered separately in extrusion-spin coating, for they are sequential processes. This section investigates initial conditions for spin coating provided by extrusion-slot coating. It will also suggest and analyze a new method for improving initial conditions.

4.8.1 Flow over a Rotating Disk during Extrusion-Spin Coating

Experiments [Ellison, 1971; Kobayashi et al., 1980; Sezeri and Giron, 1984; Malik, 1986] show that when the Reynolds number ($\mathrm{Re} \equiv \rho\Omega r^2 / \mu$) is smaller than 1×10^5, resist flow is steady state and axisymmetric with laminar motion. In the extrusion-slot coating stage, the maximum rotational speed is obtained as the extrusion head approaches the center. As long as the maximum rotational speed does not exceed the critical Reynolds number, the mass transfer coefficient is independent of radius [Kreith et al., 1959].

During the extrusion-slot coating stage of the extrusion-spin coating process, the flow over a rotating disk must remain in a laminar regime to ensure a predictable evaporation. Figure 4-20 shows the maximum rotational speed to remain in the laminar regime during extrusion-slot coating. Rotational speed varies linearly with the Reynolds number. When the rotational speed exceeds 1470 RPM, the transition of flow from laminar to transient occurs at the periphery of 200 mm wafers. These ranges assume that extrusion-spin coating takes place under standard atmospheric conditions. The rotational speed during extrusion-slot coating stays well below 1470 RPM, as shown in Figure 4-6. Thus, the flow over the wafer remains in the laminar regime.

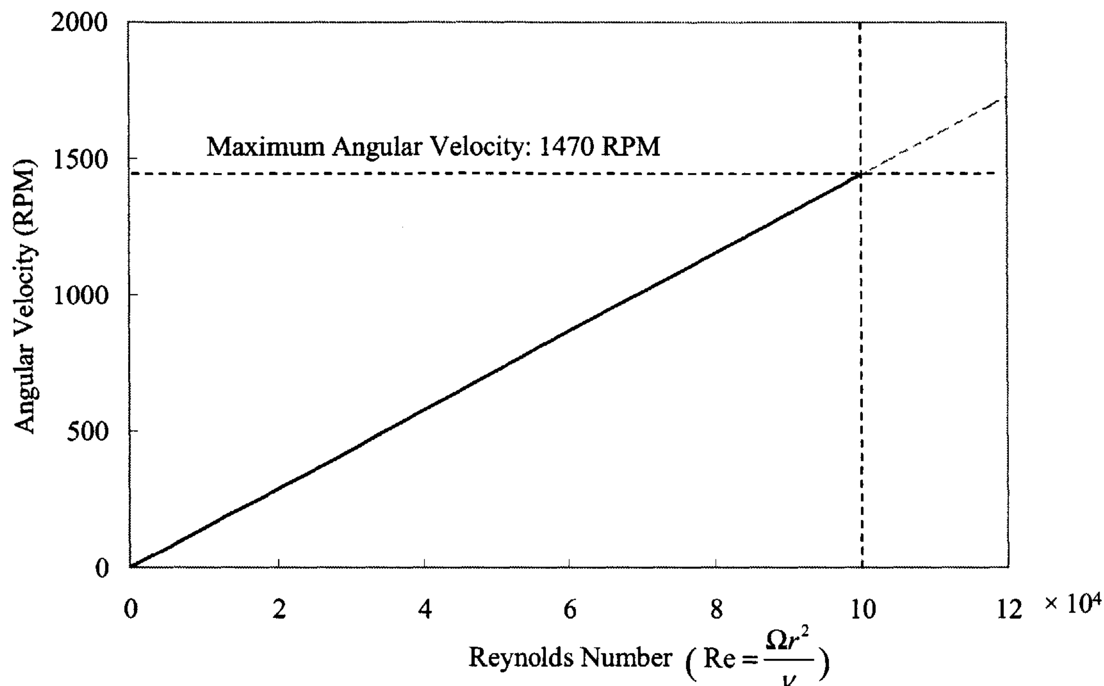

Figure 4-20: Range of rotational speeds for the flow above the rotating wafer to remain in laminar regime.

4.8.2 Evaporation of Solvent from a Spinning Disk

The previous section showed that the flow over the rotating wafer is laminar during extrusion-slot coating. The evaporation of solvent can now be theoretically analyzed.

Solvent Evaporation in a Quiescent Atmosphere

The mass transfer rate of PGMEA solvent was determined in a quiescent atmosphere. A certain amount of solvent weighting 4.862 kg was placed on a micro-scale. Weight variation was measured every minute for 10 minutes. With no solvent concentration in the surrounding atmosphere, the mass transfer rate is measured to be 1.11×10^{-6} kg/m^2·sec (Figure 4-21). The experiment was repeated three times. The variation in weights was less than 0.1%.

Fick's law of diffusion gives the diffusion coefficient of solvent surrounded by air:

$$j_{solv} = -\rho D_{solv,air} \nabla m_{solv} \tag{4.26}$$

where j_{solv} is the diffusive mass flux of PGMEA solvent, ρ is the solvent density, m_{solv} is the mass fraction of the solvent, and $D_{solv,air}$ is the binary diffusion coefficient. The experimentally obtained diffusion coefficient is 2.2×10^{-5} m^2/sec.

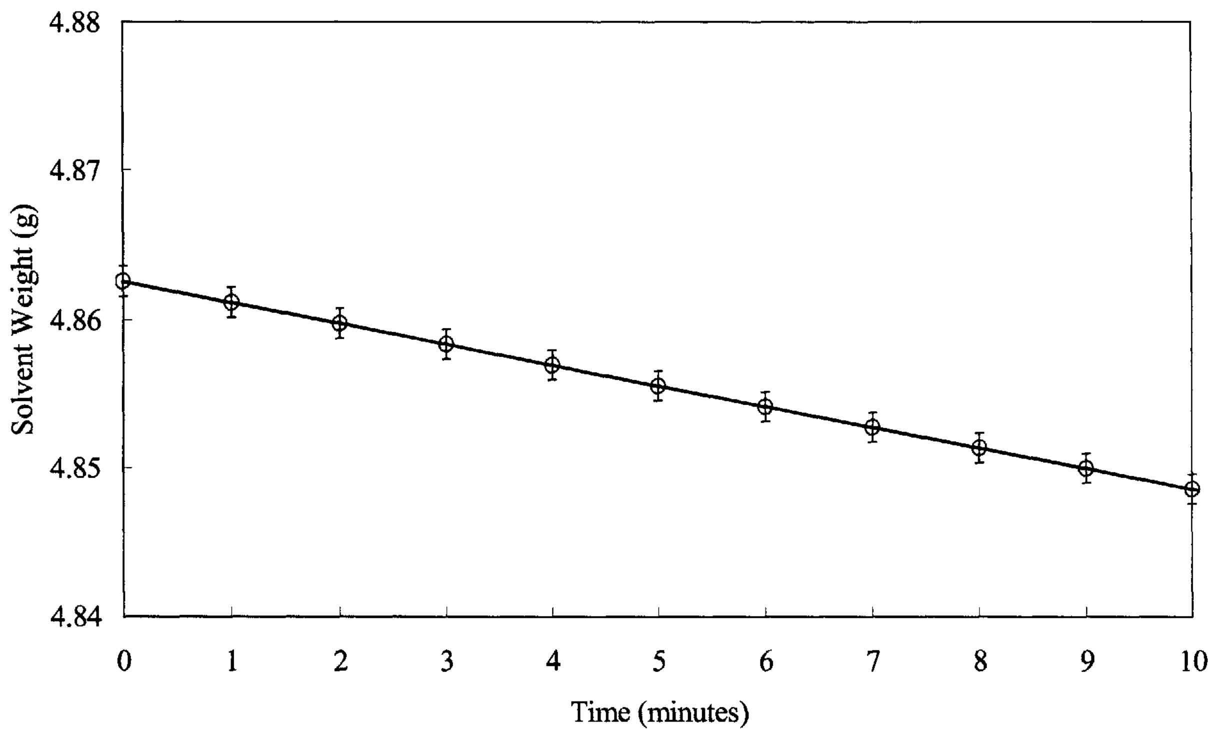

Figure 4-21: Mass transfer rate of PGMEA solvent.

Solvent Evaporation from a Rotating Disk

The mass transfer rate per unit area, $\dot{m}$, from a rotating disk, can be calculated from Mills [1987]:

$$\dot{m} = g_m \ln(1 + B_s) \quad (4.27)$$

where g_m is the mass transfer conductance at zero net mass transfer and B_s is the mass transfer driving force. When no air diffuses into the solvent and the solvent is the only species transferred:

$$B_s = \frac{m_{s,air} - m_{s,solv}}{m_{s,solv} - 1} \quad (4.28)$$

where $m_{s,air}$ is the mass fraction of solvent in the air far from the solvent surface and $m_{s,solv}$ is the mass fraction of solvent in the air just above the solvent surface. Assuming that the evaporated solvent is carried out quickly when surrounded by air, $m_{s,air} = 0$. Assuming that there is pure solvent at the liquid surface, $m_{s,solv}$ can be obtained from the saturation pressure of the solvent [AZ Product Bulletin].

The mass transfer conductance at zero net mass transfer, g_m, can be obtained by considering an analogy between convective heat transfer and mass transfer. Following Edwards et al. [1979], the heat transfer from a rotating disk in laminar flow can be obtained:

$$\mathrm{Nu}_r = \frac{0.585\,\mathrm{Re}^{1/2}}{0.6/\mathrm{Pr} + 0.95/\mathrm{Pr}^{1/3}} \quad (4.29)$$

where Nu_r is the Nusselt number, Pr is the Prandtl number and Re is the Reynolds number. Equation 4.29 is valid only when the Reynolds number is smaller than 1×10^5. Replacing the Nusselt and Prandtl numbers with the Sherwood and Schmidt numbers gives:

$$\mathrm{Sh}_r = \frac{g_m r}{\rho D_{solv,air}} \frac{0.585\,\mathrm{Re}^{1/2}}{0.6/\mathrm{Sc} + 0.95/\mathrm{Sc}^{1/3}} \quad (4.30)$$

Solving Equation 4.30 for the mass transfer conductance, g_m, yields:

$$g_m = \frac{0.585 \rho D_{solv,air}}{0.6/\mathrm{Sc} + 0.95/\mathrm{Sc}^{1/3}} \left(\frac{\Omega}{\nu} \right)^{1/2} \tag{4.31}$$

Combining Equation 4.31 and 4.28 with 4.27 gives:

$$\dot{m} = \frac{0.585 \rho D_{solv,air}}{0.6/\mathrm{Sc} + 0.95/\mathrm{Sc}^{1/3}} \left(\frac{\Omega}{\nu} \right)^{1/2} \ln \left(\frac{m_{s,air} - 1}{m_{s,solv} - 1} \right) \tag{4.32}$$

The amount of solvent evaporation at different locations on the rotating wafer during extrusion-slot coating can be obtained by integrating Equation 4.32 from the time of deposition to the end of cycle:

$$\Delta m(r,\theta) = \int_{t_0(r,\theta)}^{T} \dot{m}\, dt \tag{4.33}$$

where $t_0(r,\theta)$ is the time at which the photoresist is deposited at the radial position, r, and the angular position, θ and T is the total coating time. Figure 4-22 shows the amount of solvent evaporation at various radial positions at the end of the extrusion-slot coating process. An initial coating layer of 20 μm thickness was applied with different coating speeds on a 200 mm wafer. Each calculation was conducted at $\theta = 0$. The amount of evaporation at the periphery of the wafer is as much as 10 times the amount at the center of the wafer. Such a difference can result in uneven coating thickness. For example, using a coating speed of 80 mm/sec and an initial coating thickness of 20 μm, 1.2% of the deposited solvent evaporated at the periphery of the wafer as compared to 0.12% at the center. Sukanek's analysis (Equation 1.2) reveals that this evaporation causes the photoresist viscosity to increase by 0.1% at the periphery and 0.01% at the center. Emslie et al.'s analysis (Equation 2.10) shows that viscosity variations at the periphery and center of the wafer result in 3% and 1% coating thickness variations at the end of the spin coating

process. Assuming a final coating thickness of 1 μm, the difference in coating thickness caused by viscosity variation between the periphery and the center of the wafer is approximately 200 Å. The coating uniformity is approximately 70 Å. Therefore, it is critical to minimize the variations of solvent evaporation amount across the wafer for a uniform final coating.

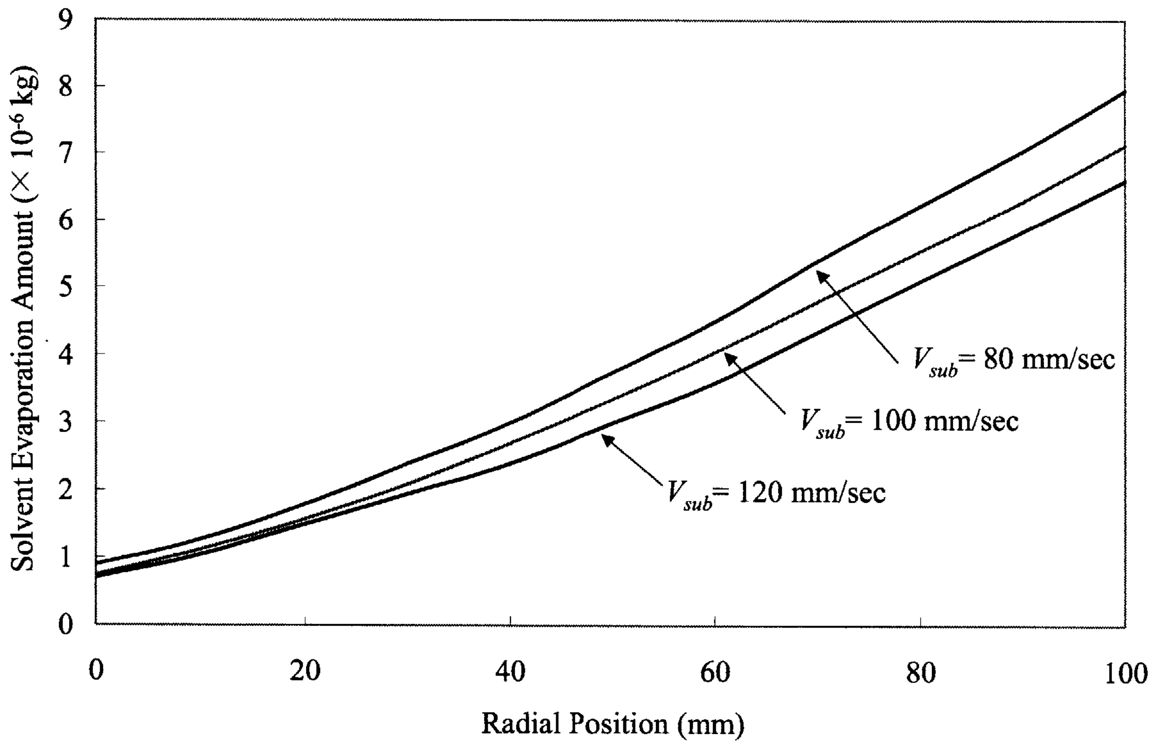

Figure 4-22: Evaporation on a rotating disk during extrusion-slot coating.

One way to decrease the solvent evaporation amount is to increase the coating speed. Figure 4-22 shows that when the coating speed increases, the total coating time decreases and the duration of the evaporation shortens. Consequently, the amount of evaporation decreases. However, the maximum coating speed is limited by defects, as discussed in Section 3.5. Another way to eliminate evaporation is to use a solvent-concentrated environment over a rotating disk. Solvent evaporation is prevented when the solvent concentration degree in the surrounding atmosphere is sufficiently high for the concentration gradient between the solvent and atmosphere to be negligible.

The following sections present theoretical analysis including the solvent-concentrated environment. The first step is to obtain the physical properties of PGMEA solvent in the gas state.

4.8.3 Physical Properties of PGMEA Solvent in Gas State

The physical properties of gaseous PGMEA solvent are required to analyze the flow over a rotating disk. This section will obtain the necessary properties.

Molecular Weight

The molecular weight of the PGMEA solvent is derived from its molecular composition. Figure 4-23 illustrates its molecular structure. From this, the molecular weight of PGMEA solvent is calculated to be 132.2.

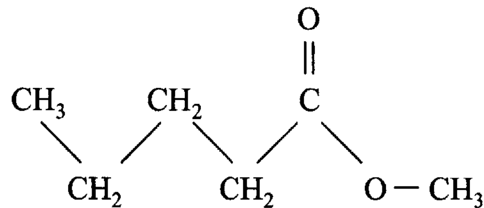

Figure 4-23: Molecular structure of PGMEA solvent.

Density

An estimation of the amount of the PGMEA solvent required to saturate a given volume of space is necessary. The PGMEA solvent saturates at 3.7 mm HG at the atmospheric pressure of 760 mm HG. This gives a fractional volume of 0.49%. Thus the volume of PGMEA solvent vapor to saturate a volume $\nabla_{chamber}$ is $0.0049 \times \nabla_{chamber}$.

Density of the PGMEA vapor can be estimated using the ratio of its atomic weight to that of a gas with a known density. PGMEA solvent is 4.72 times as dense as a nitrogen vapor of identical pressure and temperature, and has a density of 5.43 kg/m^3.

Viscosity

For organic compounds, Reichenberg [1979] present the method of estimating the viscosity of a gas:

$$\mu_{PGMEA\ Vap} = \frac{M^{1/2}T}{a^*\left[1+(4/T_c)\right]\left[1+0.36T_r(T_r-1)\right]^{1/6}}\frac{T_r\left(1+270\eta_r^4\right)}{\left(T_r+270\eta_r^4\right)} \tag{4.28}$$

where $\mu_{PGMEA\ Vap}$ is the viscosity of PGMEA vapor, M is the molecular weight of the solvent and T is the atmospheric temperature. T_c is the critical temperature defined as $T_c = 50.2 - 0.16M + 1.41T_b$. T_r is the reduced temperature defined as $T_r = T/T_c$. η_r is the reduced dipole moment given by $\eta_r = 52.46\frac{\eta^2 P_c}{T_c^2}$ where $P_c = \left(0.113 + 0.0032n_a - \sum \Delta p\right)^{-2}$ and η is the magnetic dipole moment. Finally, a^* is sum of a formula based on the atomic structure form. Reid et al. [1987] offers a formula and table to obtain the value of a^* for various chemicals. By solving Equation 4.28, the viscosity of PGMEA solvent vapor is obtained as 62.6 μPa-sec.

4.8.4 Effect of Spin Speed and Solvent Concentration on Flow above Rotating Disk

Section 2.6 reviewd previous works on the flow above a rotating disk. The studies revealed that three flow regimes can exist above a rotating disk: laminar, transient and turbulent, each of which are determined by the Reynolds number. This section studies the effect of spin speed and solvent concentration on the flow above the 200-mm rotating disks. Estimating the rotational speed and solvent concentration for the flow to remain in laminar regime is important. Once the flow above the wafer is laminar, evaporation of solvent can be predicted and thus, theoretical predictions of coating thickness and uniformity are feasible.

PGMEA vapor and air were used to analyze the flow. Table 4.1 shows the physical properties of the two. Figure 4-24 shows the corresponding radial positions obtained with Equations 2.19 and 2.21 with the given values.

Table 4.1: Comparison of density and viscosity of PGMEA solvent vapor with other gases.

Physical Property	PGMEA Vapor	Air	Water Vapor
Density (kg/m^3)	5.43	1.204	0.75
Viscosity ($\times 10^{-6}$ Pa-sec)	6.26	18.2	9.57
Kinematic Viscosity ($\times 10^{-6}$ m^2/sec)	1.15	15.1	12.8

Because the kinematic viscosity of PGMEA vapor is lower than the air by one-tenth the value, the radial positions for determining the regimes of flow over a rotating disk is decreased, as shown in Figure 4-18. Radial positions with a solvent-concentrated environment are obtained when the solvent concentration is assumed to be maintained at 100% in the surrounding area. When the solvent concentration reaches and stays at 100%, the flow above a rotating disk does not significantly affect the coating results, because there is no evaporation. In reality, 100% solvent concentration is difficult to maintain. Later experiments use concentrations of 30~80%. In such cases, the kinematic viscosity of air-solvent mixture is higher than that of pure solvent vapor but lower than the kinematic viscosity of air. Therefore, the radial positions will fall between the positions obtained using air and 100% solvent concentration.

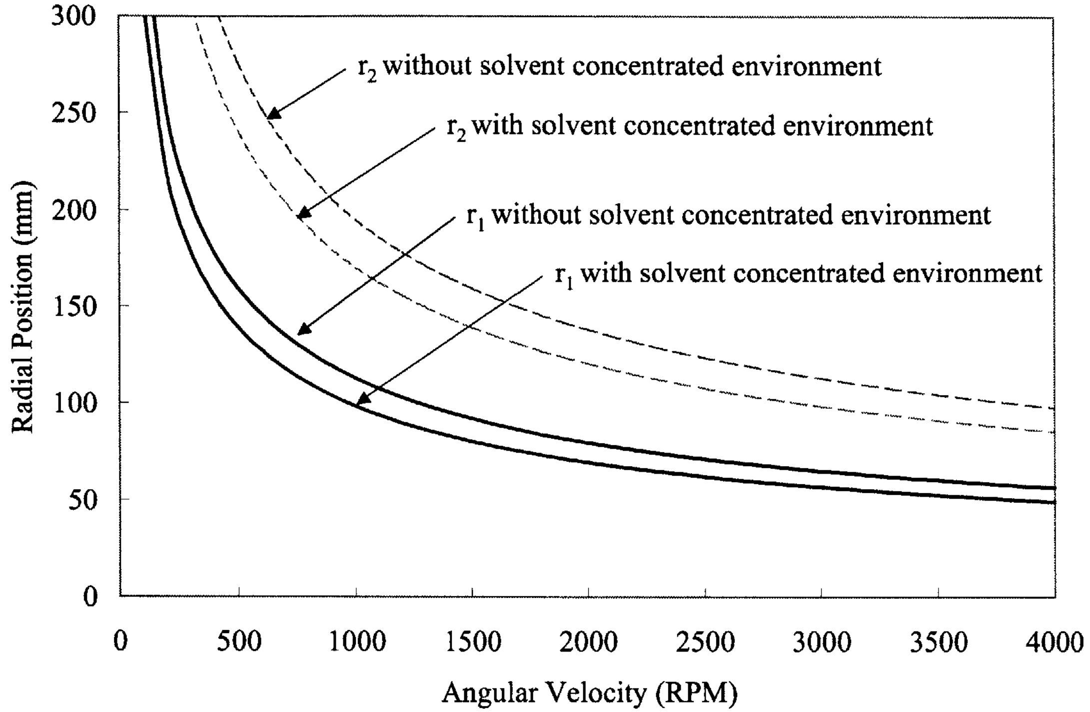

Figure 4-24: Effect of solvent-concentrated environment on flow above the rotating disk.

4.9 Summary

In this chapter, the methods of applying extrusion-slot coating on a rotating wafer were described. Two important parameters for establishing the initial coating layer were studied: initial coating thickness and uniformity. Initial coating thickness affects the coating efficiency. A thicker initial coating is desirable to for faster coating and to reduced defects in the coating layer. Thicker coatings, however, lower the coating efficiency. Initial coating uniformity affects the final coating uniformity. Because attaining a uniform final coating layer is important, the initial layer must attain the required uniformities suggested in Section 4.2.

Although extrusion-spin coating was only theoretically described in this chapter, some of its advantages over spin coating can be estimated. First, extrusion-spin coating will guarantee a higher coating efficiency because it uses less photoresist. In addition, the

extrusion-spin coating method can prevent some of the defects caused by conventional spin coating. The deposition in spin coating is only partial. It can cause two types of common defects: voids and striations. Because extrusion-slot coating coats the entire wafer with a uniform initial layer, defects caused by the spreading of resists from incomplete coverage will not appear.

However, the solvent evaporation is expected to be a problem when a thin initial coating layer is applied by extrusion-slot coating. Means for minimizing the evaporation need to be developed.

Chapter 5

Experimental Apparatus of Extrusion-Spin Coater with Solvent-concentrated Environment System

A prototype extrusion-spin coater was built to conduct experiments with the extrusion-spin coating method. Figures 5-1 and 5-2 illustrate the apparatus. An extrusion-spin coater consists of two major modules: an extrusion module and a spin coating module. The extrusion module is comprised of an extrusion head, an X-Z motion table, a gap measurement sensor, and a dispensing pump. The spin coating module is a spin coater, major components of which are a vacuum chuck, spindle rod, and motor.

Compatibility, flexibility, and precision were the three design goals for the prototype of the extrusion-spin coater. The prototype is based on a spin coater to ensure compatibility with other spin coaters. The extrusion head mount can mount different types of heads for flexibility. Accuracy and precision were the highest priority. Extrusion-slot coating requires an accurately controlled position and a coating speed with precise repeatability. Mechanical components of the extrusion-spin coater were selected to meet such requirements.

The following sections will describe each component and its functions in detail.

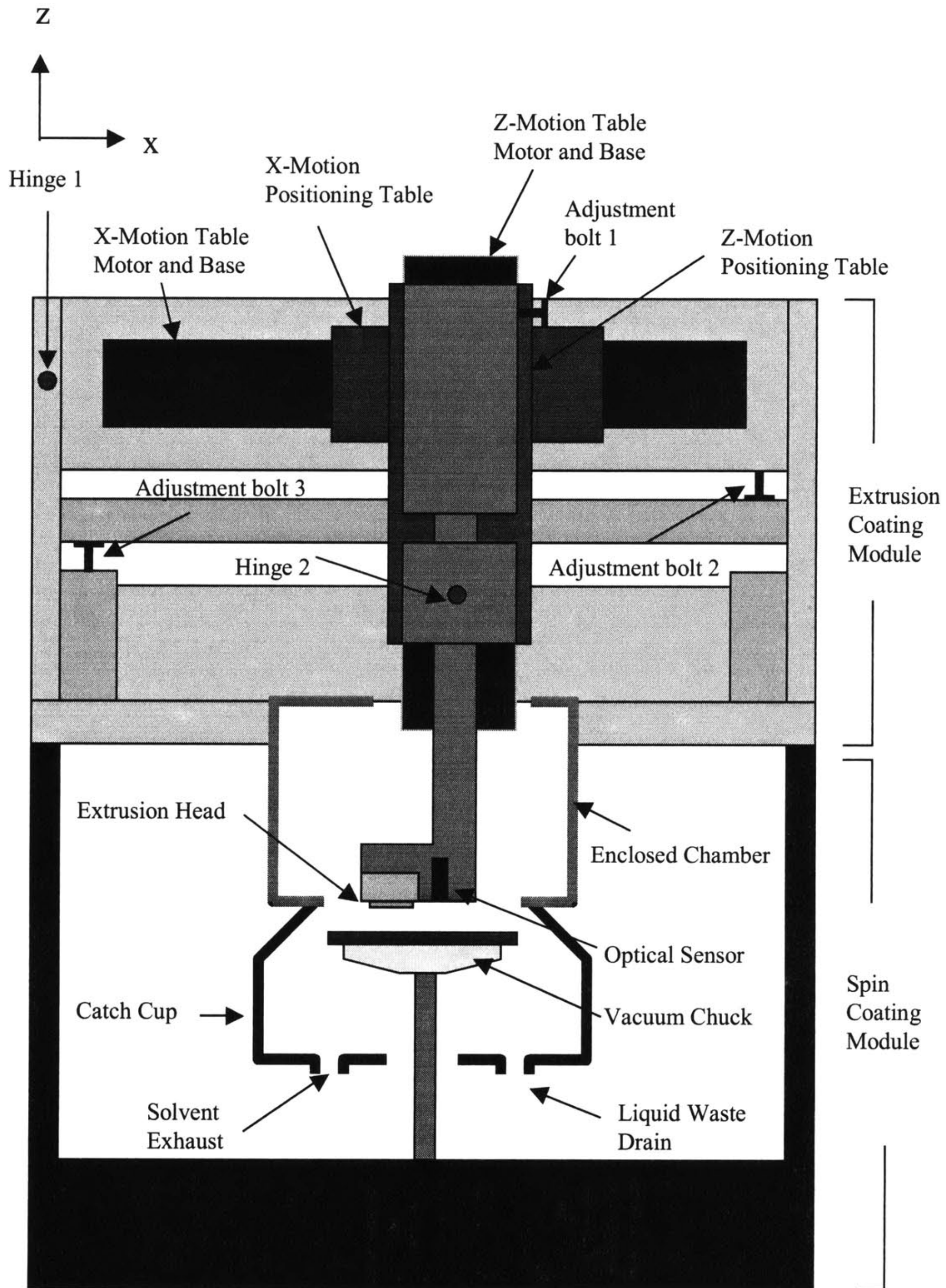

Figure 5-1: Schematic diagram of extrusion-spin coater.

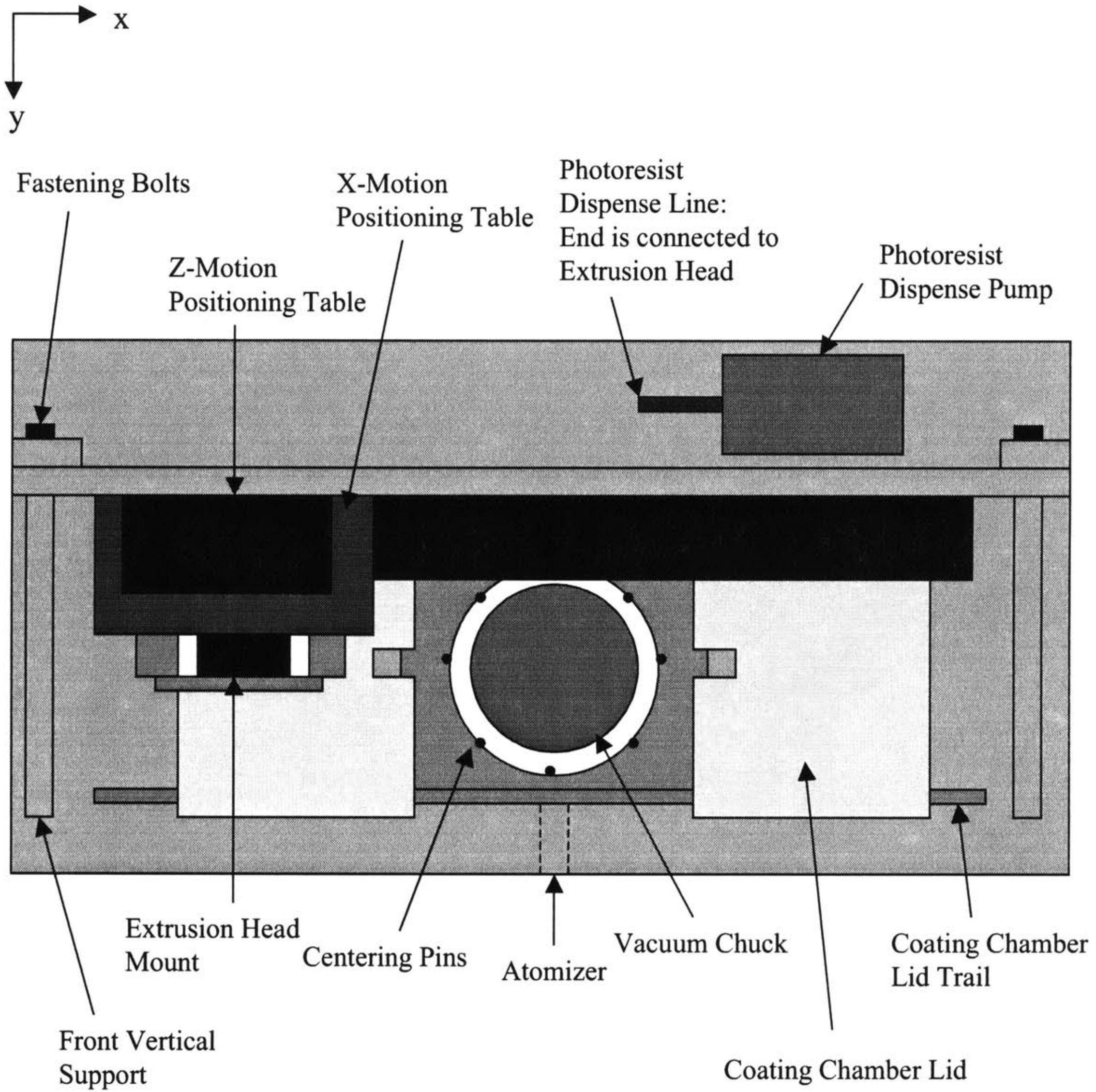

Figure 5-2: Top view of extrusion-spin coater.

5.1 Extrusion Head

Figure 5-3 is a schematic diagram of the extrusion head used for the experiments. The extrusion head is composed of two separable extrusion die pieces and a shim. The thickness, s, of the shim can be changed to allow different flow rates, Q. The shim thicknesses used in this study are 25 and 50 μm. The shim is inserted between the two extrusion die pieces. The three are bolted tightly together to prevent leaks. Photoresist is extruded through the aperture at the bottom of the head to dispense onto the slowly-spinning wafer. The gap distance between the extrusion head and the substrate is maintained between 40 to 100 μm to allow a predictable amount of neck-ins, as explained in Section 4.4.

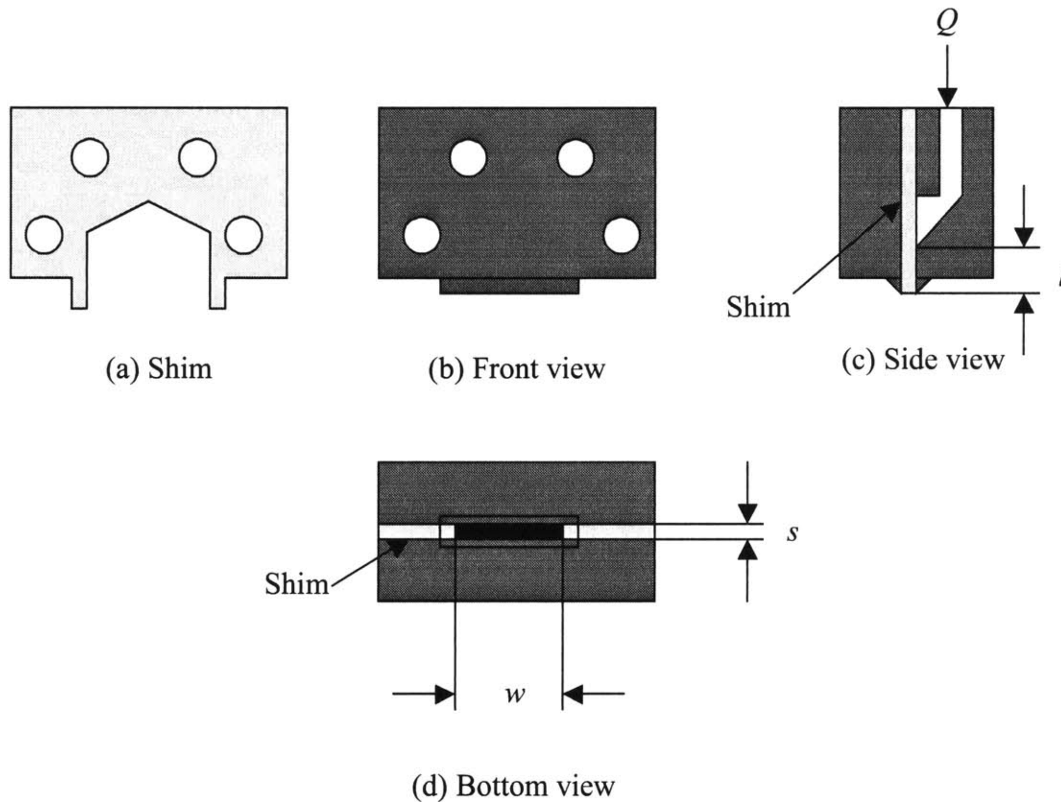

Figure 5-3: Schematic diagram of extrusion head.

Figure 5-4 shows the pressure drop in the extrusion head as obtained by Equation 3.3. The channel length is 10 mm. Depending on the type of photoresist used, different sizes of shims were used to meet the required pressure drop level. Figure 5-5 shows the relationship between the pressure drop created across the bead and various bead radii for maintaining a stable bead. For example, to maintain a 20-μm bead radius, the pressure drop must be maintained at ~ 1.5×10^3 Pa. Bead radius decreases as pressure drop reduces.

For the experiments, a 25-μm thick shim was used with a flow rate of 0.01 ml/sec or higher for deep UV resist and a 50-μm thick shim was used with a flow rate of 0.06 ml/sec or higher for i-line resist to maintain a coating bead 20-μm or bigger. It is possible to use thicker shims and lower flow rates for both resists. However, in such cases, the bead will not be formed at the fore tip of the extrusion head, resulting in unstable coating.

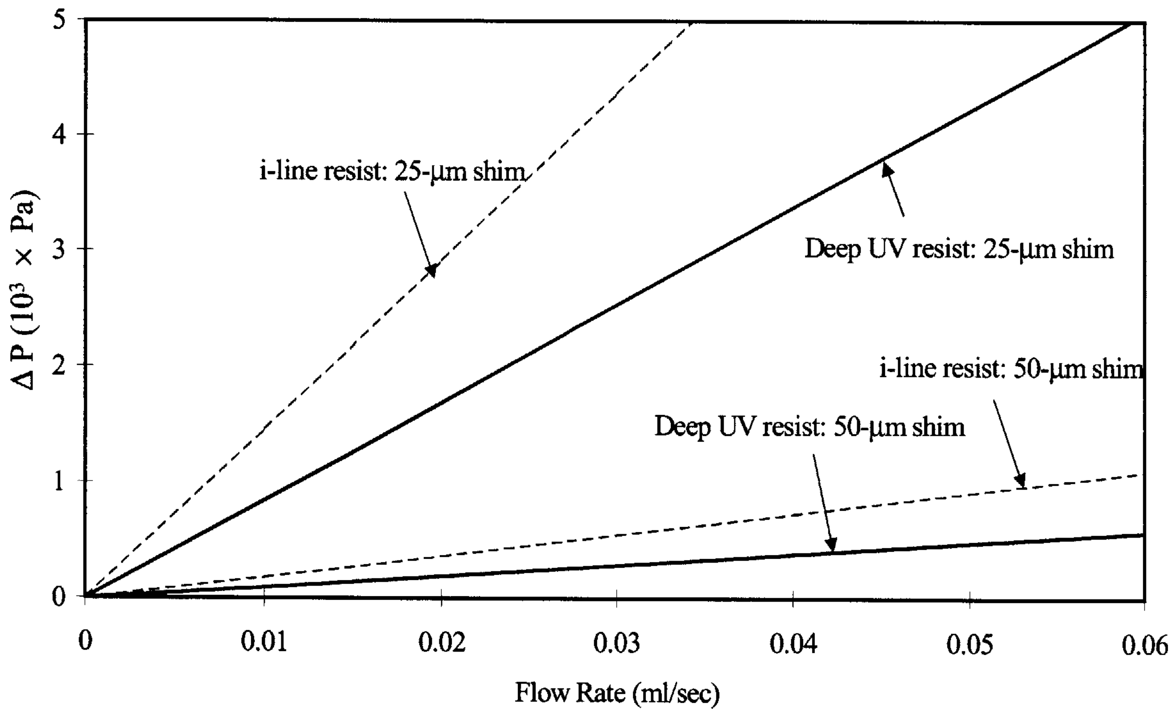

Figure 5-4: Pressure drop in extrusion head with various flow rates.

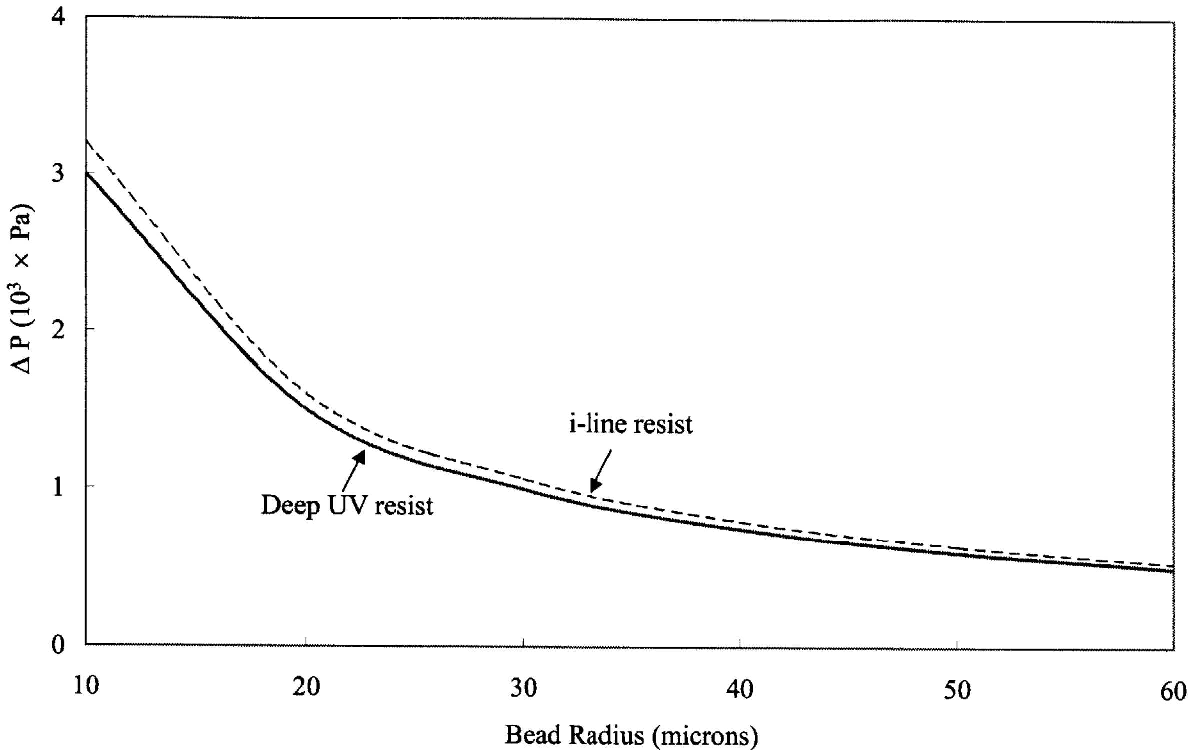

Figure 5-5: Pressure drop to maintain a stable bead.

5.2 Positioning System

The X-Z motion table positions the extrusion head precisely. Figure 5-6 shows the Daedal 800000 series table, selected to meet the design requirements. The following requirements must be met for successful extrusion-spin coating. The first requirement is positional accuracy, which is the motion table's ability to reach the same position when it moves over a certain length. It represents the precision level of the table. The positional accuracy of both the X and Z motion tables is 150 μm/m. For extrusion-spin coating, the length of table movement is less than 500 mm. Therefore, the actual error in the position of the extrusion head is only 75 μm. This error does not cause problems for the motion in the X-direction because a 75-μm overlap of photoresist affects neither the final coating thickness nor uniformity [Derksen, 1997]. It does, however, cause problems when the error occurs in Z-

direction. When the gap distance is varied by 75 μm, both the coating speed and the initial coating thickness cannot be estimated correctly, as discussed in Section 4.2.4. To solve this problem, a sensor that measures the gap distance between the extrusion head and the wafer was installed. The sensor will be described in more detail in the following section. When the Z-motion table is moving along the X-motion table, the latter table must move in a straight line along the X-axis (Figure 4-14). If the deviation from this straight line is large, the extrusion head slot misses the center to cause an uncoated center or a bubble entrapment, as discussed in Section 4.7.2. Straight line precision is 80 μm/m. When extrusion-spin coating is applied to a 200 mm wafer, the distance moved by the Z-motion table along the X-axis corresponds with the radius of the wafer. Therefore, the actual deviation from the straight line is 8 μm. Repeatability shows how accurately the same position can be reached. Tolerance of repeatability is ± 5 μm. This is satisfactory because 5 μm does not cause any significant changes in both neck-ins (Z-motion table) and overlap amount (X-motion table), as discussed in Sections 4.4, 4.5, and 4.6.

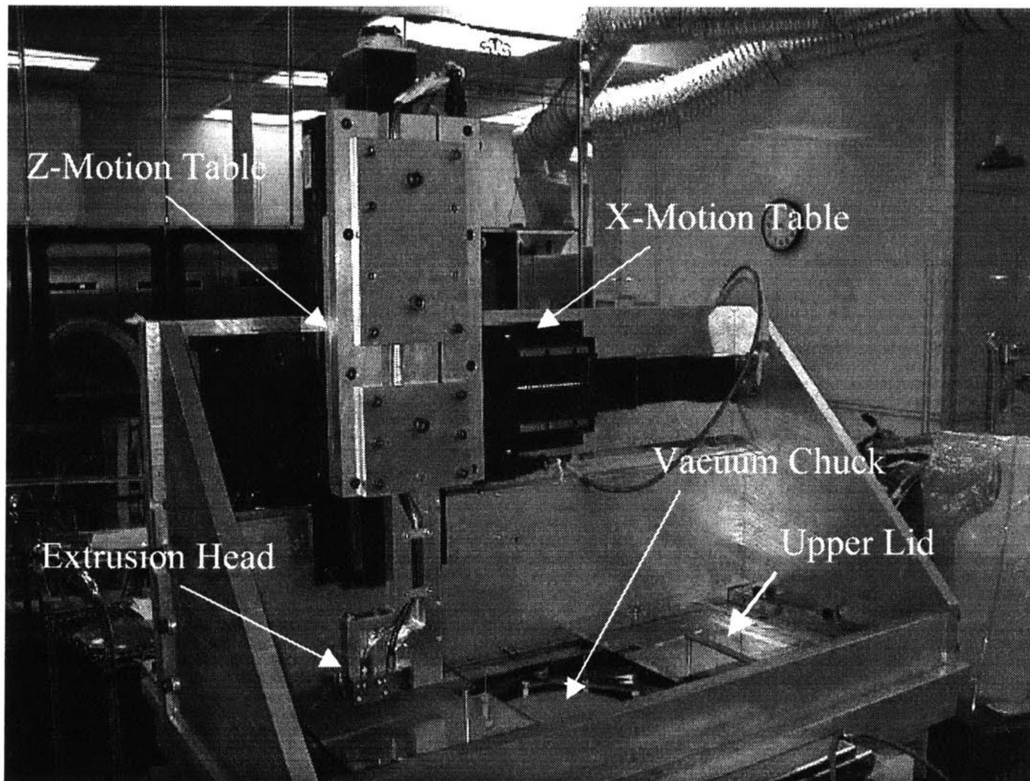

Figure 5-6: Picture of X-Z motion table.

5.3 Gap Measurement Sensor

A Philtec RC140L, a reflectance-compensated optical displacement sensor, measured the gap distance between the extrusion head and the wafer. It emits a light onto the surface of the substrate, measures the light reflected, and generates a voltage proportional to the intensity of the measured light. This particular sensor was selected because it can measure the distance for both stationary and moving targets. The sensor has a sensitivity of 4.9065 μm/mV and a linear range between 5.51 and 6.17 mm with corresponding voltage changing from 1 to 3 volts with a tolerance of ± 0.5%.

The gap variation was measured using the sensor. The wafer was loaded on the vacuum chuck and moved to the extrusion-slot coating position. The wafer was then rotated and the gap distance was measured for every 45° turn. Figure 5-7 shows the results when the given value for gap distance was 40 μm. The dotted line in the figure indicates the actual gap distance variation when the sensor did not provide any feedback. The gap varied from 40 ~ 120 μm. When the sensor provided feedback to the Z-motion positioning table, the gap variation was reduced to 40 ~ 80 μm (continuous line in Figure 5-7). Such variation causes the difference between theoretical estimations and experimental data. For example, when a 40 μm gap is given as an input during extrusion-slot coating, the actual maximum coating speed will be lower than the estimated value because of the points at which the gap distance is wider than designated. The effect of gap distance variation will be discussed in detail in Section 6.1.

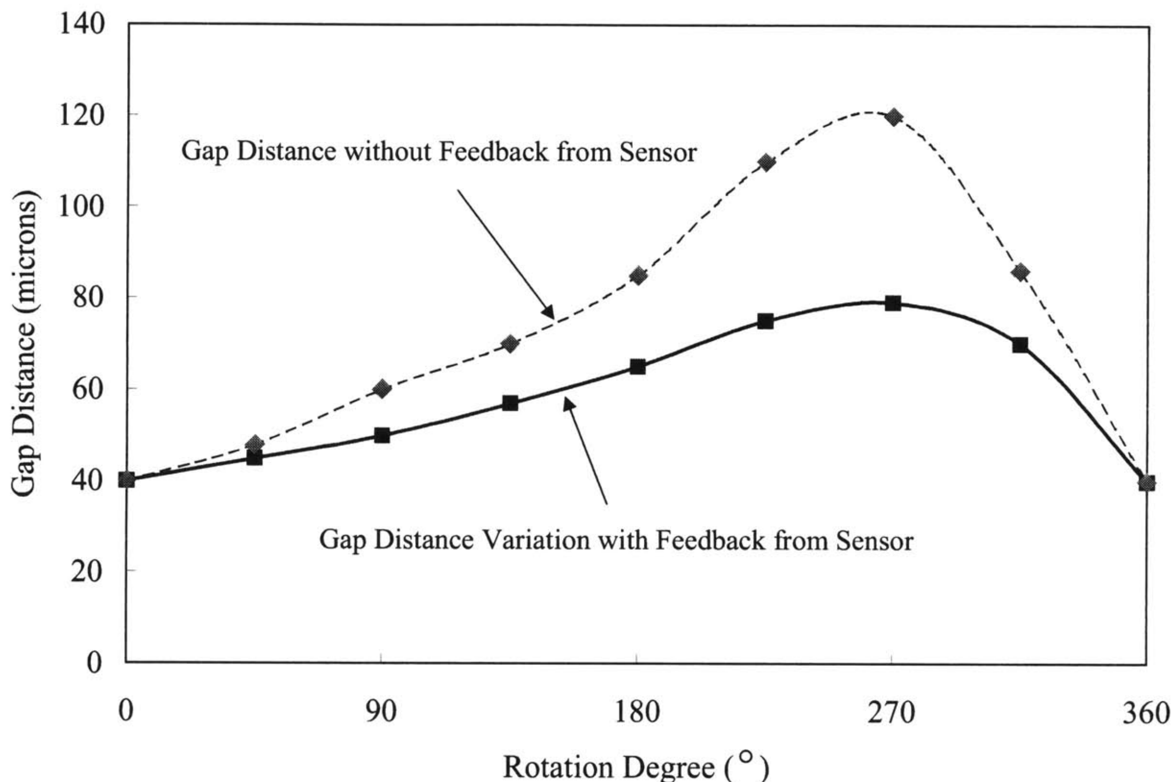

Figure 5-7: Gap variation measurement.

5.4 Photoresist Dispensing System

A dispensing pump controls the rate of the extruded flow. Two pumps were used in experiments. The first generation pump was a Millipore pump. It was used in some of the initial experiments to determine the feasibility of the extrusion-coating method. The second generation pump was a Cybor pump, designed to accommodate low flow rates.

5.4.1 First Generation Pump

A Millipore Gen-2^{Plus} photochemical dispense system was first used. It is a displacement pump with a 0.08 ml/sec minimum flow rate and 0.01 ml/sec step volume. The nominal lowest flow rate with the Millipore Gen-2^{Plus} pump is 0.08 ml/sec. However, that does not

include the uncompensated compliance of the supplying hose and the resistance in the extrusion head. The pump had to be calibrated to obtain an exact flow rate. A bleeding valve was later installed to decrease the minimum flow rate. Consequently, the minimum flow rate was reduced to 0.0348 ml/sec for i-line and 0.012 ml/sec for deep UV resist. The bleeding valve consists of two components: an on-off valve and an adjustment valve. The on-off valve turns the bleeding valve on and off. A needle valve with an adjustable dial was selected as the adjustment valve to control the flow rate. Figure 5-8 shows the pump calibration data with the bleeding valve for i-line and deep UV resists. To calibrate the flow rate, 1 ml of photoresist was dispensed at a flow rate of 0.08 ml/sec. The photoresist dispensed was weighed at intervals of 10 seconds to determine the actual dispense volume. The uncertainty in the flow rate was 2.5% for the i-line and 11.5% for the deep UV resist.

The first generation pump was used to test the feasibility of extrusion-spin coating. It, however, posed some problems. Figure 5-8 shows that when the flow rate is below 0.03 ml/sec, the pump does not provide a predictable flow rate. The flow rate can only be obtained by experimentation. In addition, the pump did not provide adequate suckback when the extrusion head reached the center of the wafer. It also had an unstable dispense at initiations. Dispense had to be repeated three to four times before the pump provided a stable dispense rate. Appendices B and C discuss suckback and unstable dispense problems, respectively.

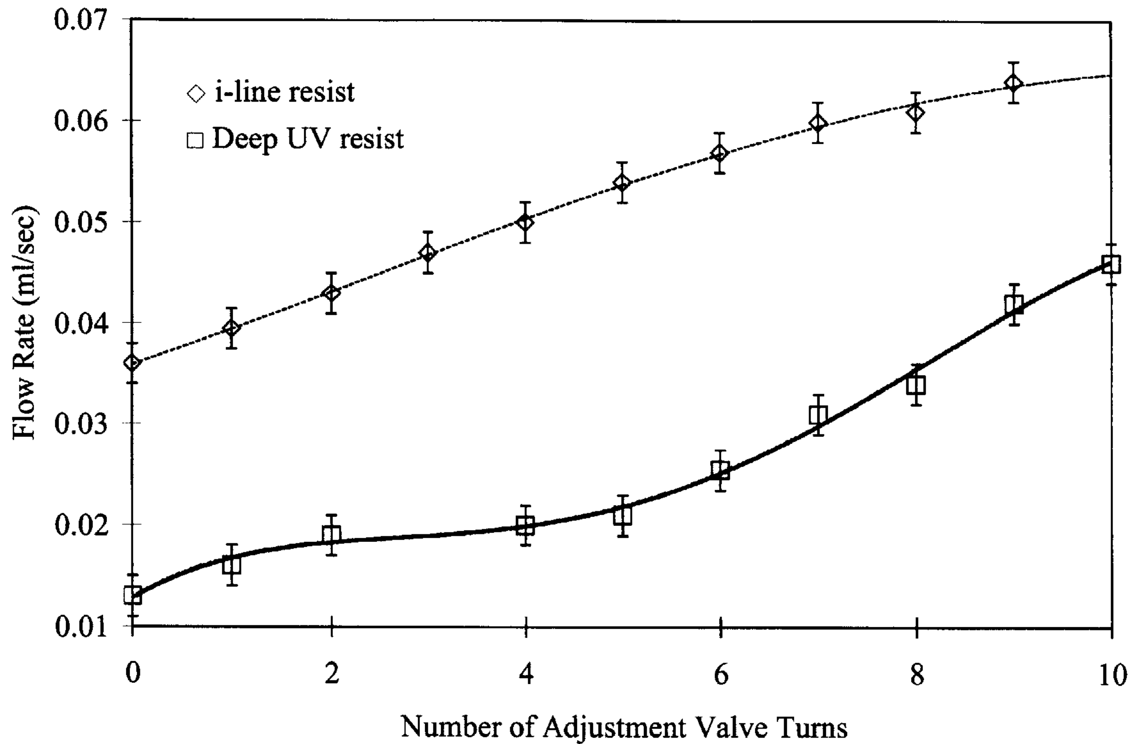

Figure 5-8: First generation pump calibration.

5.4.2 Second Generation Pump

A Cybor pump Model 5116 replaced the Millipore pump. The Cybor pump is a displacement pump with a 0.01 ml/sec minimum flow rate. The minimum suckback rate is also 0.01 ml/sec. It was selected because it can be controlled more precisely than the first generation pump. The correct amount of suckback is critical in dispensing the proper amount of photoresist at the center of the wafer (Appendix B). The bleeding valve was removed from the original experimental apparatus once the Cybor pump was added. The new pump could control the low flow and suckback rate precisely. Table 5.1 shows the detailed specifications of the Cybor pump.

Figure 5-9 shows the calibration data of the second generation pump. A programmed flow rate provides the inputs. The actual flow rate is measured. The range of the flow rates was 0.01 ~ 0.1 ml/sec. The deviation of the flow rate was within ± 5 % of

the given range. When a flow rate of 0.01 ml/sec was used, the extruded flow had a flow rate of 0.0098 ml/sec. Therefore, assuming that a total volume of 1 ml is dispensed onto the wafer using the pump flow rate of 0.01 ml/sec, the actual volume dispensed is 0.98 ml.

Table 5.1: Specifications of Cybor pump.

Parameter	Specification	
Programmable Volumes	Dispense	0.1 ml minimum
		10.0 ml maximum
	Suckback	0.0 ml minimum
		2.0 ml maximum
Programmable Rates	Dispense	0.01 ml/sec minimum
		5.00 ml/sec maximum
	Suckback	0.01 ml/sec minimum
		5.00 ml/sec maximum
Programmable Rate	Dispense	0.01 ml/sec
Resolution	Suckback	0.01 ml/sec

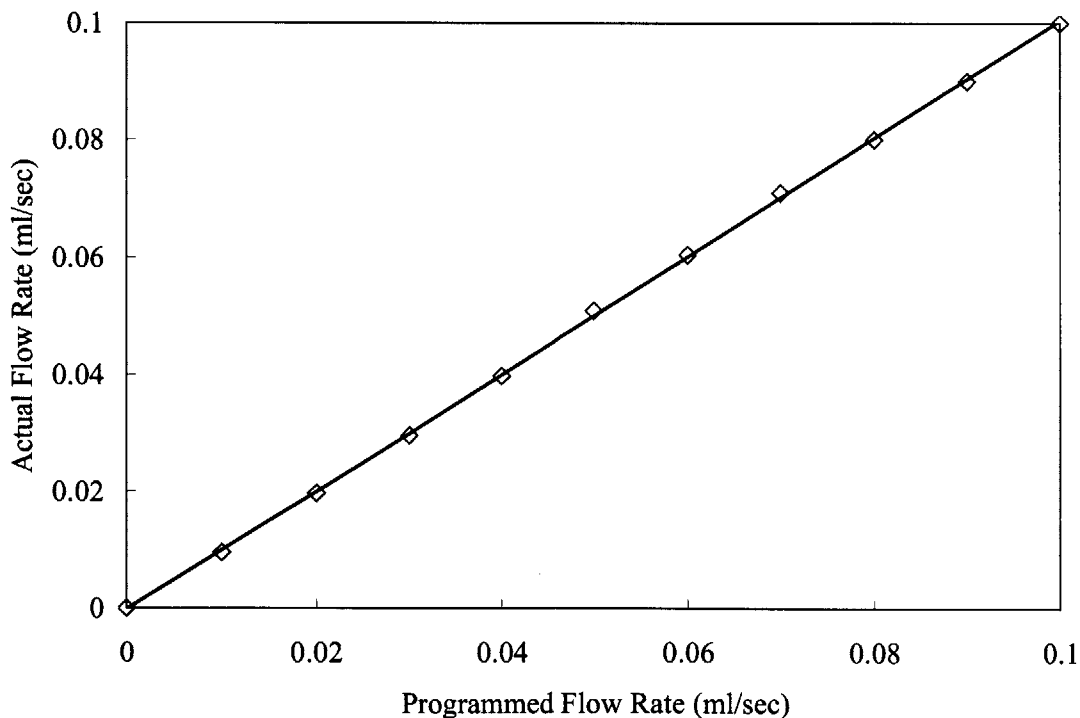

Figure 5-9: Second generation pump calibration with deep UV resist.

5.5 Spin Coater

The spin coater used for the experiments is one component of an SVG 90SE Track System. Basic components for the spin coater are a vacuum chuck, a spindle rod, a motor, and a catch cup. The vacuum chuck is made of Teflon to avoid contamination and chemical reactions. It uses 70 ~ 80 kPa of vacuum to hold a wafer during the extrusion-spin coating process. A spindle rod transmits torque from the motor to the chuck. The spindle rod mechanism is critical. Its dynamics are directly related to the spinning motion of the wafer. The catch cup surrounds the vacuum chuck during the coating process to catch and drain any photoresist flung off the wafer. It has a solvent exhaust vent through which the evaporated solvent is removed.

5.6 Control System

The control hardware for the extrusion-spin coater is divided into two systems: the positioning controller and the spinner controller. The primary controller is a Parker Compumotor AT6450 Controller with four channels of servomotor control, an analog to digital converter, and digital inputs and outputs. Two servomotor outputs control the X and Z-axis motion table. A third servomotor output controls the spinner elevation motor. The digital outputs of the controller send signals to the spinner controller, the photoresist dispense pump, the vacuum chuck, the centering pins, the Z-axis motor brake, and the spinner elevation motor brake. A 14-bit AD converter records the voltage from the optical sensor (gap measurement sensor) and updates it every 3.5 ms.

The secondary controller is a Pacific Scientific SC 755 Controller. It sets the spin speed and vertical position of the wafer. Digital inputs and outputs from the main controller feed the secondary controller with commands to run the extrusion and spin coating cycles. It generates a simulated encoder signal to allow electronic gearing of the spin speed with the X-axis motion of the primary controller.

5.7 Solvent Vaporizing Equipment

An atomizer in the enclosed chamber created small droplets of the solvent in the resists to improve evaporation and reduce excess moisture and sludge buildup. The solvent is combined with air by means of a low pressure siphon to produce an atomized spray. The atomizer can be adjusted by changing the inlet nitrogen and solvent pressure to provide fine, medium, or coarse drop size atomization. In this application, a fine atomization to support rapid evaporation is achieved by increasing the nitrogen pressure and lowering the solvent pressure. Figure 5-10 shows the atomizer setting. Figure 5-11 shows the atomizer calibration according to different nitrogen inlet pressures and different degrees of valve opening.

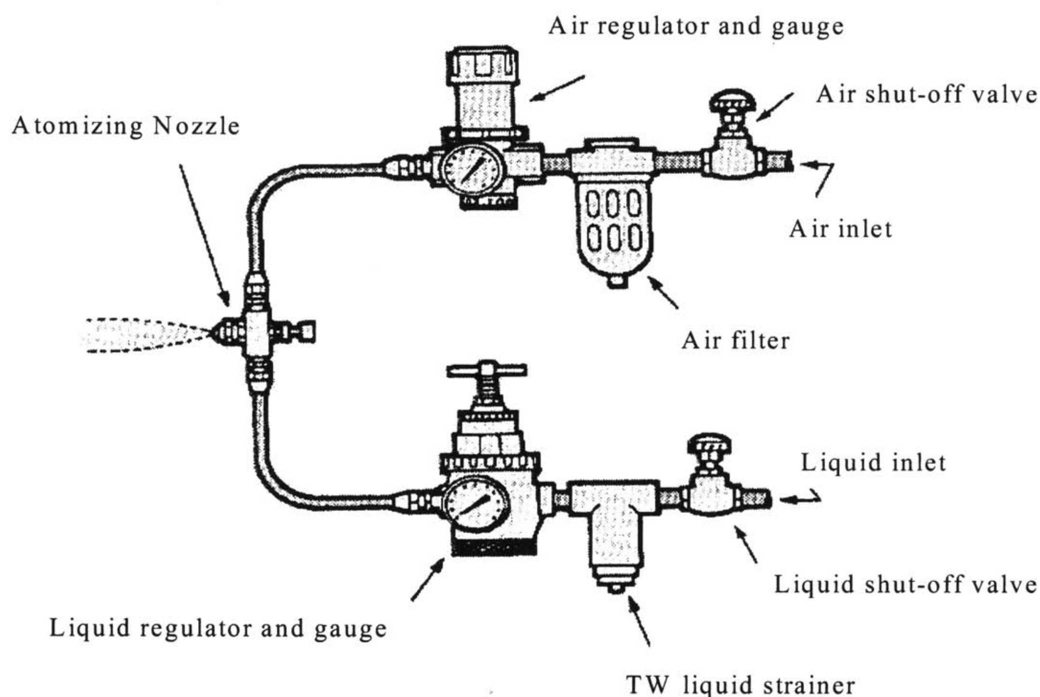

Figure 5-10: Schematic diagram of installed atomizer.

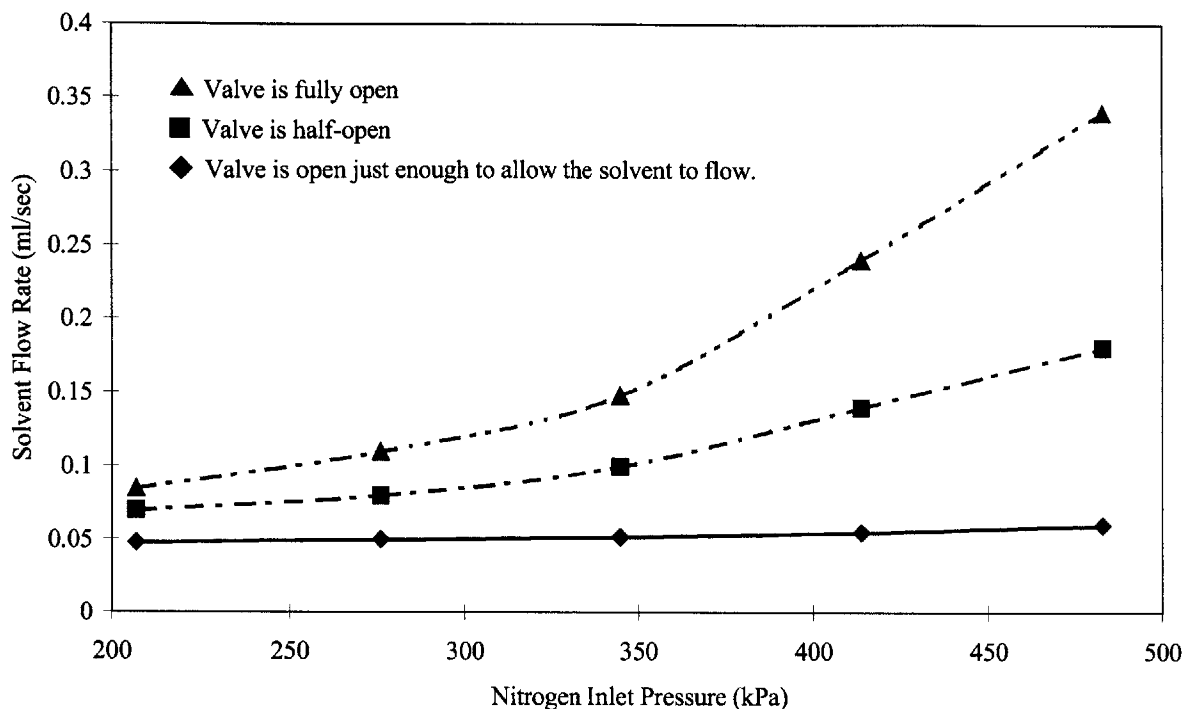

Figure 5-11: Atomizer calibration.

5.8 Solvent Concentration Measurement

A Berkeley Micro Instruments BMC200 Chemical Vapor Sensor provides a real-time measurement of airborne solvent concentrations. The sensor contains a silicon micromachined chip that detects vapor-induced mass changes in an absorbent polymer film. The BMC200 includes a micromachined flexural plate wave (FPW) sensor. The FPW vapor sensor offers very low absolute noise levels and hence very low vapor detection limits. The Chemical Vapor Sensor also contains a silicon micro-electro-mechanical system (MEMS) chip. On this chip is a micromachined membrane that is made of thin layers of silicon nitride, metal, and piezoelectric zinc oxide coated with a thin layer of polymer. Integrated on the plate are two interdigital transducers used to launch and detect ultrasonic flexural plate wavers. An oscillating voltage is applied to one transducer, producing mechanical stress in the piezoelectric zinc oxide layer. This stress generates flexural acoustic waves in the plate that travel toward the second transducer. When the

sensor is exposed to a chemical vapor, some of the chemical is absorbed into the polymer film, increasing the mass of the membrane, and lowering the velocity and frequency of the wavers [Grate, Wenzel and White, 1991]. Table 5.2 lists detailed specifications of the sensor.

The chemical vapor concentration is displayed in real time and stored for later analysis. All data were taken as frequently as every 10 milliseconds. The sensor is placed at the appropriate measurement locations in the enclosed chamber to measure the solvent concentration at various locations.

Table 5.2: Measurement specifications of sensor.

Chemicals	Most volatile organic chemicals
Chemical Sensitivity	1 Hz/ppm
Concentration Range	Zero to saturation
Resolution	1 Hz
Response Time	Sub-second
Measurement Rate	100 samples per second (max)

5.9 Alignment and Calibration

The biggest issue in designing an effective extrusion module is parallel alignment. Two alignments are critical: the X-motion table and the extrusion head. Each must be parallel aligned with the wafer. Three adjustment bolts were used to execute the necessary alignments. Adjustment bolt 2, shown in Figure 5-1, aligns the X-motion table with the wafer by rotating the upper support bar with respect to hinge 1. Adjustment bolt 1 aligns the extrusion head with the wafer coarsely by rotating the vertical support bar with respect to hinge 2. Adjustment bolt 3 is located behind the lower supporting bar, as shown in Figure 5-1. It fine-tunes the alignment of the X-motion table with the wafer.

The gap distance measuring sensor requires calibration. The sensor indicates different measurement values each time the system is turned on because the homing actions of the X-Z motion table and the spindle chuck motor vary every time the system is restarted.

The system is calibrated upon start up to attain the correct gap distance between the extrusion head and the wafer.

5.10 Operation of Extrusion Coating Module

Figure 5-12 illustrates that a cycle of the extrusion coating process consists of four major stages. In the first stage, the extrusion head scans the surface of the wafer, recording the gap distance between the wafer and the extrusion head using the sensor. In the next stage, the extrusion head comes down to the z position. The head is now away from the wafer by the required gap distance. In the third stage, the wafer is coated. The extrusion head moves toward the center of the wafer dispensing photoresist while it gets feedback from the sensor to keep the gap distance constant. At this stage, the wafer rotates with a changing rotational speed profile to keep the linear speed of the extrusion coating constant. A spiral pattern is formed, as in Figure 4-4 as velocity toward the center varies along the radial position and the tangential velocity is kept constant. In the last stage, the extrusion head is pulled away from the wafer after dispensing the proper amount of photoresist on the center region.

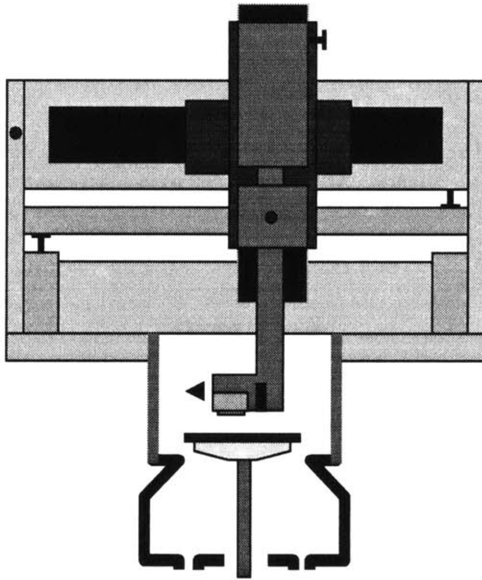

(a) Scanning wafer surface

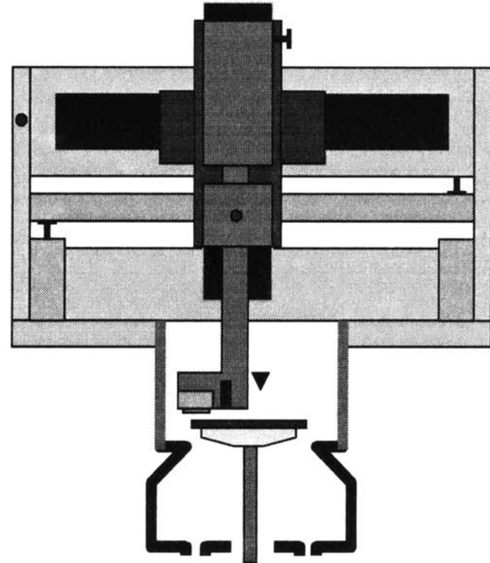

(b) Locating the coating outset position

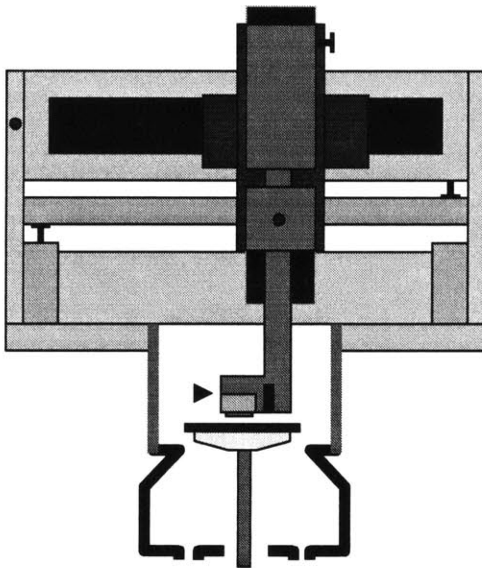

(c) Applying photoresist to the wafer using extrusion coating

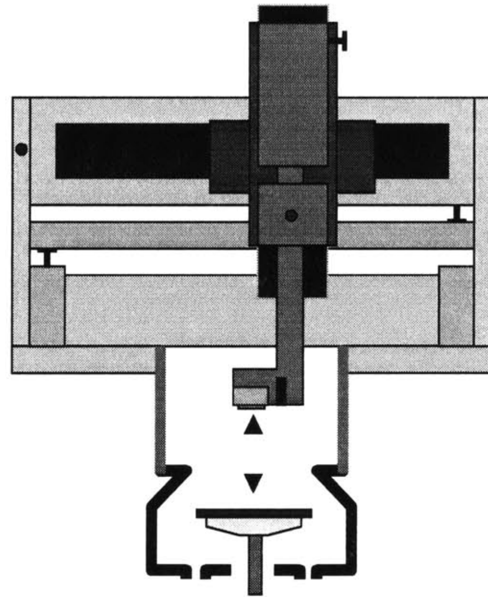

(d) End of extrusion coating Spin coating initiates

Figure 5-12: Extrusion coating operation

5.11 Operation of Spin Coating Module

The spin coating process begins when extrusion-slot coating ends. The wafer is first moved down to the spin coating position inside the catch cup. Consequently, high speed rotation begins to attain a desired coating thickness and uniformity. Varying the spin speed can control the final coating thickness. In the following experiments, high spin speeds of 1500~3000 RPM were used. An acceleration of 5000 RPM/sec is used for all experiments. At the end of the spin coating process, the wafer is unloaded to its original position and placed in an oven for the baking process.

Chapter 6

Experimental Procedures, Results and Discussion

This chapter presents the experimental results from extrusion-spin coating. All process variables and their effects on coating results are discussed. Once the effect of each process variable is identified experimentally, it is compared with theoretical estimations. Various process variables are optimized. Finally, extrusion-spin coating as a whole is evaluated.

6.1 Experimental Window of Coatability

The experimental window of coatability was produced for two photoresists: i-line and deep UV. Photoresist was deposited on a moving substrate using extrusion-slot coating. The defect-free coating speed and wet coating thickness data were collected. In this experiment, a bead vacuum was not applied.

Figure 6-1 shows the window of coatability for the possible coating regimes. The maximum coating speed and minimum initial coating thickness are also shown. A gap distance of 40 μm is used because it is the gap distance used throughout the experiments. The coating regions for deep UV and i-line resists are indicated by "◇" and "□" signs, respectively. This region indicates the coating speeds with various initial coating thicknesses that do not create defects during the extrusion-slot coating process. However, not all provide the required coating uniformity level for extrusion-spin coating. This will be discussed in Section 6.8. The continuous line that connects "◆" indicates the maximum extrusion coating speeds (80 ~ 170 mm/sec) with various initial coating thicknesses for deep UV resist. The dotted line that connects "■" shows the maximum coating speeds (80 ~ 140 mm/sec) for i-line resist. The lower bound lines for both photoresists indicate the

lowest flow rates the pump could deliver for each photoresist. Ruschak's theoretical analysis (Section 3.4.2) indicates that the range of maximum coating speeds are 90 ~ 180 mm/sec and 110 ~ 170 mm/sec for deep UV and i-line resists, respectively. Both theoretical maximum speeds are calculated for an 80 μm gap distance. When a gap distance of 40 μm is given as an input, the actual gap distance varies from 40 to 80 μm as shown in Section 5.3. If the gap distance can be maintained at 40 μm throughout the entire rotation, the maximum coating speed can be higher than the actual data. However, due to the gap variation during the rotation, the actual maximum coating speed is restrained by the largest gap distance. A comparison of Ruschak's analysis and experimental data indicates that his equation provides a good envelope for estimating maximum coating speeds.

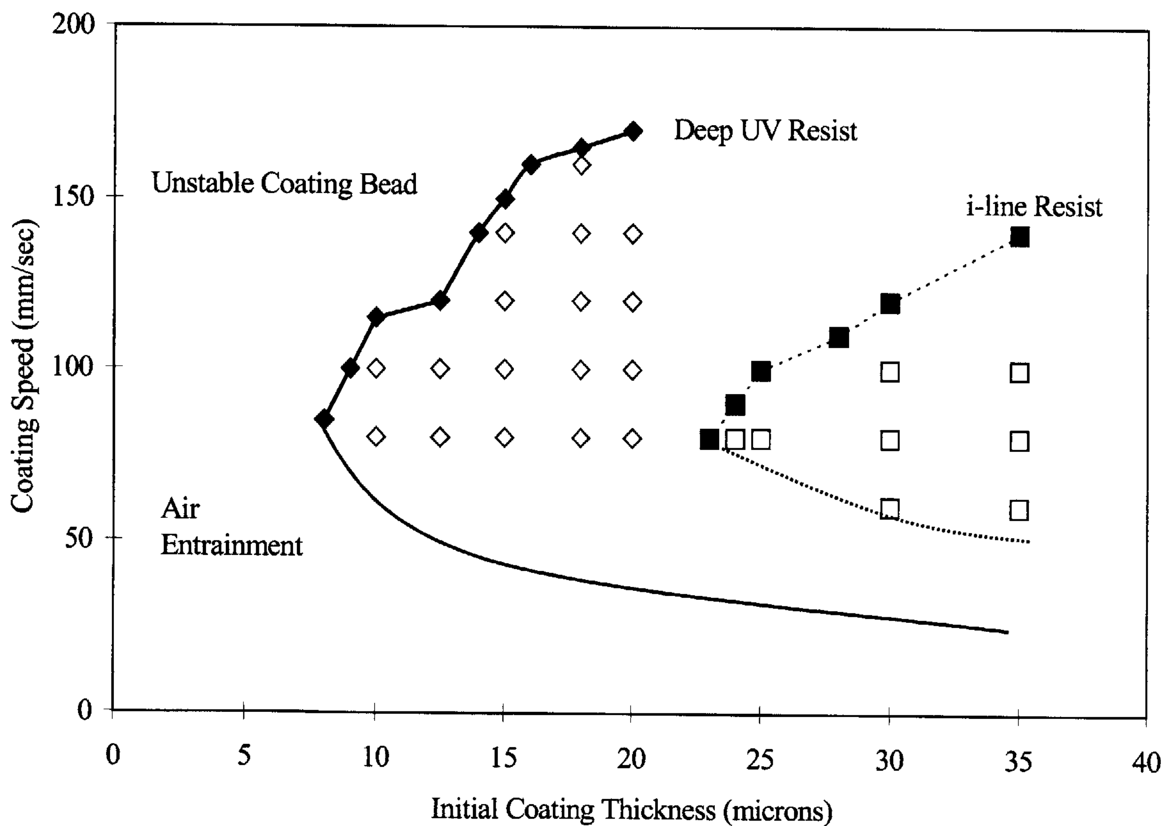

Figure 6-1: The window of coatability for extrusion-slot coating.

Figure 6-1 shows that the lower viscosity of deep UV resist allowed higher coating speeds and thinner coatings than those attained by i-line resist. The figure also indicates that as the coating thickness increases, the maximum coating speed increases. Such phenomena are consistent with Ruschak's analysis (Equation 3.5). The most useful information provided is the estimation of maximum coating speed and minimum coating thickness. From this information, minimum extrusion coating times and maximum coating efficiencies can be obtained using Figures 4-8 and 4-3, respectively.

6.2 Inspection of Coated Wafers

For all experiments, wafers were inspected twice: before and after the coating. Defects in the coated layer cause final thickness variations. If a bare wafer contains defects such as nicks or bumps, they will cause defects in the coated layer. If particles adhere to the coated layer during the coating process, they will also cause defects. Inspection of defects on bare and coated wafers is relatively easy and does not require any instruments. All the defects described in Sections 1.6 and 2.5 can be detected with bare eyes when the coated wafer is exposed to UV light. For experiments, all the bare and coated wafers were inspected. Only the defect-free coated wafers were measured using a spectral interferometer to obtain mean coating thickness and uniformity.

6.3 Experimental Procedure

For each experiment, the extrusion head and the X-motion table were aligned with respect to the wafer, the gap measurement sensor was calibrated, the extrusion head was cleaned to remove dry photoresist at the slot, and the wafer was inspected. Each experiment was conducted in accordance with the following procedures:

- The vacuum chuck was raised to the wafer-loading position and the wafer was placed on it.
- The wafer was centered on the chuck using the spin coating modules centering pin.
- The vacuum was turned on at 70 kPa to secure the wafer to the chuck.
- The wafer was lowered to the extrusion coating position.
- The extrusion head was positioned at the periphery of the wafer with the inner edge of the extrusion head slot exactly above the outer edge of the wafer.
- The gap between the extrusion head and the wafer was adjusted to desired distance (40 μm).
- When a solvent-concentrated environment was used, solvent vapors were inserted into the coating chamber until the concentration in the chamber reached 80%.
- The spinner began rotating at an initial rotational speed corresponding to the specified extrusion coating speeds (80~120 mm/sec).
- The pump started dispensing photoresist at a programmed flow rate (0.01~0.04 ml/sec).
- The extrusion head moved inward along the X-axis at a speed proportional to the wafer's rotational speed.
- The sensor feedback maintained a constant gap distance during extrusion-slot coating.
- The coating speed was maintained constant by increasing the wafer's rotational speed and the extrusion head's radial speed.
- When the leading edge of the extrusion head reached the critical radius (r = 20 mm), the wafer stopped accelerating and remained at a constant speed for the rest of the coating process.
- The extrusion head continued moving inward until it reached a specified position.
- The pump stopped dispensing and began suckback at a specified rate (0.01~0.02 ml/sec) to remove the excessive resist at the center of the wafer.
- The wafer stopped rotating.
- When a solvent-concentrated environment was used, the solvent vapor flow was stopped.

- The wafer was lowered into the catch cup and the extrusion head was removed from the coating area.
- The wafer began high spin speed coating (1500~3000 RPM).
- The spin coating of the wafer was stopped and the wafer was raised up to the loading position.
- The vacuum was turned off and the wafer was removed from the chuck.
- The wafer was baked in an oven (110°C for 30 seconds).
- The thickness and uniformity of the coated layer was measured using a Prometrix spectral interferometer.

6.4 Experimental Conditions

During initial experiments, the extrusion-spin coater was located in a laminar flow hood which provided filtered air to eliminate particles in the experimental area. The temperature in the room was unregulated and ranged from 15 to 28 °C. The relative humidity was also unregulated and ranged from 21 to 49%. Later, the extrusion-spin coater was moved to a clean room. The temperature and the humidity were then regulated to 23 °C and 43%, respectively.

6.5 Initial Experimental Results

Experiments to determine the feasibility of extrusion-spin coating were carried out using two types of photoresist: an i-line (AZ 1512) and a deep UV (AZ DX 1200 P). As listed in Table 1.1, the two photoresists have similar values of densities and surface tensions, but the viscosity of the i-line photoresist is 19 mPa-sec while that of the deep UV photoresist is 11 mPa-sec.

A set of experiments with each of the two photoresists tested the effectiveness of the extrusion-spin coating process in the absence of a controlled environment (e.g. temperature, humidity, and solvent-concentrated environment). An initial coating layer was applied

using extrusion-slot coating. After the initial coating was applied, each wafer was accelerated at 5000 RPM/sec to a rotational speed of 3000 RPM. The spin speed was maintained for 40 seconds. Following the high-speed spin process, each wafer was baked at 110°C for 30 seconds.

For all experiments, the final coating thickness was measured using a Prometrix spectral interferometer. Typically, 49 points on a coated wafer were selected and the thickness at each point was measured. Figure 6-2 and 6-3 show the initial coating results with i-line and deep UV resists, respectively. Coating uniformities were measured with various initial coating thicknesses. Both figures also indicate benchmarks for the two resists. The benchmarks were established using the conventional spin coating method with 20 ml of center dispense. Because the initial experiments were conducted in an uncontrolled environment, there could be a limitation in achieving the required coating thickness and uniformity. The benchmark indicates the best coating uniformity attained by conventional spin coating. It was necessary to compare the results between extrusion-spin and conventional spin coating methods to test the potential of extrusion-spin coating.

The theoretical prediction in Section 4.8.2 indicated that solvent evaporation during extrusion-slot coating will affect the coating uniformity. To verify the hypothesis, the coating uniformities with various extrusion-slot coating times were examined. For i-line resist (Figure 6-2), coating times of 21~26 seconds were used. For deep UV resist (Figure 6-3), coating times of 17~22 seconds were used. With the shorter coating time, coating uniformity has less deviation from the mean coating thickness (better coating uniformity). Two stages of uneven evaporations are involved, during extrusion-slot coating and during spin coating. During the extrusion-slot coating stage, evaporation occurs without the solvent-concentrated environment due to the spiral coating pattern. It takes approximately 20~40 seconds to complete extrusion-slot coating depending on the coating speed (Section 4.3). The photoresist dispensed at the edge of the wafer evaporates because a spiral shape forms while the extrusion head is moving from the edge to the center of the wafer. This causes the photoresist at the edge to be more viscous than the photoresist at the center. As a result, during the spin coating stage, the photoresist at the edge does not spread out as much as the photoresist at the center, leaving the thicker coating profile at the edge. Figures 6-2 and 6-3 corroborate this conclusion. As the coating time was increased, coating

uniformity became worse because the difference in the viscosities of photoresist grew. The second uneven evaporation occurs during the spin coating stage. It plays a partial role in degrading the coating uniformity. As Figure 4-12 indicates, a spin speed of 3000 RPM creates a transient regime above the edge of the rotating wafer that causes faster evaporation than in the laminar regime. The result is, again, a more viscous resist and a thicker coating profile on the periphery of the wafer.

Figure 6-4 shows the typical coating thickness profile from the initial coating results. Deep UV resist was used with 0.093 ml of dispense, 25 μm initial coating thickness, 3000 RPM high spin speed and 20 seconds of spin coating time. Mean coating thickness was 0.72 μm and coating uniformity was 22 Å. As predicted, a thinner coating is formed at the center region than at the periphery region. These phenomena correspond with the analysis in Section 4.8.2.

Despite the failure to meet the required coating uniformity (5Å), initial coating results strongly imply that extrusion-spin coating has the potential to be a more efficient method than conventional spin coating. Results in Figures 6-2 and 6-3 show that using both i-line and deep UV resists, coating uniformities obtained by extrusion-spin coating are either the same or better than the conventional spin coating with only one-twentieth of the resist amount used.

Initial experiments indicate that deep UV is more suitable for the extrusion-spin coating method because it can produce better coating uniformity with less dispense. As the industry trend is also moving from i-line to deep UV, the rest of this thesis will study the results of deep UV.

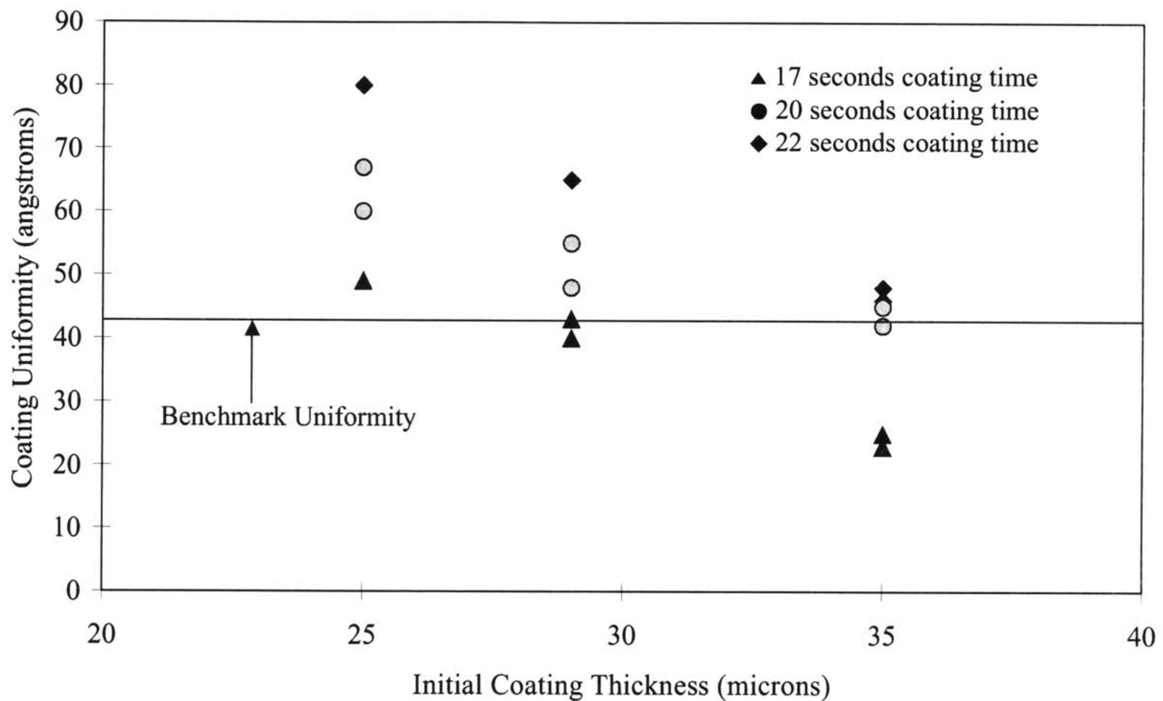

Figure 6-2: Uniformity data for an i-line resist.

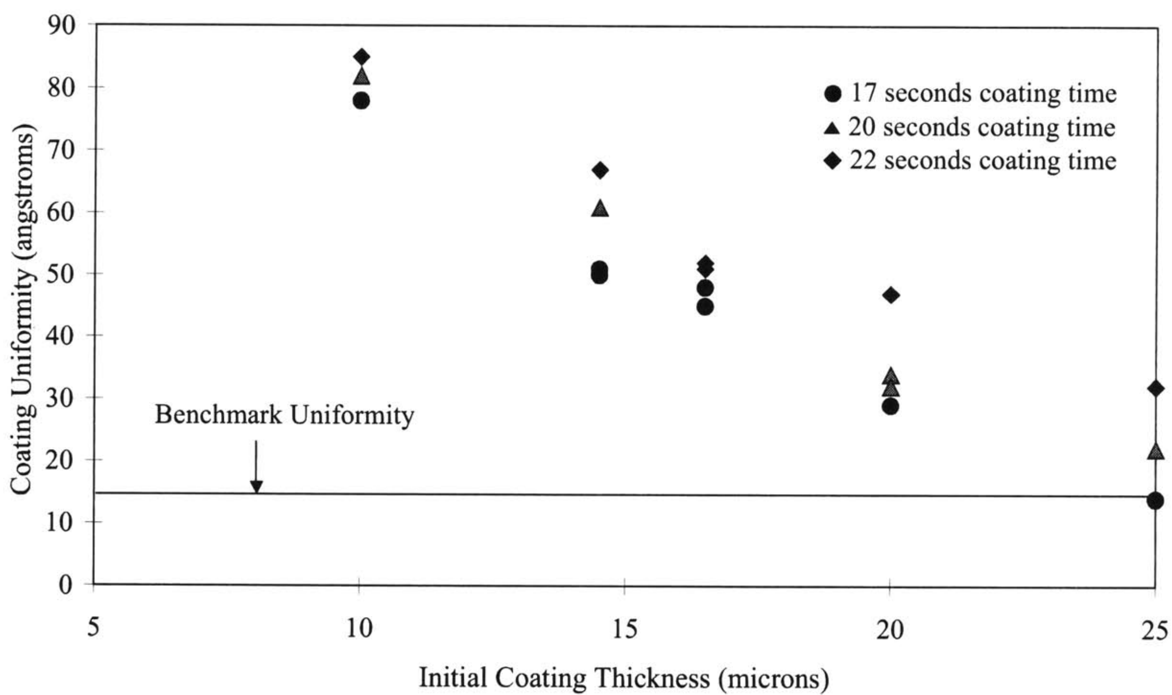

Figure 6-3: Uniformity data for a deep UV resist.

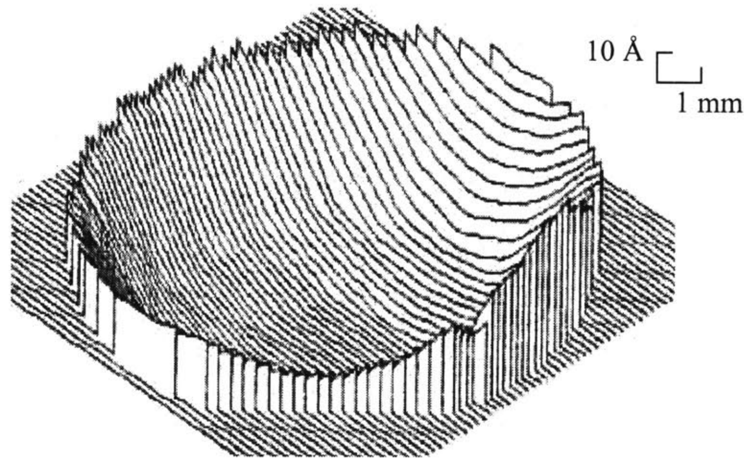

Figure 6-4: Coating thickness profile from initial coating results.

6.6 Initial Solvent-concentrated Environment

The model of Emslie et al. (Equation 2.10) predicts that an initially uniform coating will remain uniform throughout the spin coating process, provided that the density and viscosity also remain constant, independent of time and radial position on the wafer. One way to maintain the density and viscosity of the photoresist constant over the entire wafer is to create a solvent-concentrated environment. When the solvent concentration in the environment is over 80%, the solvent concentration gradient between the environment and the photoresist film reduces. The mass transfer rate was again measured by a micro-scale using same method in Section 4.8.2. The solvent evaporation rate was reduced to 1.2×10^{-7} $kg/m^2 \cdot sec$ from 1.1×10^{-6} $kg/m^2 \cdot sec$. Using 80% solvent concentration, coating speed of 80 mm/sec and initial coating thickness of 20 μm, 0.12% of the deposited solvent evaporated at the periphery of the wafer compared to the 0.02% at the center. This evaporation caused the photoresist viscosity to increase by 0.01% at the periphery and 0.004% at the center. Using Emslie et al.'s analysis (Equation 2.10), viscosity variations

between the periphery and center of the wafer result in 5 Å coating uniformity, assuming the final mean coating thickness is 1 μm. This uniformity meets the required level.

Initial experiments tested the potential of a solvent-concentrated atmosphere. Figure 6-5 illustrates the results from the initial experiments. In the previous section, the established benchmark uniformity using spin coating did not meet the required uniformity level. The best coating uniformity was 15 Å using deep UV resist. A new benchmark uniformity was established using extrusion-spin coating, using 6.89 ml of deep UV resist with 60% solvent concentration. As a consequence, a coating uniformity of 6 Å was obtained. Three experiments were conducted afterwards with an equal amount (0.81 ml) of photoresist. The coating uniformity improved as the concentration of the solvent in the atmosphere increased. Figure 6-5 also indicates that by using the extrusion-spin coating method approximately equal uniformity with benchmark is obtained using only one-ninth the amount of photoresist.

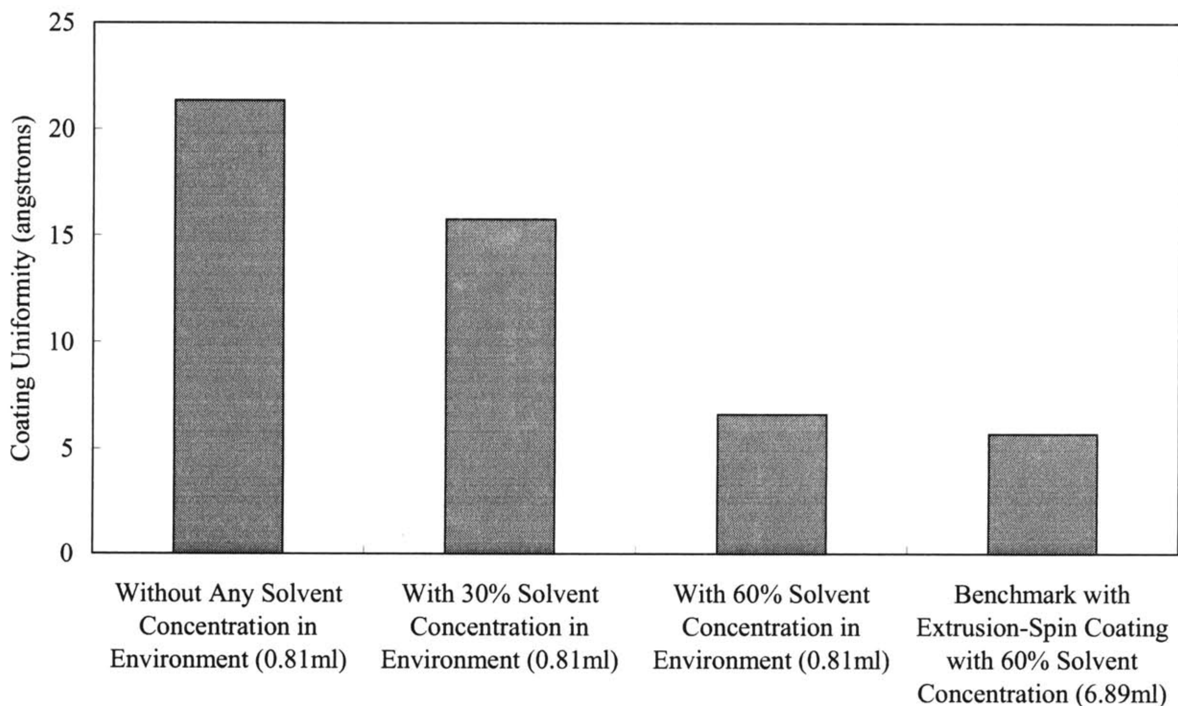

Figure 6-5: Coating uniformity improvement with increasing solvent concentration in environment.

6.7 Extrusion-Spin Coating with Solvent-concentrated Environment

6.7.1 Solvent Concentration Measurements during Extrusion-Spin Coating Process

The BMC200 Chemical Vapor Sensor measured the solvent concentration in the enclosed chamber at various locations on the wafer with respect to time. Solvent concentration was uniform over the entire wafer except, at the periphery regime. Figures 6-6 and 6-7 illustrate the measurement results at the center and the periphery of the wafer, respectively. All curves indicate the concentration measurement during the extrusion-spin coating process. Solvent vapor was introduced into the chamber for 20 seconds before the extrusion-slot coating, which was conducted for 30 seconds with continuous inflow of the solvent vapor. The solvent vapor input was then stopped and spin coating began. The spin coating step lasted 30 seconds. After the spin coating, the wafer was unloaded to its original position. The first and third curves indicate the concentration measurement with the exhaust valve closed. The second curve indicates the measurement when the exhaust valve was opened to allow outflow of the solvent vapor during the entire coating process.

Solvent concentration reached the 80% saturation in 20 seconds with the exhaust valve closed (no outflow of solvent vapor). The solvent concentration level was maintained well above 80% during the extrusion coating process. However, after the solvent vapor input ceased at the end of extrusion-slot coating (20~50 seconds), solvent concentration decreased during the spin coating process (50~80 seconds). This indicates that there was a leak in the coating chamber.

Several attempts were made to stop the leak in the coating chamber. However, the structure of the existing spin coater prevented such efforts. Design of the spin coater will have to be modified to eliminate the leak. All the experiments in this thesis were conducted with the presence of a leak.

The solvent concentration reached 80% saturation in about 40 seconds with the exhaust valve open. The slope of the second curve in Figure 6-6 is moderate compared to

those of the first and third curves before spin coating. It took a longer time to reach the same concentration level. In addition, twice the amount of solvent vapor had to be inserted into the coating chamber to achieve the same concentration level as compared to the case with no exhaust flow. After the extrusion-slot coating ended, the slope of the solvent concentration was steeper than the first and third curves. The solvent concentration decreases more quickly with an exhaust flow than not. This was caused by the exhaust of the solvent vapor, in addition to the leak in the coating chamber.

Solvent Concentration Variation at Periphery of Wafer

Figure 6-7 shows the solvent concentration variation at the periphery of the wafer as a function of time. The wafer periphery is located at the boundary of the enclosed chamber and catch cup. There is an opening of 10 mm around the periphery of the wafer. Most of the solvent vapor leak occurs through this opening. Figures 6-6 and 6-7 show this clearly. They show that in the first 50 seconds of cycle time, the increase in solvent concentration is almost identical. However, when solvent inflow ceases and spin coating begins, the decrease rate of solvent concentration is higher at the edge of wafer than at other regions. In the other regions, the solvent vapors take 80~90 seconds to be completely exhausted. At the periphery of the wafer, however, it takes only about 50 seconds due to the existing leak. This leak affects the coating thickness, profile and uniformity. The effect of the leak will be discussed in the following section.

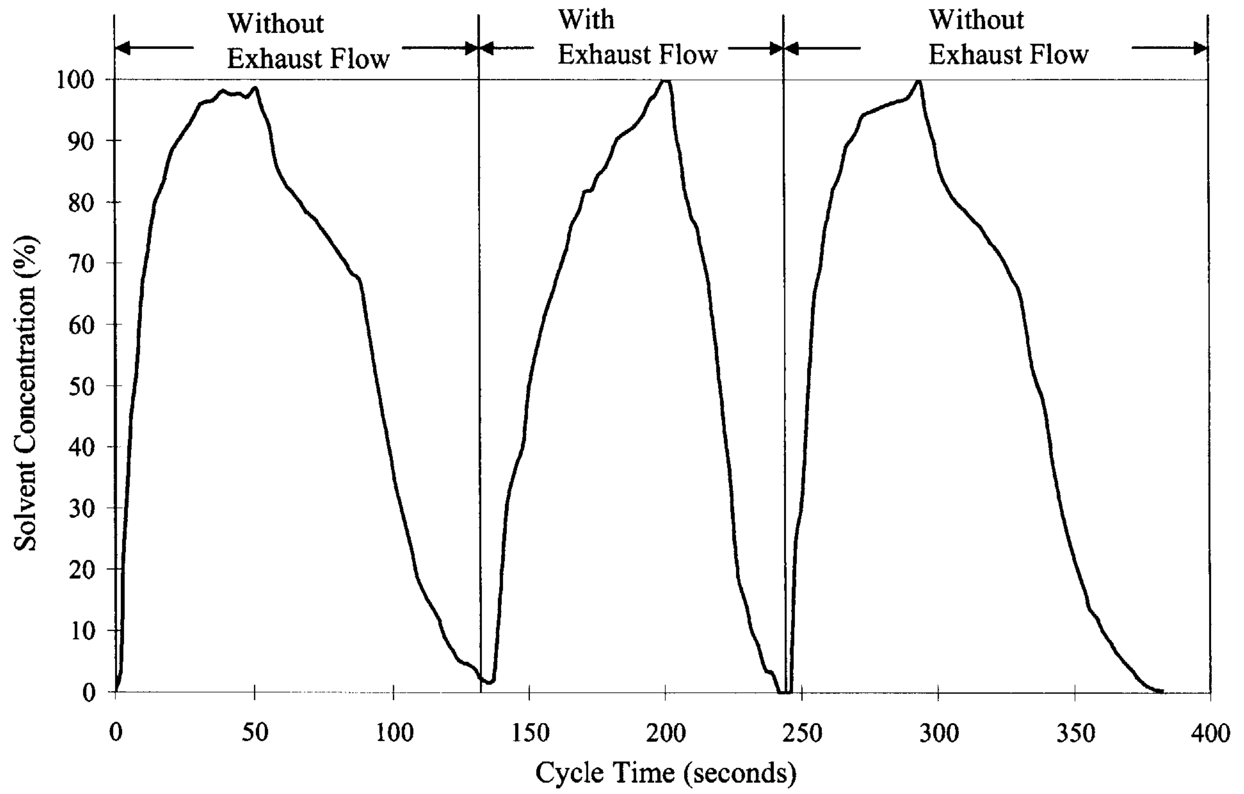

Figure 6-6: Solvent concentration measurement at the center of the wafer.

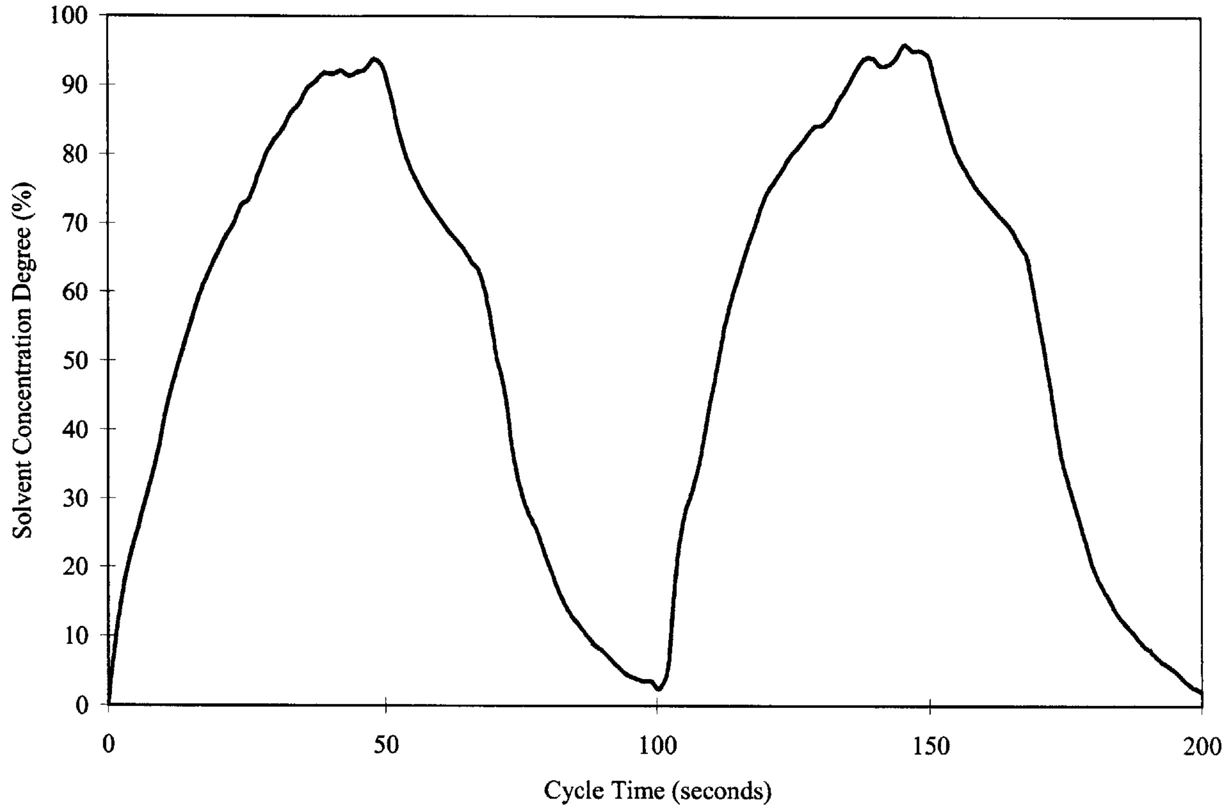

Figure 6-7: Solvent concentration measurement at edge of wafer.

6.7.2 Unsteady Solvent-concentrated Environment

The solvent concentration was not constant during the extrusion-spin coating process due to the leak. Thus, the term "solvent concentration degree," will refer to the average concentration degree during the extrusion-slot coating process in this thesis. For example, the first graph in Figure 6-6 indicates an approximate 90% solvent concentration.

Solvent concentration variation during the coating process was particularly a problem with an exhaust flow. Figure 6-8 shows the coating uniformity in both cases, with and without the exhaust flow. The coating uniformities were worse (more deviation from the mean coating thickness) with the exhaust flow than without. Predicting coating thickness was also difficult. Therefore, all the experimental data presented in the rest of this thesis were collected only when the exhaust flow was prevented.

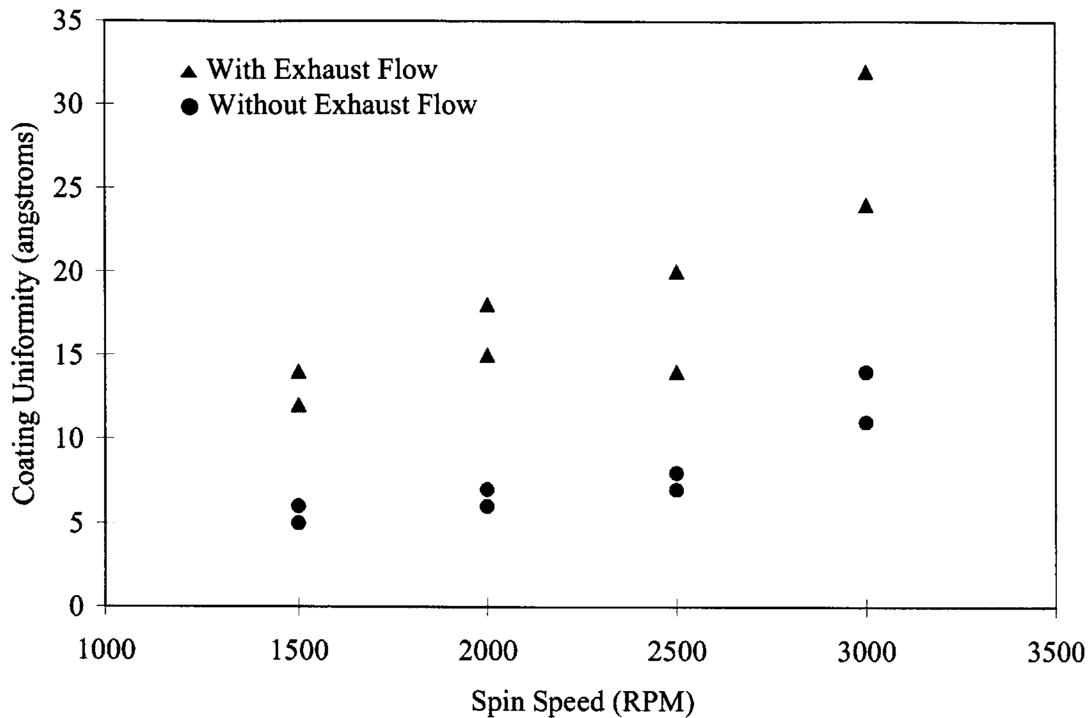

Figure 6-8: Comparison of coating uniformities.

Although the exhaust valve in the spin coater was kept closed, the leak at the periphery of the wafer allowed the solvent vapor to act as if there was an exhaust flow. The leak flow has lower flow rate than the normal exhaust flow. Its rate can be estimated by using information from Figure 6-6. We recorded the durations for solvent vapor to be completely exhausted from the coating chamber after a cycle of extrusion-spin coating. They are 10 and 50 seconds with and without the exhaust flow, respectively. Because the coating chamber was maintained closed during the entire coating cycle, the evacuation of the solvent vapor in the absence of exhaust flow was only caused by the leak. From this, the rate of leak flow can be estimated to be approximately one-fifth the exhaust flow rate. Bornside et al.'s simulations [1993] indicate that the existence of downward flow at the periphery of a rotating wafer expedites the transition of laminar flow to a turbulent one. The effect of exhaust flow, however, is not quantified and should be studied in the future.

6.8 Initial Coating Layer Thickness

Thicknesses and uniformities of an initial coating layer are important because they affect the final coating thickness and uniformity. Extrusion-slot coating provided an initial coating layer to the wafer. The wafer was removed and baked before spin coating. A Prometrix spectral interferometer measured the thickness of 49 points on the wafer. In all cases, the initial coating thickness was thinner than the programmed thickness by 1~5%. For example, when 20-μm initial layer was programmed to be deposited, the actual initial layer varied from 19.95 to 19.99 μm. This happened because the actual pump flow rate is lower than the programmed rate, as discussed in Section 5.4.2. Coating uniformities varied from 50 to 300 Å, depending on initial coating thickness. The coating uniformities were better with the thicker coatings. The specific ranges for initial coating uniformity are 100 to 300 Å with 10 μm thick initial coating layer applied, 80 to 250 Å with 20 μm thick initial coating layer, and 50 to 200 Å with 30 μm thick initial coating. Figure 4-4 shows the approximate calculation of the final coating uniformity from the initial coating uniformities. Assuming high spin speed between 1500 and 2000 RPM is used, such a range of initial coating uniformities results in a variance in the final coating uniformity: between 25 and 40 Å for 10 μm, 2 and 16 Å for 20 μm, and 1 and 6 Å for 30 μm initial thicknesses. In the experiments, a 20 μm initial coating thickness was used because it can meet both coating uniformity (5 Å or better) and efficiency (25% or better) requirements.

Most of the measurements indicated that the coating layer at the center of the wafer was thicker than all other locations. Such deviations were expected because of the overlap at the center created by the spiral coating, as shown in Figure 4-5. The thickness at the center was as much as 1~5 μm thicker than at other locations when the first generation pump was used. Such deviation decreased to 50~200 Å with the second generation pump.

6.9 Experimental Observations

Some experimental observations from the initial experiments provide valuable insights for successful application of the extrusion-spin coating process in the future:

- With less than 80% solvent concentration, spin coating time is an unimportant process variable. At high spin speeds over 2500 RPM, spin coating time does not affect the final coating thickness as long as the time is more than 20 seconds. However, its significance increases as spin speed decreases. When high spin speed is lower than 1500 RPM, spin coating time should not be less than 30 seconds. If a coating time of less than 30 seconds is used, the spreading of photoresist will cease before reaching a steady state, producing unpredictable results. In all cases, the spin coating time should be long enough for the spreading (with solvent-concentrated environment) and evaporation of photoresist (without solvent-concentrated environment) to reach a steady state.
- Normally, solvent vapor inflow stops after extrusion-slot coating. However, the mechanical leak caused the solvent concentration level to decrease after solvent vapor inflow ceased. The inflow of solvent vapor was continued during spin coating to compensate for the loss. The rate of inflow varied from 0.05 to 0.3 ml/sec. However, experiments indicated that it was almost impossible to maintain 100% solvent concentration (a fully saturated environment) without condensation occurring inside the coating chamber.
- A pool of resist deposited at the center of the wafer resulted in an unacceptable coating uniformity (Appendix B). The second generation pump with a precise suckback, removed the excessive amount of resist.

6.10 Prediction of Coating Uniformity

Prediction of coating uniformity is possible using Bornside et al.'s model (Equation 2.18) if the mass transfer coefficient, k, can be experimentally obtained. An initial coating thickness of 20 μm and an extrusion coating speed of 80 mm/sec were used for all experiments to estimate a value of k. Experimental results indicated that coating uniformity was mostly affected by high spin speed and solvent concentration degree. Figure 6-9 and 6-10 illustrate the coating thickness profile when the high spin speed was relatively fast (2500 RPM) and slow (1500 RPM), respectively. The coating thickness profile had a thicker edge area when high spin speed was over 2500 RPM. The region in which the radial position on the wafer was less than 60 mm from the center had a uniformity of less than 5 Å. However, the flow regime above the edge of the wafer becomes turbulent where the high spin speed and mass transfer coefficient are increased, resulting in rapid evaporation of photoresist. As a result, the viscosity at the periphery becomes higher than at the other locations on the wafer. The photoresist did not spread out as much as the photoresist at the inner radial region, creating a thicker edge. The coating uniformity dramatically worsened due to the thicker edges. The uniformity reading was between 20 and 50 Å. On the contrary, when a high spin speed of 1500 RPM was used, the coating profile had a thicker center and thinner edge. The coating uniformity was more desirable with this profile. All coating results had the uniformity of 5 ~ 10 Å.

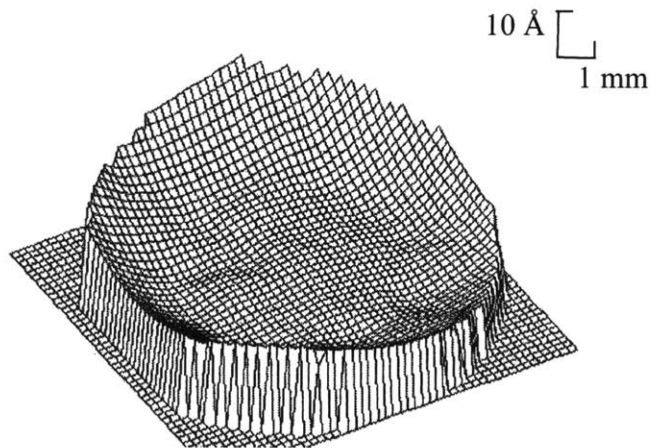

Figure 6-9: Coating thickness profile with spin coating speed of 2500 RPM in ~90% solvent-concentrated environment.

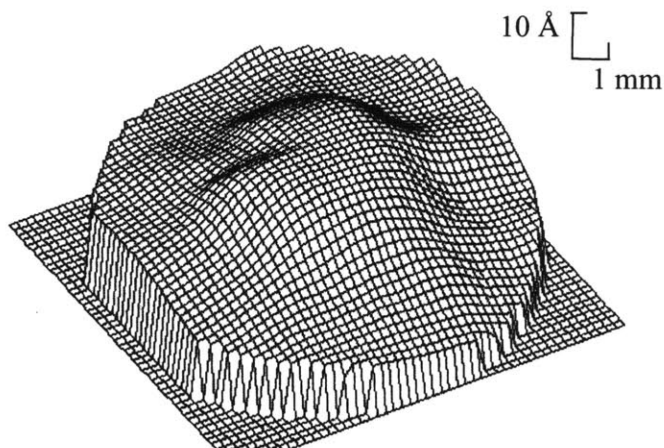

Figure 6-10: Coating thickness profile with spin coating speed of 1500 RPM in ~90% solvent-concentrated environment.

6.10.1 Mass Transfer Coefficient

The mass transfer coefficient k is the dominant factor in deciding the coating thickness and uniformity in the presence of evaporation from a rotating disk. Bornside et al.'s model (Equation 2.18) shows the relationship between the final coating thickness, h_f, and k. From their model, when the initial properties of the photoresist are known, k can be calculated by measuring the final thicknesses at different locations on a wafer. Figure 6-11 shows the values of calculated ks at three radial positions from the center of the wafer. Solvent

concentration degrees used for the calculations were 0%, 30%, and 60%. When the solvent concentration degree was over 80%, solvent evaporation was negligible. It was no longer valid to predict the final coating thickness from Equation 2.18. The mass transfer coefficient with a zero solvent-concentrated environment (0% concentration) is smaller than Kreith et al.'s theoretical estimation (Figure 2-8) by approximately one-fourth. This is because although no solvent concentration was used, the solvent evaporated from the photoresist was not carried away instantly, and so vapor remained in the surroundings. However, the mass transfer coefficient increases as the location on the wafer approaches the periphery because the leak near the periphery of the wafer more quickly carries the vapor.

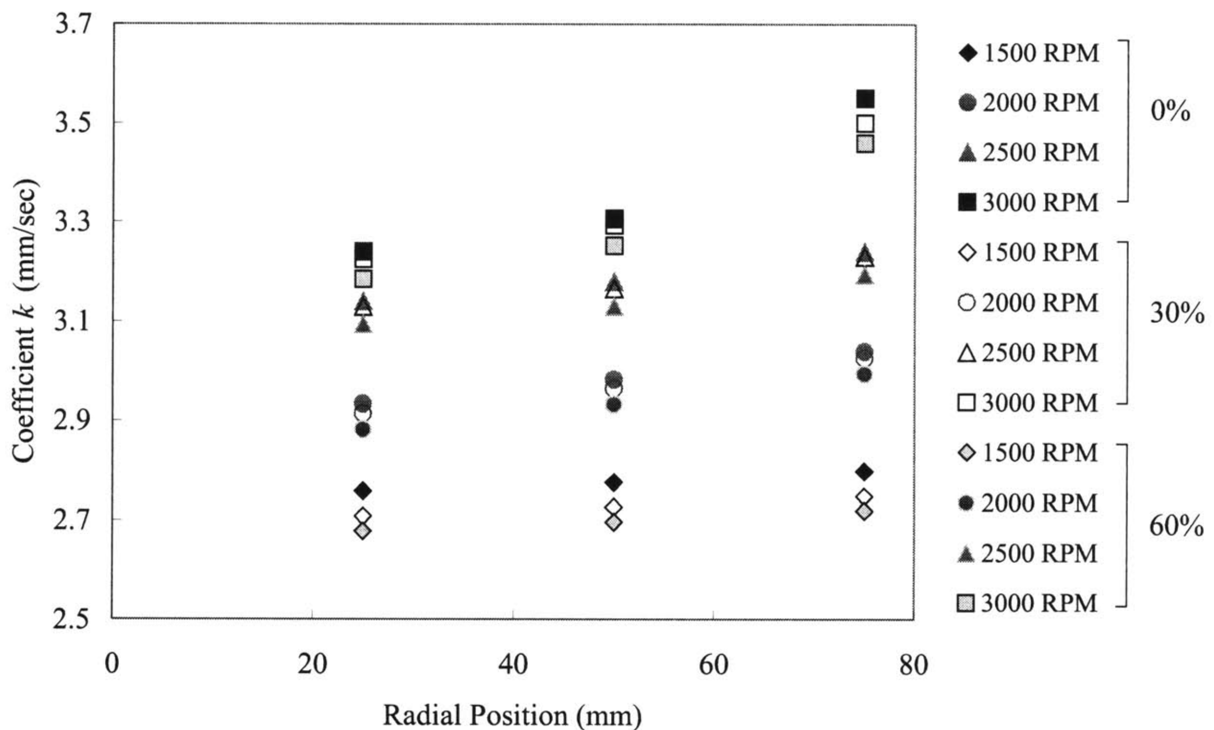

Figure 6-11: Calculated mass transfer coefficient k in various radial positions.

6.10.2 Coating Uniformity Prediction Curve

Figure 6-12 shows the coating uniformity improvement as solvent concentration increases. The three curves in the figure were obtained by applying Bornside et al.'s model with the mass transfer coefficient obtained in Figure 6-11. The curves were extended to 100% solvent concentration. Figure 6-12 indicates that the prediction curve corresponds with the actual data at 80% solvent concentration when spin speeds of 1500 and 2000 RPM were used. At 100% concentration, the actual data deviated from the prediction curve by 4~8 Å. This deviation is caused by the fact that the initial coating layer is not completely uniform, as discussed in Section 6.8. However, when 3000 RPM of spin speed was used, the coating uniformity became unpredictable. This experimental result corresponds with the discussion in Section 6.7. Solvent evaporation took place at the periphery of the wafer due to the leak. The solvent vapor flow above the periphery of the wafer remained very close to, if not in the turbulent regime, thus increasing the mass transfer coefficient.

Estimation of the coating uniformity with different solvent concentrations and a high spin speed is now possible for a 200 mm wafer. The prediction curve from Figure 6-12 shows the precision of ± 3 Å from 0 to 60% solvent concentrations for high spin speeds below 3000 RPM.

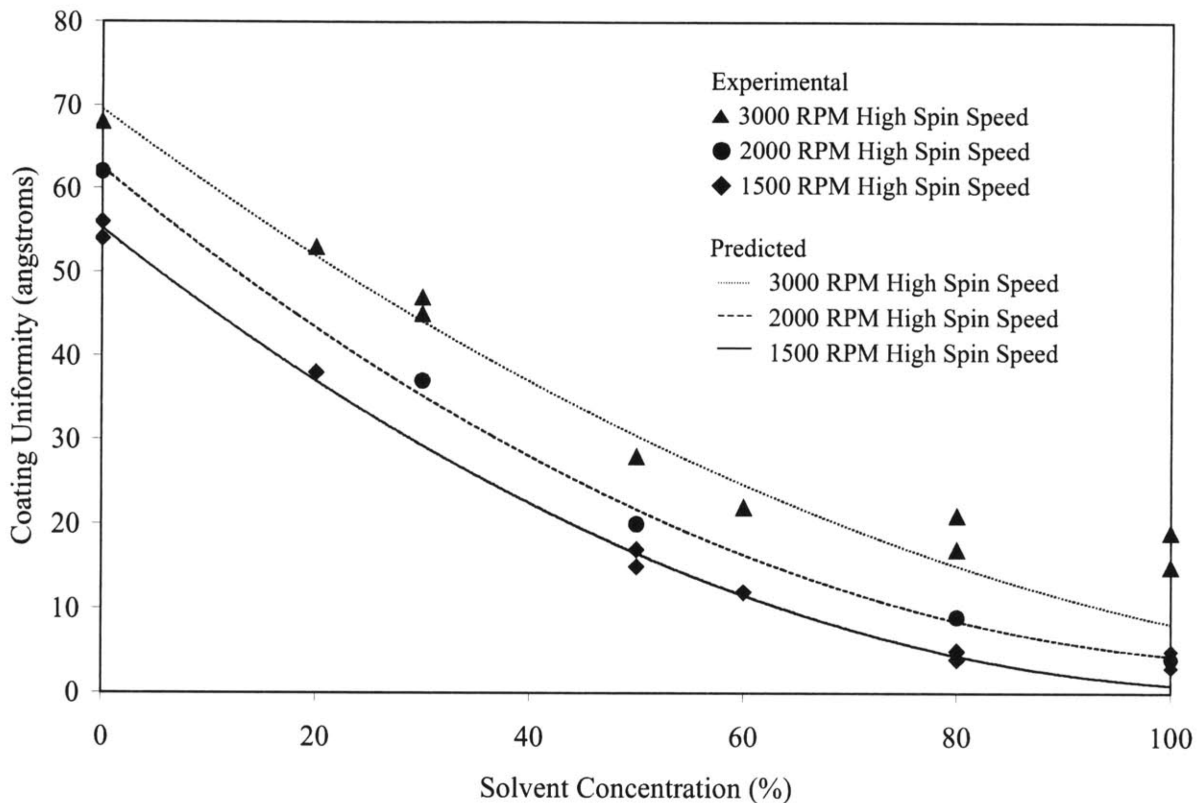

Figure 6-12: Coating uniformity results with different high spin speeds.

6.11 Mean Coating Thickness

Section 6.10 explained that the coating uniformity can be estimated by knowing the initial conditions and values of relevant process variables. In this section, a method for estimating the mean coating thickness will be discussed.

One of the most attractive features of the extrusion-spin coating process is that the final coating thickness can be predicted from process variables, such as initial coating thickness, spin coating speed and spin coating time. Experiments explored the relationship between the listed process variables and the final coating thickness. An initial coating thickness of 20 μm was used to obtain a coating efficiency of 25%. Spin coating speeds ranging from 1500 to 2500 RPM were used. The spin coating time varied from 30 to 50 seconds. The solvent concentration degree was at least 80% to eliminate the effect of

solvent evaporation on coating thickness. As a result, mean coating thicknesses were obtained as shown in Figure 6-13, 6-14, and 6-15. Different spin coating times were used for the three figures. The continuous line in each figure indicates the theoretical prediction by Emslie et al.'s model (Equation 2.10). All data were collected when the extrusion-spin coating process reached a steady state at which the coating uniformity was less than 10 Å.

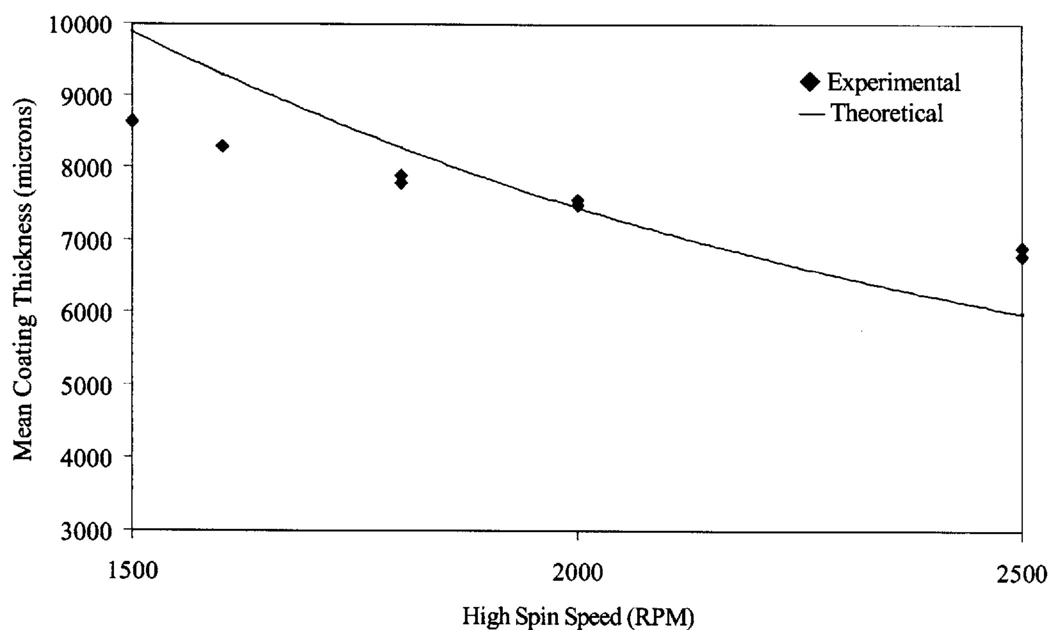

Figure 6-13: Mean coating thickness results with 30 seconds of spin coating time and different high spin speeds.

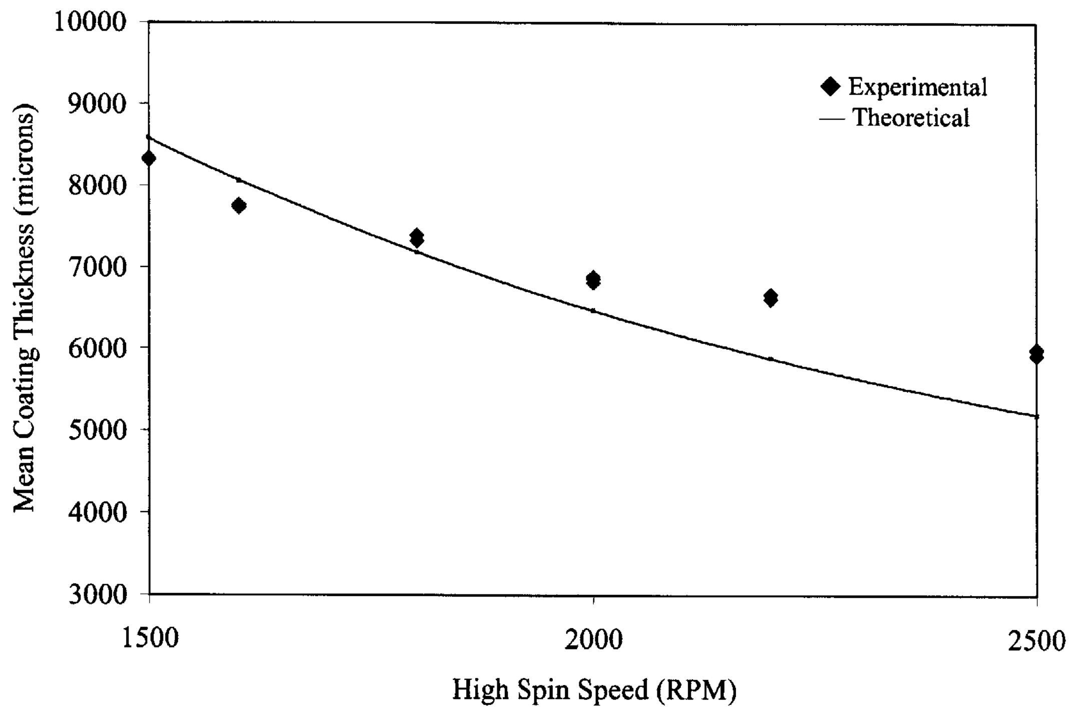

Figure 6-14: Mean coating thickness results with 40 seconds of spin coating time and different high spin speeds.

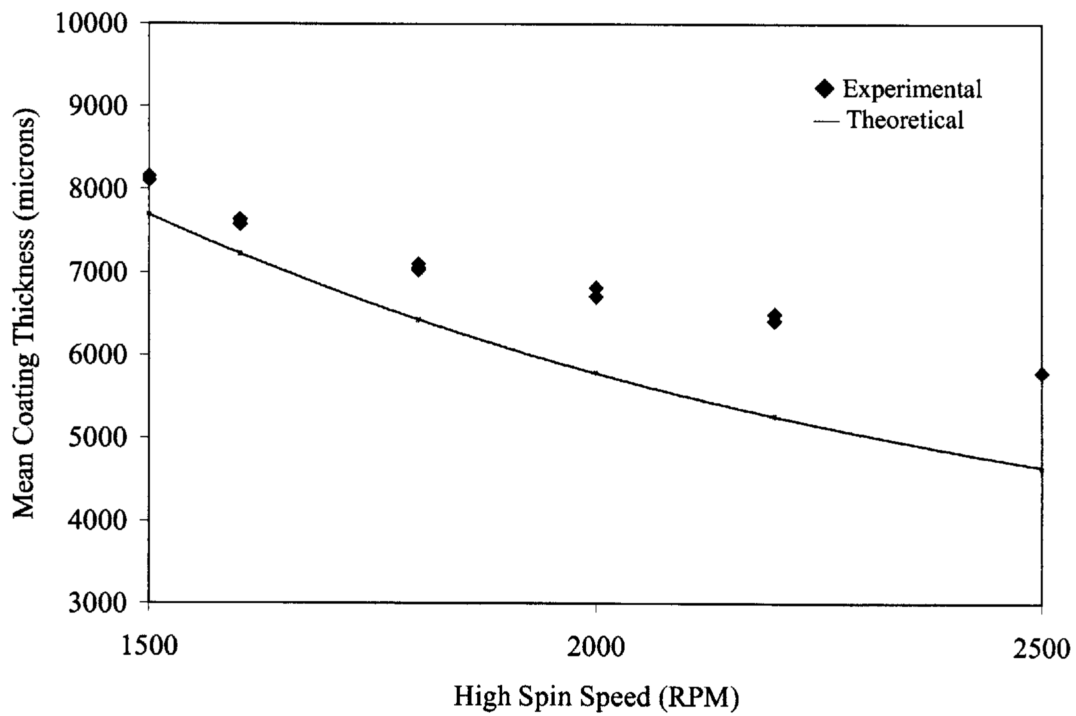

Figure 6-15: Mean coating thickness results with 50 seconds of spin coating time and different high spin speeds.

Results in Figures 6-13, 6-14, and 6-15 indicate that the mean coating thickness variance is inversely proportional to the rotational speed and the coating time. Thickness decreases as high spin speed and spin coating time increase. This trend corresponds with Emslie et al.'s model. However, experimental data did not exactly match Emslie et al.'s theoretical prediction. Instead, the empirical coefficient that varied almost linearly with spin speed was obtained.

6.11.1 Coating Thickness Coefficient

The correlation coefficient between theoretical and experimental coating thickness is defined as:

$$K(\Omega,t)=\frac{(h_f)_{\text{experiment}}}{(h_f)_{\text{theory}}} \tag{6.1}$$

where $(h_f)_{\text{experiment}}$ is the final coating thickness obtained in experiments, $(h_f)_{\text{theory}}$ is the theoretical coating thickness obtained by Equation 2.10. Figures 6-13, 6-14, and 6-15 show both experimental and theoretical final coating thicknesses. High spin speeds and spin coating times are also indicated. From this, the values of $K(\Omega,t)$ can be calculated. Figure 6-16 shows the value of $K(\Omega,t)$ with various high spin speeds and spin coating times. The figure also provides the empirical relationship between the thickness coefficient, $K(\Omega,t)$, and the process variables, Ω and t.

$$K(\Omega,t)=0.0002\Omega+f(t) \tag{6.2}$$

$$f(t)=0.0123t+0.1385 \tag{6.3}$$

Using Equations 6.2 and 6.3, the value of $K(\Omega,t)$ can be obtained with an error of ± 1%. This error causes the variation between predicted and actual final coating thicknesses to be within ± 100 Å.

The ideal value of $K(\Omega,t)$ is 1 so consequently Emslie et al.'s equation can be directly applied in real situations. However, this is not true because their assumptions are not always valid. The density and viscosity of photoresist do not remain constant during the entire coating process. Figure 6-6 indicates that during the spin coating process, solvent concentration at the periphery of the wafer drops below 80% after the first 10 seconds. This means that after the first 10 seconds, the effect of evaporation on coating thickness is no longer negligible. To eliminate the evaporation of the solvent, the concentration in the coating chamber must be maintained at 100% during both the extrusion-slot and spin coating processes. In real situations, this is almost impossible. As mentioned in Section 6.9, when the inside of the coating chamber was fully saturated, solvent vapors condensed. The condensed vapors dripped onto the spinning wafer, causing defects in final dry coating.

Although Emslie et al.'s assumptions are not fully satisfied, the prediction of the coating thickness was still possible by obtaining the coefficient $K(\Omega,t)$. Two important facts can be obtained by studying $K(\Omega,t)$. First, the effect of spin coating time on coating thickness has limitations. For a specific high spin speed, there is a point at which viscous drag exceeds centrifugal force. From this point, the photoresist will cease to spread out, even if the wafer keeps rotating. From the experimental results, this point is estimated to be between 40 and 50 seconds. At 50 seconds of coating time, all the experimental data showed a thicker coating than the theoretically calculated ones, as shown in Figure 6-15. Second, all the experimental data showed thicker coating than the predicted ones when high spin speeds above 2000 RPM were used. This is due to solvent evaporation. Figure 4-24 shows that the flow over the radial position of 80 mm from the center of wafer will remain in the transient regime, causing a higher solvent evaporation rate than in the laminar regime. This higher evaporation rate will cause a thicker coating around the periphery of the wafer, increasing the mean coating thickness.

The coating thickness coefficient $K(\Omega,t)$ provides correction for such differences between the theoretical analysis and the actual data. Using this value of $K(\Omega,t)$, and provided that the solvent concentration degree in the coating chamber is over 80%, final coating thickness can be predicted when initial wet coating thickness, density and viscosity of photoresist, high spin speed, and spin coating time are given. The variation between the

actual mean coating thickness and predicted coating thickness using $K(\Omega,t)$ is $\pm$ 100 Å. This coefficient does not include regions over 2500 RPM because both coating uniformity and evaporation rate became unpredictable above this rotational speed.

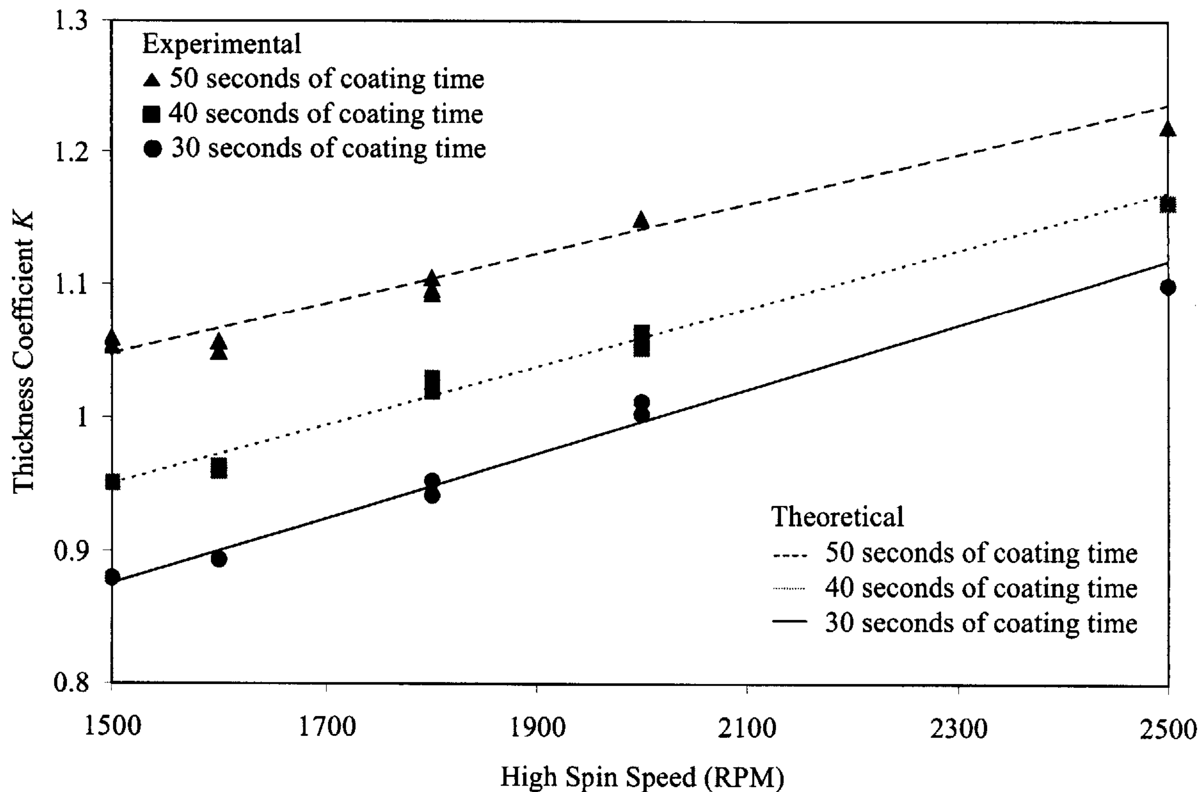

Figure 6-16: *K* coefficient value according to different spin speed and spin coating time.

Prediction of coating thickness for 200 mm wafers is possible using the values of $K(\Omega,t)$ obtained in this section. The following conditions must be met.

- The solvent concentration degree in the environment must be maintained at over 80% during extrusion-slot and spin coating.
- The initial coating layer must have reached a certain uniformity level to yield the required coating uniformity.
- The initial coating layer must not contain defects.

- The Reynolds number of the flow above a rotating wafer must remain between 1×10^5 and 1.66×10^5, which correspond with high spin speeds of 1500 and 2500 RPM, respectively.

Once these conditions are satisfied, the coating thickness coefficient $K(\Omega,t)$ obtained can be applied to various sizes of wafers to predict coating thicknesses with different initial conditions.

6.12 Summary

Initial experimental results without any controlled environments showed that extrusion-spin coating has the potential to be an efficient photoresist coating method. However, coating uniformity was not acceptable. This problem was solved by adding a solvent-concentrated environment.

Extrusion-spin coating eliminates the unpredictable dispense stage in a spin coating process. Coating thickness and uniformity become predictable by obtaining mass transfer and coating thickness coefficients, k and $K(\Omega,t)$, respectively. For the correct estimation of coating thickness, the flow over the wafer in the extrusion-spin coating process remains close to, if not in, the laminar regime. Experiments indicated that the spin coating speed should not exceed 2500 RPM for predictable results. In addition, solvent concentration must be higher than 80% to make the extrusion-spin coating process deterministic.

Chapter 7

Conclusions and Future Work

7.1 Evaluation of Extrusion-Spin Coating Method

Extrusion-spin coating is a viable alternative to spin coating if a few challenges can be overcome. It can produce uniform coatings at thicknesses below 1 μm in approximately one minute at efficiencies of 25% or higher. Extrusion-spin coating also meets the coating uniformity requirements (standard deviation of 5 Å) of photoresist coating in microlithography. In addition, by replacing the conventional dispense method in spin coating with an efficient extrusion-slot coating, the process becomes deterministic. The relationships between process variables and coating results can be obtained. Therefore, it is easy to predict and control the coating outputs, such as coating thicknesses and uniformities.

7.2 Evaluation of Process Variables

Extrusion-spin coating adds three process variables to the conventional spin coating method: extrusion coating speed, initial coating thickness, and solvent concentration degree in environment. The other main process variables with extrusion-spin coating are high spin speed and spin coating time.

Extrusion coating speed is important when the solvent concentration degree in the environment is less than 80%. A different amount of evaporation at the periphery and at other locations on a wafer causes viscosity variation on a wafer and will lead to uneven coating thicknesses. With faster coating speeds, evaporation is reduced. Correspondingly, the coating uniformity improves. When the solvent concentration is over 80%, extrusion coating speed is no longer the important parameter affecting coating uniformity.

Initial coating thickness affect mean coating thickness (when an 80% or higher solvent-concentrated environment is used), coating uniformity (when less than an 80% solvent-concentrated environment is used) and coating efficiency (in both cases). When the solvent concentration in the environment is less than 80%, initial coating thickness is the critical factor in determining the coating uniformity. Thicker initial coating layers contain more solvent. The variation in viscosity with a thicker initial coating layer is smaller than with a thinner coating layer and thus, the resulting coating uniformities improve. When the solvent concentration in the environment is higher than 80%, the initial coating thickness does not affect the coating uniformity. An optimum initial coating layer is obtained by using the maximum extrusion coating speed and the minimum coating thickness which do not create defects.

The solvent concentration degree affects the final coating thickness and uniformity. Coating uniformity improves by increasing the concentration degree. The solvent concentration must be over 80% before extrusion-slot coating begins to attain predictable final coating thickness with uniformities of 5 Å.

High spin speed during the spin coating process mainly affects the final coating thickness. High spin speed also affects the coating uniformity when the solvent concentration degree is lower than 80%. However, the relationship between high spin speed and coating uniformity is hard to analyze theoretically. Experiments must be conducted to find such a relationship.

The effect of the spin coating time on coating thickness and uniformity is small compared to the other process variables. However, it must be sufficiently long to reach a steady state of coating thickness and uniformity.

7.3 Solvent Consumption

One of the main issues with extrusion-spin coating is the amount of solvent consumption during the coating process. It takes approximately 1 ml of the solvent in liquid state to saturate an experimental coating chamber with a volume of 38×10^6 mm^3. Because solvent is an environmentally hazardous product, minimizing the solvent consumption is desirable. Unlike the photoresist, solvent vapor can be recycled. Development of a solvent vapor recycling system is necessary for both environmental and economical reasons.

7.4 Concluding Remarks

Extrusion-spin coating provides three major advantages over conventional spin coating .

- Coating efficiency is higher. Spin coating requires an abundant dispense of photoresist to ensure an initial thin layer over the entire wafer. The initial uniform layer is obtained in the middle of the spin-off stage when most of the applied photoresist has already been thrown out. Extrusion-spin coating starts with that thin layer of coating, eliminating the waste. Thus, it produces minimal waste, resulting in increased coating efficiency.
- Common defects from spin coating are prevented. To achieve an initial thin uniform layer, spin coating uses an excessive amount of resist to prevent defects caused by lack of resist supply. Extrusion-slot coating covers the entire wafer with a uniform layer. Therefore, it eliminates defects such as voids or striations.
- Extrusion-spin coating provides an initial uniform layer for spin coating. The method provides a deterministic coating process that makes the prediction and control of the final coating thickness and uniformity possible.

Despite the advantages listed above, extrusion-spin coating still needs to be improved upon before it can replace current spin coating in industrial applications. In the following section, such areas will be touched upon and directions for improvement will be suggested.

7.5 Future Work

The prototype of an extrusion-spin coater was built and tested with 200 mm wafers. The results corroborated the predictions of positive aspects of the extrusion-spin coating method. However, there are four important issues that must be solved before extrusion-spin coating can replace spin coating.

- The spinner chuck runout must be minimized or eliminated to achieve a stable deposit of photoresist layer in the extrusion-slot coating stage. A spin coater that can accommodate a non-wobbling rotation at low rotational speeds need to be developed.
- A method for using a coating bead vacuum is desirable for reducing the coating time.
- Further experiments have to be conducted with various sizes of wafers to find a scalability of coating results obtained from 200 mm wafers. In this way, the results from this thesis can be extended to predict and control coating thickness and uniformity with various sizes of wafers.
- The design of the solvent generating system must be improved upon to minimize the use of the solvent for a smaller environmental impact. Because solvent vapors are not as easily contaminated as photoresist, recycling of solvent vapors is a good possibility. Solvent waste from the creation of the solvent-concentrated environment could be minimized or even eliminated.

With these challenges met, extrusion-spin coating will be an effective replacement for spin coating.

Appendix A: Behavior of Resist Films with Evaporation

Meyherhofer [1978] analyzed the behavior of resist film on a rotating disk with evaporation. In addition to Emslie et al.'s model (Equation 2.10), he added the effect of evaporation. At the start of spinning, the solids concentration of the resist is uniform. The solvent evaporation over the entire surface area causes the solids content, c, to increase. As h_{wet} is independent of r, c is also independent of r. Both solid and solution are assumed to have density unity to simplify the discussion. The volume of the photoresist is equal to the volume of the solvent (L) plus the volume of the solid (S). While real solutions do not obey this assumption, the difference is small over the concentration ranges used and does not affect the final results [Lawrence, 1988]. With the definition of L and S, $c(t)$ and h_{wet} are expressed as:

$$c(t) = S/(S+L) \qquad \text{(A.1)}$$

$$h_{wet} = S + L \qquad \text{(A.2)}$$

The change in solid concentration affects the behavior of coating flow through the change in viscosity. Rates of changes of S and L due to outflow and evaporation are:

$$\frac{dS}{dt} = -c\frac{1}{r}\frac{\partial(rq)}{\partial r} = -c\frac{2\Omega^2 h^3}{3\nu} \qquad \text{(A.3)}$$

$$\frac{dL}{dt} = -(1-c)\frac{2\Omega^2 h^3}{3\nu} - e \qquad \text{(A.4)}$$

where e is the evaporation rate.

Equations A.3 and A.4 are expressed in terms of rate of change of volume per unit area (m/sec). The final film thickness, h_f is equal to the final solid thickness, S_f. It can be obtained by integrating the two equations (A.3 and A.4) from the initial thickness and solid

concentration values to the point where all the solvent evaporates and only the solid film remains ($L = 0$).

The kinematic viscosity ν can be estimated using Sukanek's viscosity model (Equation 1.2) and rewritten as:

$$\nu = \nu_l + (1 - \nu_l)\left(\frac{c}{c_0}\right)^n \tag{A.5}$$

The exponent n typically has values around 1.5~2.5 for photoresist solutions [Jenekhe, 1983]. While Equations A.3, A.4, and A.5 cannot be solved analytically, an approximate value of h_f is estimated by Meyerhofer. He assumed that, at the outset, evaporation is negligible until the liquid film thins to a value $h_{1/2}$ at which the evaporation and outflow contributions in Equation A.4 are equal:

$$(1 - c_0)\frac{2\Omega^2 h^3}{3\nu} = e \tag{A.6}$$

Appendix B: Center Overlap

A set of experiments was conducted with different volumes of photoresist and concentration degrees. Figure B-1 shows the coating uniformity problems with the first-generation pump. When the pump did not have proper suckback at the center of the wafer, it deposited excessive resist. Two consecutive bars in the figure indicate the coating uniformities with/without including the center coating thickness. At low solvent concentration levels (C_s < 80%) the difference between the two is not distinct because overall coating uniformity is bad. However, when a high solvent concentration is achieved (C_s > 80%) the center problem became evident. Figure B-2 shows the typical coating thickness profile when an excessive amount of photoresist is applied at the center region. The coating thickness at the center is much thicker than the thicknesses of other locations of wafer. By calculating the coating uniformity including and excluding the center region, the coating uniformity varied as much as 50 Å. This problem was completely solved when the pump was replaced with the second-generation pump that had a suckback control precise down to 0.01 ml/sec.

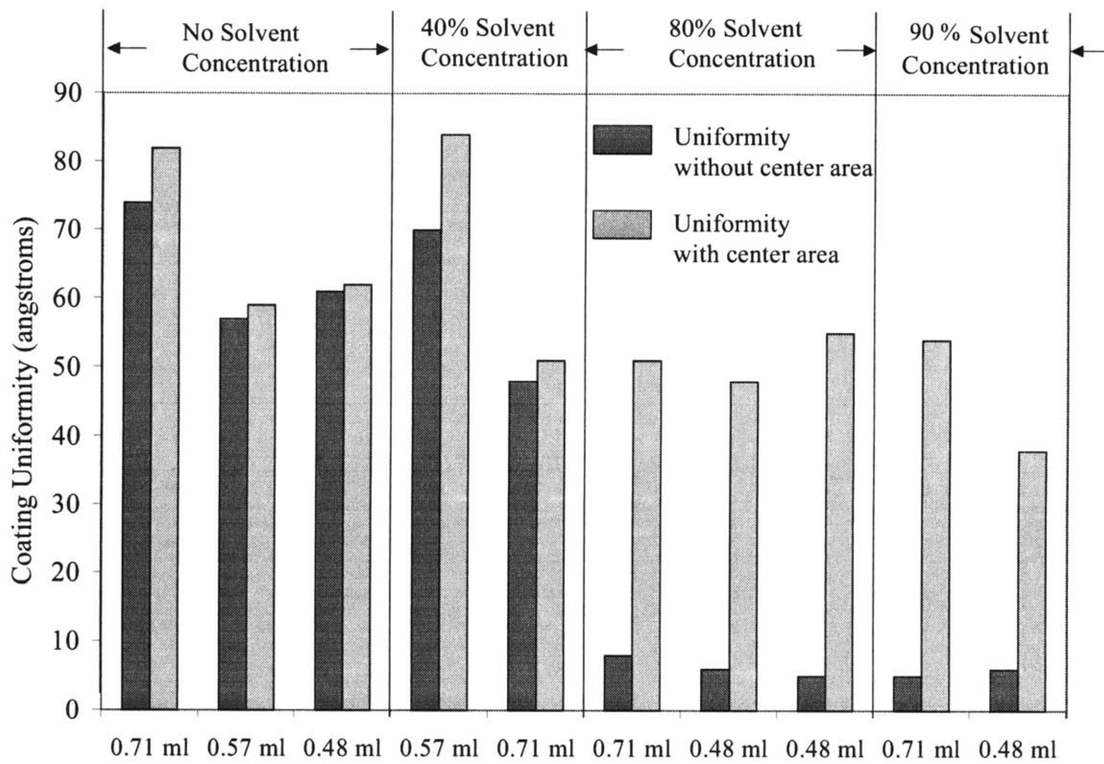

Figure B-1: Center problem occurs when proper amount of suckback at the center is missing.

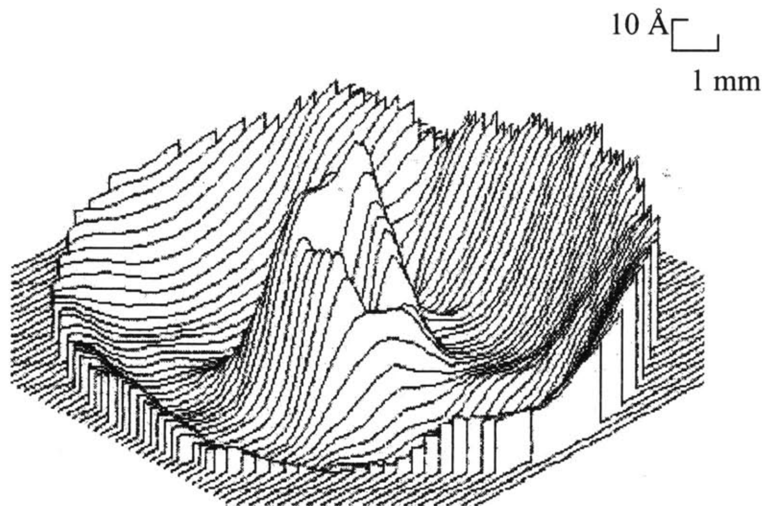

Figure B-2: Coating thickness profile with excessive dispense at center.

Appendix C: Pump Stability

Pump stability was another issue to be considered when experiments were conducted. As more and more experiments were conducted with the same process variables, pump dispense reached a steady-state and coating results became stable. Figure C-1 shows the coating uniformity improvement with repetitive use of the pump. The same values of process variables were used for all sets of experiments: 20 μm initial coating thickness and 40 μm gap distance. Valid coating results were obtained only after the pump reached a stable state. Throughout the experiments, each experiment was repeated 4~6 times. Only valid coating results were collected.

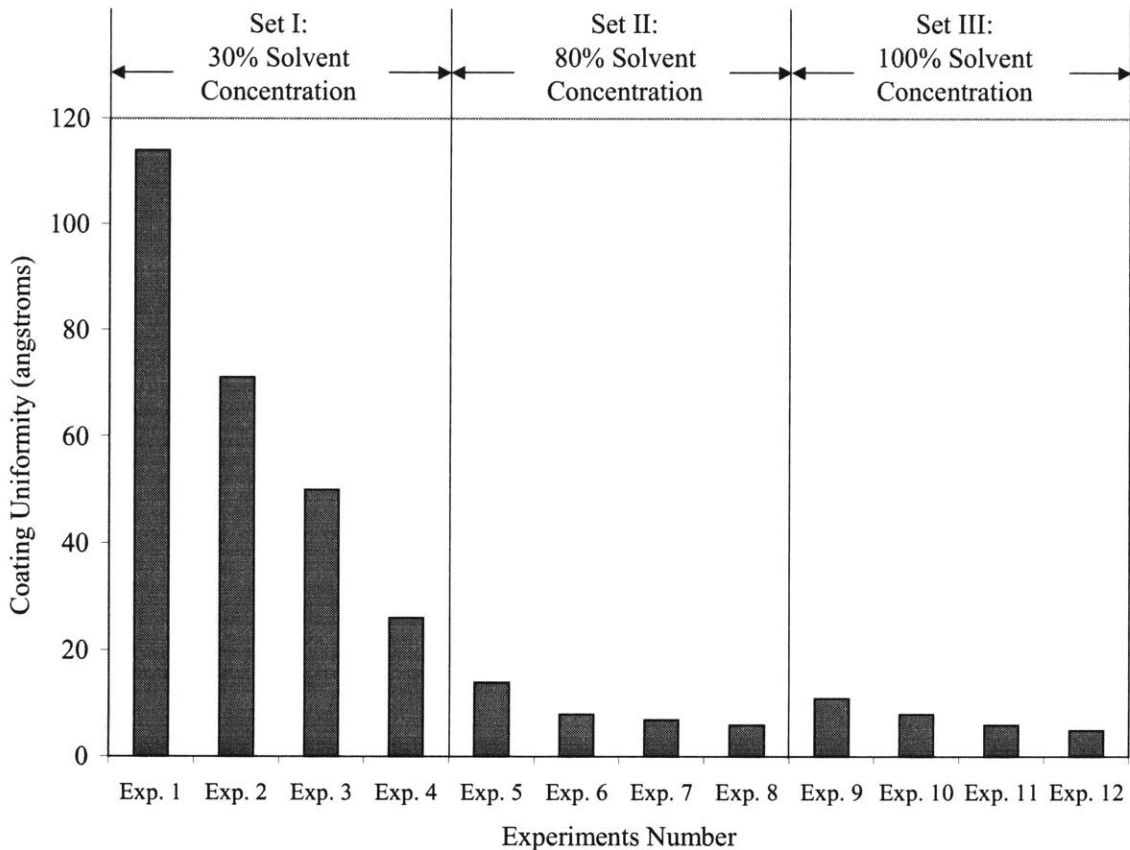

Figure C-1: Coating uniformity improvement with steady-state pump dispense.

Bibliography

A. Acrivos, M. J. Shah and E. E. Peterson. On the flow of a non-Newtonian liquid on a rotating disk. *Journal of Applied Physics*, 31(6), 1960.

A. W. Adamson. Physical Chemistry of Surfaces, 4th Edition, Wiley, New York, 1982.

American Society for Testing and Materials, Published Methods and Procedures, "Standard Methods for Testing Photoresists in Microelectronic Fabrication," Test Std F-66 84, 1984.

AZ Product Bulletin. AZ series positive photoresists. Hoechst Celanese Corporation.

S. Bagen and C. Newquist. Extrusion coating of polymer films for low-cost flat panel display manufacturing. *1996 Display Manufacturing Technology Conference, Digest of Technical Papers*, 3, 1996.

J. Bargon. Lithographic Material, *Methods and Materials in Microelectronic Technology*, Plenum Publishers, New York, 1984.

A. E. Beguin. Method of coating strip material. U.S. Patent 2,681,234, June 1954.

N. E. Bixler. *Stability of a coating flow*, PhD thesis, University of Minnesota, 1982.

E. Bokelberg and W. Venet. Effects of relative-humidity variation on photoresist processing, *SPIE: Advances in Resist Technology and Processing XII*, 2438, 1995.

D. E. Bornside, C. W. Macosko, and L. E. Scriven. On the modeling of spin coating, *Journal of Imaging Technology*, 13(4), August 1987.

D. E. Bornside, C. W. Macosko, and L. E. Scriven. Spin coating: One-dimensional model, *Journal of Applied Physics*, 66(11), December 1989.

D. E. Bornside and R. A. Brown. Method for low pressure spin coating and low pressure spin coating apparatus. U.S. Patent 5,358,740, October 1994.

D. E. Bornside and R. A. Brown. The effect of gas phase convection on mass transfer in spin coating, *Journal of Applied Physics*, 71(2), 15 January 1993.

M. J. Bowden. A Perspective on Resist Materials for Fine Line Lithography, *Materials for Microlithography*, Advances in Chemistry Series, No. 266, American Chemical Society, 1984.

R. Burley and B. S. Kennedy. An experimental study of air entrainment at a solid-liquid-gas interface, *Chem. Eng. Sci.*, 1976.

R. Burley and B. S. Kennedy. A study of dynamic wetting behavior of polyester tapes, *Br. Polymer J.*, 1976.

R. Burley and B. S. Kennedy. *Wetting, spreading and adhesion*, chapter 15. Academic Press, London, 1978.

S. A. Campbell. The Science and Engineering of Microelectronic Fabrication, Oxford University Press, 1996.

J. F. Chen et al. "Design and analysis of across chip linewidth variation for printed features at 130 nm and below." *SPIE*, vol. 3998, 2000.

B. T. Chen. Investigation of the solvent evaporation effect on spin coating of thin films, *Polymer Engineering and Science*, 23(7), May, 1983.

E. J. Choinski. Patch coating: taking the spin out of thin, *Information Display*, 7(11), 1991.

M. H. Clarkson, S. C. Chin, and P. Shacter. Visualization of flow instabilities on a rotating disk, *Am. Inst. Aero. Astro.* J. 18:1541, 1980.

E. Cohen and E. Gutoff. *Coating and Drying Defects*, John Wiley and Sons, New York, 1995.

P. Das and U. Sengupta. Krypton Fluoride Excimer Laser for Advanced Microlithography, Microlithography, chapter 4, Marcel Dekker, Inc., 1998.

W. J. Daughton and F. L. Givens. An investigation of the thickness variation of spun-on thin films commonly associated with the semiconductor industry, *Journal of the Electrochemical Society*, 129(1), January 1982.

K. Denbigh. *The Principles of Chemical Equilibrium, 4th edition.* Cambridge University Press, Cambridge, England, 1981.

J. Derksen. *A new method for semiconductor lithography: Fluid layer overlap in extrusion-spin coating.* SM Thesis, Mechanical Engineering, Massachusetts Institute of Technology, 1997.

B. M. Deryagin and S. M. Levi. *Film coating theory.* Focal Press, London, 1964.

K. Doren, W. Freitag and D. Stoye. Water-Borne Coatings, The Environmentally Friendly Alternative, Hanser Publishers, New York, 1995.

D. K. Edwards, V. E. Denny and A. F. Mills. *Transfer Processes.* Hemisphere, Washington, D.C., 2nd edition, 1979.

D. J. Elliott. *Microlithography: Process Technology for IC Fabrication*, chapter 3. McGraw-Hill Book Company, New York, 1986.

B. T. Ellison and I. Cornet, *J. Electrochem. Soc.* 118:68, 1971.

A. G. Emslie, F. T. Bonner, and L. G. Peck. Flow of a viscous liquid on a rotating disk, *Journal of Applied Physics*, 29(5), May 1958.

F. Fahrni and A. Zimmermann. Coating device. U.S. Patent 4,109,611, April 1978.

H. L. Faust. *Menisci studies in bead coating*, MS Thesis, Dept. of Chem. Eng., Drexel University, Philadelphia, 1975.

B, I, Fedorov, G. Z. Plavnik, I. V. Prokhorov, and L. G. Zhukhovitskii. Transitional flow conditions on a rotating disk, *J. Eng. Phys.* 31, 1448 (1976)

W. W. Flack, D. S. Soong, A. T. Bell, and D. W. Hess. A mathematical model for spin coating of polymer resists, *Journal of Applied Physics*, 56(4), August 1984.

N. Fraysse and G. M. Homsy. An experimental study of rivulet instabilities in centrifugal spin coating of viscous Newtonian and non-Newtonian fluid, *Phys. Fluids* 6(4), April 1994.

A. M. Goethals et al. 193 nm lithography on a full field scanner, *SPIE* vol. 3679, March 1999.

J. W. Grate, S. W. Wenzel and R. M. White. Flexural Plate Wave Devices for Chemical Analysis, *American Chemical Society*, 1991.

S. Granger and J. Blunt. Engineering Coatings, Abington Publishing, 1998.

N. Gregory, J. T. Stuart and W. S. Walker, Phil. Tfahns. R. Soc. London, Ser. A 248, 155 (1955).

E. B. Gutoff. Simplified design of coating die internals, *Journal of Imaging Science and Technology*, 37(6), 1993.

E. B. Gutoff. *Modern Coating and Drying Technology*. VCH Publishers, Inc., 1992.

J. Hens and W. Mues. Laser-dopler measurements in the vicinity of a moving contact line, *AIChE Meeting*, New Orleans, LA, 1988.

L. E. Higgins and B. G. Scriven. Capillary pressure and viscous pressure drop set bounds on coating and bead operability, *Chemical Engineering Science*, 35, 1980.

S. A. Jenekhe, Rheology and spin coating of polymide solutions, Polymer Eng. Sci. 23, 830 (1983).

P. Joos, M. Bracke and P. Van Remoortere. The dynamics of wetting. *AIChE*, Orlando, March 1990.

R. Kobayashi, Y. Kohama, and Ch. Takamadate. Spiral vortices in boundary layer transition regime on a rotating disk, *Acta Mech.* 35:71, 1980.

Y. Kohama. Study on boundary layer transition of a rotating disk, Acta Mech. 50:193, 1984.

F. Kreith, J. H. Taylor, and J. P. Chong. Heat and mass transfer from a rotating disk, *Journal of Heat Transfer*. 81:95-105, 1959.

R. J. LaPorte. Hydrophilic polymer coatings for medical devices, Technomic Publishing Company, Inc., 1997.

C. J. Lawrence. The mechanics of spin coating of polymer films, *Phys. Fluids* 31(10), October 1988.

K. Y. Lee, L. Liu and T. Liu. Minimum wet thickness in extrusion-slot coating, *Chemical Engineering Science*, 47(7), 1992.

W. A. Levinson, A. Arnold and O. Dehodgins. Spin coating behavior of polymide precursor solutions, *Polymer Engineering and Science*, Vol. 33, No. 15, August 1993.

M. Maenhoudt et al. Feasibility of printing 0.1 μm technology with optical lithography, *SPIE* Vol. 3679, March, 1999.

M. R. Malik. The neutral curve for stationary disturbances in rotating-disk flow, J. Fluid Mech. 164, 275 (1986)

D. Meyerhofer. Characteristics of resist films produced by spinning, *Journal of Applied Physics*. 49(7), 3993, July 1978.

S. Middleman and A. K. Hochberg. *Process Engineering Analysis in Semiconductor Device Fabrication*, chapter 9. McGraw-Hill, Inc., New York, 1993.

A. F. Mills. *Heat and Mass Transfer*, chapter 10. Richard D. Erwin, Inc., 1995.

K. Millsaps, and K. Pohlhausen. Heat Transfer by Laminar Flow From a Rotating Plate, *Journal of the Aeronautical Sciences*, vol. 19, p120, 1952.

W. Moreau, K. Cornett, J. Fahey, L. Linehan, M. Montgomery, R. Smith, and R. Wood. The shot size reduction of photoresist formulations, *SPIE: Advances in resist technology and processing XII*, 2438, 1995.

W. M. Moreau. Semiconductor Lithography: Principles, Practices and Materials. Plenum Press, New York, 1988.

W. Mues, J. Hens and L. Boiy. Observation of a dynamic wetting process using laser-doppler velocimetry, *AIChE Journal*, 35(9), 1989.

U. Okoroanyanwu, C. Pike and H. J. Levinson. Process induced defects in sub-0.15 µm device patterning using 193 nm lithography, *SPIE* Vol. 3998, 2000.

T. Patton, *Paint flow and pigment dispersion*, Wiley, New York, 1979.

Photoresists for microlithography. *Solid State Technology*, June 1993.

W. W. Pulkrabek and R. M. Wabrek. Single-Pass Curtain Coating, *Materials and Manufacturing Processes*, 8(3), 1993.

W. S. Rees, Jr. *CVD of Nonmetals*, VCH, 1996.

D. Reichenberg. *Symp. Transp. Prop. Fluids and Fluid mixtures*, Natl. Eng. Lab, East Kilbride, Glasgow, Scotland, 1979.

R. C. Reid, J. M. Prausnitz, and B. E. Poling. *The Properties of Gases and Liquids*. McGraw-Hill, Inc., New York, fourth edition, 1987.

K. J. Ruschak. Limiting flow in a pre-metered coating device, *Chemical Engineering Science*, 1976.

L. Sartor. *Slot coating: Fluid mechanics and die design*, PhD thesis, University of Minnesota, 1990.

A. Z. Sezeri and A. Giron, Int. J. Number. Methods Fluids 4, 989 (1984)

P. H. Singer. Trends in Resist Design and Use, *Semiconductor International*, August 1985.

B. W. Smith. Optics for Photolithography, Microlithography, chapter 3, Marcel Dekker, Inc., 1998.

B. W. Smith. Resist Processing, Microlithography, chapter 8, Marcel Dekker, Inc., 1998.

N. H. Smith. NACA TN 1227, 1947.

E. M. Sparrow and J. L. Gregg. Mass transfer, flow, and heat transfer about a rotating disk, *Journal of Heat Transfer*. 82:294-302, 1960.

L. E. Stillwagon and R. G. Larson. Leveling of thin films over uneven substrates during spin coating, *Physics of Fluids A*, 2(11), November, 1990.

J. Sturtevant et al. Characterization of CD control for sub-0.18 μm lithographic patterning, *SPIE* Vol. 3679, March, 1999.

Substituted Resist Materials, Solid State Technology, May 1985.

P. C. Sukanek. Spin coating, *Journal of Imaging Technology*, 11(4), August 1985.

J. A. Tallmadge, C. B. Weinberger and H. L. Faust. Bead coating instability: A comparison of speed limit data with theory, *AIChE*, 25, 1979.

T. Ueno. Chemistry of Photoresist Materials, Microlithography, chapter 8, Marcel Dekker, Inc., 1998.

G. Vandenberghe, T. Marschner and K. Ronse. CD-control comparison for sub-0.18 μm patterning using 248 nm lithography and strong resolution enhancement techniques, *SPIE* Vol. 3679, March, 1999.

Th. Von Karman, Z. Angew. *Math. Mech.* 1:233, 1921.

C. Wagner. Heat transfer from a rotating disk to ambient air, *Journal of Applied Physics*, vol. 19, 1948.

C. T. Wang and S. C. Yen. Theoretical analysis of film uniformity in spinning processes, *Chemical Engineering Science*, Vol. 50, No. 6, 1995.

Z. W. Wicks, F. N. Jones and S. P. Pappas. Organic coatings science and technology, John Wiley and Sons, New York, 1994.

S. P. Wilkinson and M. R. Malik. Stability experiments in the flow over a rotating disk, *Am. Inst. Aero. Astro. J.* 23:588, 1985.

C. G. Willson. Organic Resist Materials – Theory and Chemistry, Introduction to Microlithography, Advances in Chemistry Series, No. 219, American Chemical Society, Washington, D.C., 1983.

S. Wolf and R. N. Tauber. Silicon Processing for the VLSI Era: Volume 1 – Process Technology. Lattice Press, Sunset Beach, CA, 1986.

S. Yen and C. Wang. The Film Formation of a Newtonian Fluid on a Spinning Disc with Evaporation, *Journal of The Chin. I. Ch.* E., Vol. 26, 1995.

Z. Zawidski, *Phys. Chem.* 35, 129, 1990.